Study of Influence of Vehicle Shape and Stiffness on the Lower Extremity Injury of Child and Adult Pedestrians

Tsuyoshi Yasuki

Abstract

World Health Organization (WHO) reported that road traffic injuries will become the third leading contribution of the global burden of disease (WHO, 2004). The Institute for Traffic Accident Research and Data Analysis (ITARDA) reported that vulnerable road users accounted for a significant proportion of the road accident fatalities (ITARDA, 2008). The distributions of the injuries of the vulnerable road users such as the pedestrians are head, face, neck, chest, abdomen, pelvis, arm, and legs. The fractures of the tibia bone and the ruptures of the knee joint ligament are the frequent injuries of the pedestrians collided by a car or a sport utility vehicle (SUV). Studies of injury mechanisms of the pedestrians of the several sizes are more important research area now.

The mechanism of the fracture of tibia bone and the rupture of knee joint ligament of the pedestrian were studied by a Finite Element (FE) model of the pedestrian in this study. The FE model of the pedestrian was developed and validated with the test result of the Postmortem Human subject (PMHS) in the literatures. The FE model was a reliable method for researching the relationship of the fracture of tibia bone and the rupture of knee joint ligament to the shape and the stiffness of the front of the impacting vehicles.

The relationships of the fracture of tibia bones and the rupture of knee joint ligaments to the shape and the stiffness of the impacting car were dependent on the sizes of the pedestrians such as American male 50%-ile (AM50%ile), American female 05%-ile (AF05%ile), and six-year old child (6YO). The results by the FE model of these three pedestrians indicated the different kinematic and the injury mechanism from each other. Optimizing the shape and the stiffness of the car was possible by the FE model of these three pedestrians and the optimized shape and the stiffness of the vehicle indicated neither the fracture of tibia bones nor the rupture of knee joint ligaments for the pedestrians such as AM50%ile, AF05%ile, and 6YO. The FE model of the pedestrian can be one of design tools for the pedestrian protection in future.

The fractures of tibia bones and the ruptures of the knee joint ligaments are the frequent injuries of the pedestrians, but both injuries were not observed in one accident simultaneously and the reason for this was unknown. This study clarified that the bending of the tibia and the bending of the knee joint occurred simultaneously at first

and the risk of fracture of tibia bone came second. If the tibia bones did not fracture, then the risk of the rupture of the knee joint ligament came last.

The risk of the rupture of knee joint ligament of the pedestrians collided by the SUV increased as the knee-bending angle increased. Adding the lower bumper absorber on the SUV was a potential countermeasure of decreasing the knee-bending angle in the case impacted by the SUV.

Utilization of the FE model of the pedestrians for researching the pedestrian protection has just begun and the method is new and reliable for the researches of not only kinematic but also injuries of the pedestrians. The present findings on the kinematic and the injury may contribute to enhancement of the bio-fidelity of the testing devices such as the lower legform impactor.

Acknowledgements

This study was carried out at Advanced CAE division of Toyota Motor Corporation, Toyota, Japan with suggestions by Biomechanics and Human-Machine Systems Research Group, Biomechanics Laboratory, Department of Mechanical Science and Engineering, Graduate School of Engineering, Nagoya University, Nagoya, Japan.

The author would like to thank those who have helped me throughout the study:

Dr. Eiichi Tanaka, Professor, Graduate School of Engineering, Nagoya University, Nagoya, Japan, for his continued support and encouragement.

Dr. Koji Mizuno, Professor, Graduate School of Engineering, Nagoya University, Nagoya, Japan, for his constructive criticism and valuable suggestions.

Dr. Toshiro Matsumoto, Professor, Graduate School of Engineering, Nagoya University, Nagoya, Japan, for his reviewing this thesis and for his help.

Dr. Tadashige Ikeda, Associate Professor, Graduate School of Engineering, Nagoya University, Nagoya, Japan, for reviewing this thesis and for his help.

Mr. Junji Hasegawa, former Manager, Toyota Motor Corporation, Toyota, Japan, for his development of a human FE model and cooperation.

Dr. Yuichi Kitagawa, Project General Manager, Toyota Motor Corporation, Toyota, Japan, for his valuable suggestions and support.

Mr. Yasuo Yamamae, Toyota Technical Development Corporation, Toyota, Japan, for his cooperation on this study and his kindness.

All my colleagues at Advanced CAE division of Toyota Motor Corporation, Toyota, Japan and Toyota Technical Development Corporation, Toyota, Japan for their support.

Finally, I am grateful to Satoko and friends for their support throughout this study.

Tsuyoshi Yasuki

Toyota, Japan, January, 2015

Contents

Abstract i
Acknowledgements iii
Contents iv
Abbreviations viii
Nomenclature ix

1 Introduction 1
1.1 Review of literatures on pedestrian safety research 1
1.1.1 Statistical distribution of pedestrian 1
1.1.2 Distribution of pedestrian injury by impact test of full-body PMHS 12
1.2 Differences in the pedestrian injuries based on the statistical database and the full-body PMHS impact test 20
1.3 Methods for reconstructing injuries occurring in pedestrian accidents 21
1.3.1 PMHS tests 21
1.3.2 Full-scale dummy tests 24
1.3.3 Multibody simulations 26
1.3.4 Simulations of human FE model 28
1.4 Objective of the present study 30

2 Validation of tibia and knee-joint ligament injuries assessed using human FE model 33
2.1 Introduction 33
2.2 Validation of THUMS 34
2.2.1 Structure of modified THUMS 34
2.2.2 Stiffness of tibia, femur, and fibula 36
2.2.3 Stiffness of knee joints 37
2.2.4 Bending and shearing of lower extremity unit 41
2.3 Validation of SUV stiffness 44
2.3.1 Stiffness of hood 45
2.3.2 Stiffness of bumper 47
2.3.3 Kinematics of full-scale pedestrian model 49
2.3.4 Injuries sustained by full-scale pedestrian model 56
2.4 Discussion 59

2.4.1 Trajectory of the HJ2 THUMS and contact force of the SUV 59
2.4.2 Injuries sustained by the HJ2 THUMS and contact force of the SUV 61
2.5 Limitations 63
2.6 Conclusions 63

3 Assessment of the tibia and knee-joint ligament injuries sustained by a pedestrian impacted by a vehicle 65
3.1 Introduction 65
3.2 Accident reconstruction methods 66
3.2.1 FE model of a sedan 69
3.2.2 Boundary and initial conditions 70
3.3 Results 71
3.3.1 Kinematics 71
3.3.2 Knee-bending angle and rupture of knee-joint ligaments 72
3.3.3 Injury of knee joint 73
3.4 Discussion 73
3.5 Conclusions 74

4 Relationships between the shape and stiffness of a vehicle and the tibia and knee-joint ligament injuries 77
4.1 Introduction 77
4.2 Methods of parametric study 77
4.2.1 FE model of urethane blocks 78
4.2.2 Parametric studies 80
4.3 Results 82
4.3.1 Kinematics 82
4.3.2 Injury 83
4.3.3 Relationships between the strain of the MCL and the stiffness of block #3 and position of block #4 85
4.4 Discussion 88
4.4.1 Relationships between the strain of the MCL and the kinematics of the lower leg 88
4.5 Conclusions 90

5 Assessment of tibia and knee-joint ligament injuries sustained by a pedestrian impacted by an suv 93

5.1 Introduction 93
5.2 Method 93
5.2.1 FE model of the pedestrian 94
5.2.2 FE model of the SUV 94
5.2.3 Initial conditions 96
5.3 Results 96
5.3.1 Kinematics 96
5.3.2 Injury 98
5.4 Discussion 98
5.5 Conclusions 98

6 Relationships between the stiffness of an SUV and the tibia and knee-joint ligament injuries 101
6.1 Introduction 101
6.2 Methods of parametric study 101
6.2.1 Human FE model 101
6.2.2 FE model of urethane blocks 102
6.3 Results 104
6.3.1 Kinematics 104
6.3.2 Injury 104
6.4 Discussion 105
6.4.1 Relationships between the femur fracture and the stiffness of block #4 105
6.4.2 Relationships between the stiffness of block #6 and the MCL rupture 106
6.5 Conclusions 107

7 Comparative study of the kinematics and injury sustained by the lower leg of the modified thums with the lower legform impactor 109
7.1 Introduction 109
7.2 Mechanical characteristics of the lower legform impactor 109
7.2.1 Lower leg 109
7.2.2 Knee joint 110
7.2.3 Kinematics and contact forces 111
7.2.4 Knee-bending angle 113
7.3 Discussion 114
7.3.1 Potential risk of injuries 114

7.3.2 Bio-fidelity of the lower legform impactor 115
7.4 Conclusions 115

8 Analytical study of the kinematics and knee-bending angle of the lower legform impactor 117
8.1 Introduction 117
8.2 Development of rigid body and spring model 117
8.3 Validation of the model 117
8.4 Results 124
8.4.1 Knee-bending angle and upper tibia acceleration as functions of contact force 124
8.4.2 Interaction of $F2$ and $F3$ with the knee-bending angle 126
8.5 Discussion 128
8.6 Conclusions 129

9 General discussion and conclusion 131
9.1 Methodology 131
9.1.1 Evaluation of accuracy of deformation of the front end of a vehicle 131
9.1.2 Evaluation of kinematics of the mathematical model using the PMHS test 132
9.1.3 Evaluation of injury considered in the mathematical model using the PMHS test 132
9.1.4 Parametric studies 132
9.2 Important results from the present study 133
9.2.1 Bifurcation of lower leg injuries 133
9.2.2 Cause of increase in the knee-bending angle of the lower legform impactor 133
9.2.3 Influence of the shape and stiffness of the front end of a vehicle 133
9.3 Future studies 134
9.4 Conclusion 134

References 137
Publications 144

Abbreviations

ACL	Anterior Cruciate Ligament
AF05%ile	American female 05%-ile
AIS	Abbreviated Injury Scale
AM50%ile	American male 50%-ile
AM95%ile	American male 95%-ile
BMD	Bone Mineral Density
CG	Center of Gravity
CVS	Crash Victim Simulation
EEVC	European Enhanced Vehicle Safety Committee
EEVCWG17	EEVC Working Group 17
EuroSid-2	ES-2 side impact dummy
ESV	Enhanced Safety of Vehicle
EU	European Union
FEM	Finite Element Method
FE model	Finite Element model
HIC	Head Injury Criteria
Hybrid 3	Hybrid III 50th Percentile Male Crash Test Dummy
IHRA	The International Harmonized Research Activities.
ISO	International Organization for Standardization
ITARDA	Institute for Traffic Accident Research and Data Analysis of Japan
JARI	Japan Automotive Research Institute
LCL	Lateral Collateral Ligament
MADYMO	Mathematical Dynamic Model
MAIS	Maximum Abbreviated Injury Scale
MCL	Medial Collateral Ligament
NCAC	FHWA/NHTSA National Crash Analysis Center
NCAP	New Car Assessment Program
NHTSA	National Highway Traffic Safety Administration
PCL	Posterior Cruciate Ligament
PMHS	Postmortem Human Subject
SUV	Sport Utility Vehicle
TNO	The Dutch Research Corporation
TRL	Transportation Research Laboratory in England
WHO	The World Health Organization

Nomenclature

F_1	Contact force between the hood and the lower leg form impactor
F_2	Contact force between the upper bumper and the lower leg form impactor
F_3	Contact force between the lower bumper and the lower leg form impactor
I_1	Momentum inertia of the femur of the lower leg form impactor
I_2	Momentum inertia of the tibia of the lower leg form impactor
k	Bending stiffness of Knee joint
L_0	Distance between center of the knee joint and the bottom of tibia
L_1	Distance between center of gravity of the femur and the bottom of tibia
L_2	Distance between center of gravity of the tibia and the bottom of tibia
M	Moment acting on knee joint of the lower leg form impactor
m_1	Mass of the femur of the lower leg form impactor
m_2	Mass of the tibia of leg of the lower leg form impactor
x_0	Displacement of the knee joint in x-direction
x_1	Displacement of center of gravity of the femur in x-direction
x_2	Displacement of center of gravity of the tibia in x-direction

1 Introduction

Automobiles have been indispensable to people's lives in industrialized societies. The World Health Organization (WHO) reported that, in the near future, road traffic injuries will become the third leading contribution to the global burden of disease (World Health Organization, 2004). The Institute for Traffic Accident Research and Data Analysis (ITARDA) reported that vulnerable road users accounted for a significant proportion of road accident fatalities (ITARDA, 2008). A combination of road engineering, vehicle design, and enforcement by laws is one of the best-suited approaches to reduce the number of injuries caused to vulnerable road users. However, vehicle-to-pedestrian collisions will remain a frequent problem in most countries for the foreseeable future. Currently, research on effective countermeasures to reduce the number of pedestrian fatalities is attracting considerable interest.

1.1 Review of literatures on pedestrian safety research

Although research on pedestrian safety has been conducted since the 1960s (Severy et al., 1966), the safety of pedestrians was not a major consideration in vehicle design until the 1980s. Public interest in the New Car Assessment Program (NCAP) and the regulation of vehicle design for the safety of pedestrians are currently prevalent. Literatures on pedestrian safety research published after 1980 are reviewed in this section.

1.1.1 Statistical distribution of pedestrian

The pedestrian safety working group of the International Harmonized Research Activities (IHRA) collected data on the recent pedestrian accidents that occurred in Australia, Europe, Japan, and the USA in a common format (Mizuno, 2005). This dataset provided information on 1605 pedestrian accidents, 9463 injuries, 6158 abbreviated injury scale 1 (AIS1) injuries, and 3305 AIS2-6 injuries. Mizuno discussed the distribution of the pedestrian injury, injury risk as a function of age, and vehicle impact speed (see Table 1.1). The distribution of the AIS2-6 pedestrian injuries sustained by adults and children, categorized in terms of each body part, is summarized in Table 1.2. The injuries to the head and the legs accounted for one-third of the AIS2-6 injuries. The distribution of injury severities of pedestrians in the above mentioned four

countries is shown in Figure 1.1. Approximately 70% of the injuries were rated as maximum AIS (MAIS) 1-2 injuries; further, approximately 20% and 10% of the injuries were rated as MAIS3-4 and MAIS5-6 injuries, respectively.

Table 1.1
Injuries Categorized by the Country and Frequency; Adapted from Mizuno (2005)

Region	Cases	Injuries	AIS1	AIS2-6
Australia	65	345	182	163
Germany	782	4056	2616	1440
Japan	240	883	523	360
USA	518	4179	2837	1342
Total	1605	9463	6158	3305

Table 1.2
Distributions of AIS2-6 Pedestrian Injuries in the USA, Germany, Japan, and Australia; Adapted from Mizuno (2005)

Body region	USA	Germany	Japan	Australia	Total
Head	32.70%	29.90%	28.90%	39.30%	31.40%
Face	3.70%	5.20%	2.20%	3.70%	4.20%
Neck	0.00%	1.70%	4.70%	3.10%	1.40%
Chest	9.40%	11.70%	8.60%	10.40%	10.30%
Abdomen	7.70%	3.40%	4.70%	4.90%	5.40%
Pelvis	5.30%	7.90%	4.40%	4.90%	6.30%
Arms	7.90%	8.20%	9.20%	8.00%	8.20%
Legs	33.30%	31.60%	37.20%	25.80%	32.60%
Unknown	0.00%	0.40%	0.00%	0.00%	0.20%
Total	100%	100%	100%	100%	100%

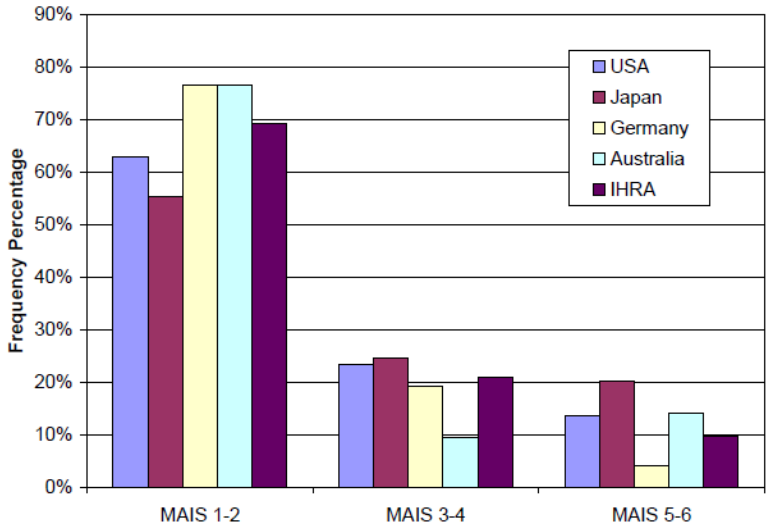

Figure 1.1. Distribution of injury severities of pedestrians; adapted from Mizuno (2005).

The distribution of the AIS2-6 pedestrian injuries sustained by adults and children, categorized in terms of the body part and the vehicle contact point, is summarized in Table 1.3. Out of the injuries sustained by both the adults and the children by the front bumper of the vehicle, 3% were caused to the head and 68% were caused to the lower leg (see Table 1.3). The distribution of the pedestrian injuries, categorized in terms of the body part and vehicle contact point for the adults as a function of the body part and the striking vehicle component, is summarized in Table 1.4. Out of the injuries sustained by the adults by the front bumper of the vehicle, 3% were caused to the head and 71% were caused to the lower leg (see Table 1.4). The distribution of pedestrian injuries, categorized in terms of the body part and Vehicle Contact Point for children as a function of the body part and the striking vehicle component, is summarized in Table 1.5. Out of the injuries sustained by children by the front bumper of a vehicle, 4% were caused to the head, 47% were caused to the lower leg, and 30% were caused to the femur (see in Table 1.5). From the database of information on pedestrian injuries complied by the IHRA, it can be inferred that the front bumper was the most frequent source of vehicle contact and that the lower leg was the most frequently injured body part of a pedestrian.

Table 1.3
Pedestrian Injuries Categorized by the Body Part and Vehicle Contact Point–All Age Groups; AIS2-6; Adapted from Mizuno (2005)

	Head	Face	Neck	Chest	Abdo-men	Pelvis	Arms	Legs					Un known-	Total
								Overall	Femur	Knee	Lower leg	Foot		
Front bumper	24	2	0	3	5	3	6	19	59	76	476	31	1	705
	3%	0%	0%	0%	1%	0%	1%	3%	8%	11%	68%	4%	0%	100%
Top surface of bonnet/wing	223	15	2	139	44	43	86	23	3	1	1	2	1	583
	38%	3%	0%	24%	8%	7%	15%	4%	1%	0%	0%	0%	0%	100%
Leading edge of bonnet/wing	15	2	4	43	78	85	35	50	40	6	30	1	0	389
	4%	1%	1%	11%	20%	22%	9%	13%	10%	2%	8%	0%	0%	100%
Windshield glass	344	56	12	30	5	12	23	2	0	0	1	1	1	487
	71%	11%	2%	6%	1%	2%	5%	0%	0%	0%	0%	0%	0%	100%
Windshield frame /A pillar	168	28	5	35	7	14	31	5	1	0	0	0	2	296
	57%	9%	2%	12%	2%	5%	10%	2%	0%	0%	0%	0%	1%	100%
Front Panel	5	1	0	9	13	7	6	9	14	11	35	3	0	113
	4%	1%	0%	8%	12%	6%	5%	8%	12%	10%	31%	3%	0%	100%
Others	45	7	1	38	12	13	15	15	9	5	39	18	0	217
	21%	3%	0%	18%	6%	6%	7%	7%	4%	2%	18%	8%	0%	100%
Total	824	111	24	297	164	177	202	123	126	99	582	56	5	2790
	30%	4%	1%	11%	6%	6%	7%	4%	5%	4%	21%	2%	0%	100%

Table 1.4
Pedestrian Injuries Categorized by the Body Parts and Vehicle Contact Point–Adults (Age > 15); AIS2-6; Adapted from Mizuno (2005)

	Head	Face	Neck	Chest	Abdo-men	Pelvis	Arms	Legs					Un known-	Total
								Overall	Femur	Knee	Lower leg	Foot		
Front bumper	20	2	0	2	3	3	3	16	29	69	429	29	0	605
	3%	0%	0%	0%	0%	0%	0%	3%	5%	11%	71%	5%	0%	100%
Top surface of bonnet/wing	140	9	1	122	39	35	73	21	3	1	1	2	1	448
	31%	2%	0%	27%	9%	8%	16%	5%	1%	0%	0%	0%	0%	100%
Leading edge of bonnet/wing	7	2	1	36	65	80	28	46	33	5	24	1	0	328
	2%	1%	0%	11%	20%	24%	9%	14%	10%	2%	7%	0%	0%	100%
Windshield glass	303	52	11	28	3	10	22	1	0	0	1	1	0	432
	70%	12%	3%	6%	1%	2%	5%	0%	0%	0%	0%	0%	0%	100%
Windshield frame /A pillar	159	28	5	34	7	14	29	5	1	0	0	0	2	284
	56%	10%	2%	12%	2%	5%	10%	2%	0%	0%	0%	0%	1%	100%
Front Panel	0	1	0	8	13	6	5	9	9	10	32	3	0	96
	0%	1%	0%	8%	14%	6%	5%	9%	9%	10%	33%	3%	0%	100%
Others	33	7	0	29	9	12	11	6	4	5	26	13	0	155
	21%	5%	0%	19%	6%	8%	7%	4%	3%	3%	17%	8%	0%	100%
Total	662	101	18	259	139	160	171	104	79	90	513	49	3	2348
	28%	4%	1%	11%	6%	7%	7%	4%	3%	4%	22%	2%	0%	100%

Table 1.5
Pedestrian Injuries Categorized by the Body Parts and Vehicle Contact Point–Children (Age < 16); AIS2-6; Adapted from Mizuno (2005)

	Head	Face	Neck	Chest	Abdo-men	Pelvis	Arms	Legs					Un known-	Total
								Overall	Femur	Knee	Lower leg	Foot		
Front bumper	4	0	0	1	2	0	3	3	30	7	47	2	1	100
	4%	0%	0%	1%	2%	0%	3%	3%	30%	7%	47%	2%	1%	100%
Top surface of bonnet/wing	83	6	1	17	5	8	13	2	0	0	0	0	0	135
	61%	4%	1%	13%	4%	6%	10%	1%	0%	0%	0%	0%	0%	100%
Leading edge of bonnet/wing	8	0	3	7	13	5	7	4	7	1	6	0	0	61
	13%	0%	5%	11%	21%	8%	11%	7%	11%	2%	10%	0%	0%	100%
Windshield glass	41	4	1	2	2	2	1	1	0	0	0	0	1	55
	75%	7%	2%	4%	4%	4%	2%	2%	0%	0%	0%	0%	2%	100%
Windshield frame /A pillar	9	0	0	1	0	0	2	0	0	0	0	0	0	12
	75%	0%	0%	8%	0%	0%	17%	0%	0%	0%	0%	0%	0%	100%
Front Panel	5	0	0	1	0	1	1	0	5	1	3	0	0	17
	29%	0%	0%	6%	0%	6%	6%	0%	29%	6%	18%	0%	0%	100%
Others	12	0	1	9	3	1	4	9	5	0	13	5	0	62
	19%	0%	2%	15%	5%	2%	6%	15%	8%	0%	21%	8%	0%	100%
Total	162	10	6	38	25	17	31	19	47	9	69	7	2	442
	37%	2%	1%	9%	6%	4%	7%	4%	11%	2%	16%	2%	0%	100%

Results of the analysis of the injury level in terms of the age group are shown in Figure 1.2. From this figure, it can be inferred that children aged 15 and younger tend to suffer from a greater number of AIS1 and AIS2 (35%) injuries than adults. Further, adults aged 61 and older suffer from the highest number of moderate and serious injuries (approximately 30%).

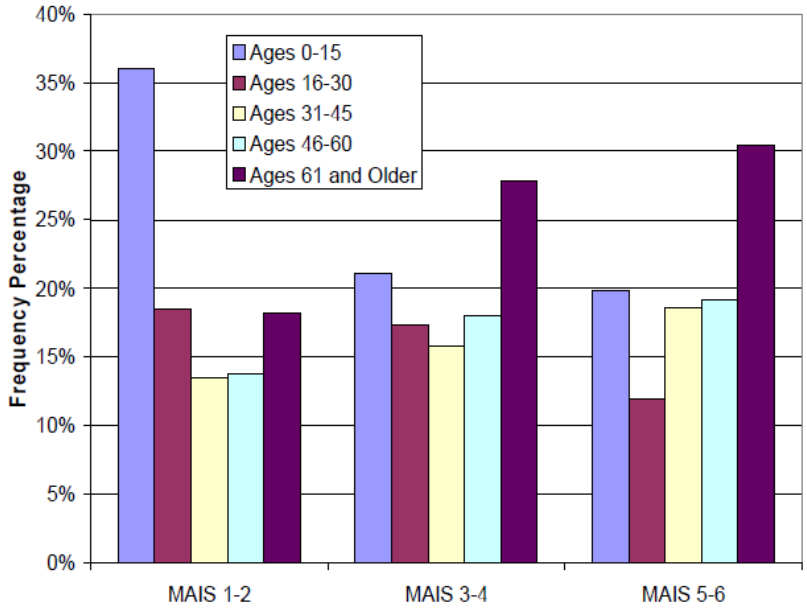

Figure 1.2. Pedestrian injuries as functions of age and injury severity; adapted from Mizuno (2005).

The cumulative frequency of the impact velocities on a per case basis for each country is shown in Figure 1.3. From this figure, it can be observed that the USA shows a larger percentage of injuries at lower velocities than the other three countries. Further, age classifications were grouped as children (age 15 years and younger) and adults (age 16 years and older). All the body parts were included for both the children and the adults in Figure 1.4, with distributions shown for MAIS2-6 and MAIS3-6 injuries. The distinction of injury distribution between the children and the adults was evident in this figure. In most cases, the children were injured at slightly lower impact velocities than the adults. Head injury distributions are shown in Figure 1.5. In the case of adults, the distributions of MAIS3-6 and MAIS4-6 injuries were almost identical, and the MAIS2-6 injuries were distributed at lower velocities. In the case of children, a similar distinction was observed between the MAIS2-6, 3-6, and 4-6 injury curves, and the distributions roughly showed the relationship between the injury severity and the impact velocity. The distributions of leg injuries sustained by children and adults are shown in Figure 1.6. As compared with the head injuries, the severity of leg injuries was less affected by the impact velocity. Children suffered from leg injuries at lower velocities than adults did. The number of traffic accidents and fatalities occurring as a result of traffic accidents in Japan has decreased since 2004 up to 2007, (see Figures 1.7 and 1.8).

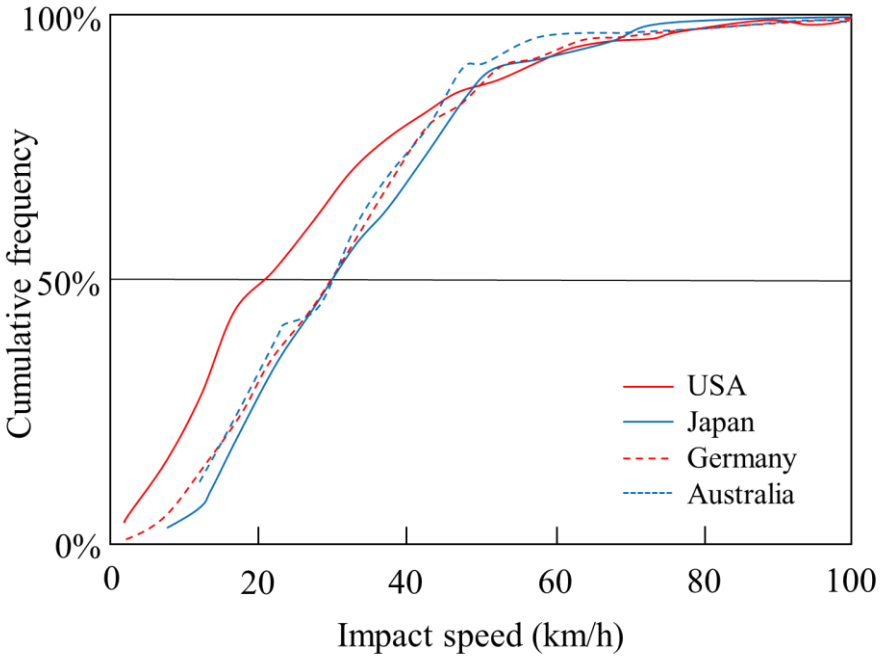

Figure 1.3. Cumulative frequency of vehicle impact speed for pedestrian injury accidents in the USA, Japan, Germany, and Australia; adapted from Mizuno (2005).

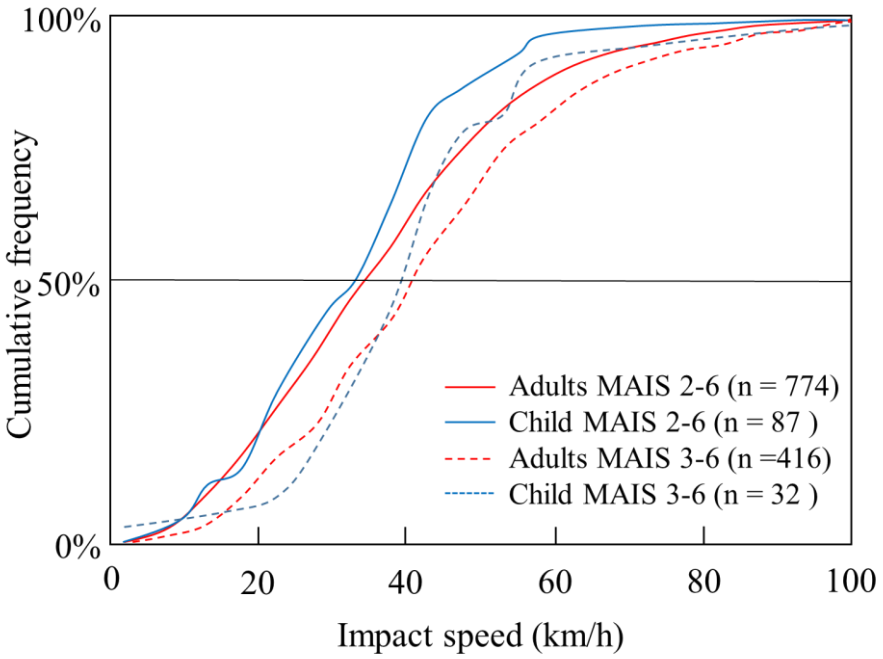

Figure 1.4. Impact velocities by MAIS level–All body parts; adapted from Mizuno (2005).

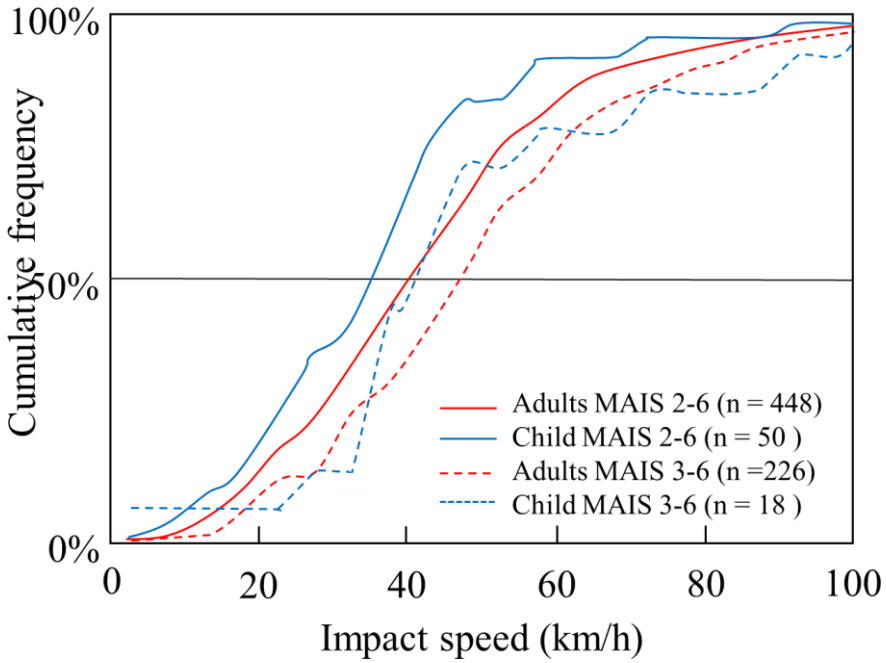

Figure 1.5. Impact velocities by MAIS level–Head injuries; adapted from Mizuno (2005).

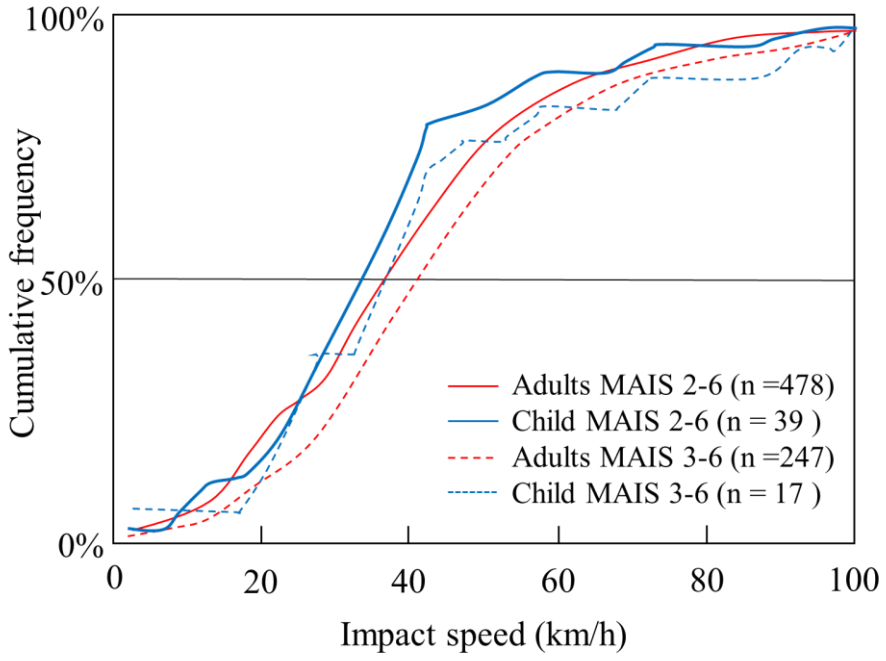

Figure 1.6. Impact velocities by MAIS level–Leg injuries; adapted from Mizuno (2005).

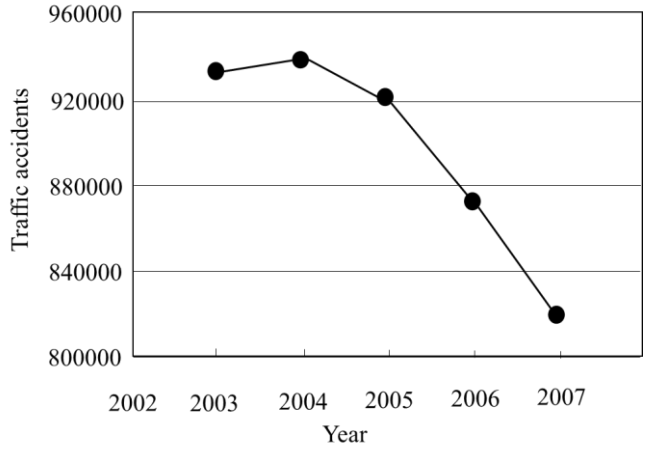

Figure 1.7. Trend in the number of traffic accidents occurring in Japan (ITARDA, 2008).

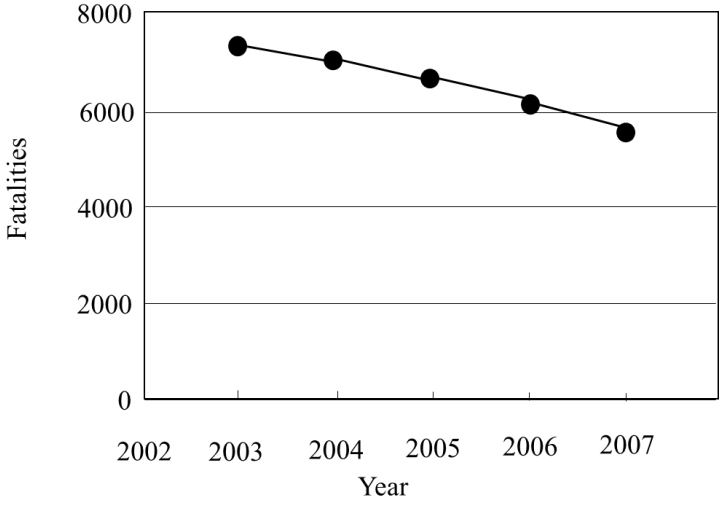

Figure 1.8. Trend in the number of traffic fatalities occurring in Japan (ITARDA, 2008).

The number of fatalities occurred as a result of traffic accidents in Japan in 2007 was 5,744, of which 30% were pedestrians. Out of all the injuries sustained by pedestrians, 17% were serious injuries, 58% were head injuries, and 37% were injuries caused to the lower extremity, which was found to be the most frequently injured body part. Vehicle-to-pedestrian collisions remained a frequent problem in Japan.

Out of the total number of fatalities that occurred as a result of traffic accidents of pedestrians in Japan, 74% occurred as a result of pedestrians crossing streets (see Table 1.6); 70% occurred as a result of traffic accidents of pedestrians who were older than sixty-five years of age (see Table 1.6); and 57% occurred as a result of traffic accidents of pedestrians crossing streets, along with severe injuries (see Table 1.7).

These statistics of traffic accident data indicated that the injuries sustained by pedestrians crossing streets were high priority in this research area.

Table 1.6
Fatalities Occurred as a Result of Traffic Accidents of Pedestrians in Japan; Adapted from ITARDA (2008)

Age	0-6	7-12	13-15	16-18	19-24	25-29	30-49	50-64	65-74	75-	Sub total	Frequency
Facing	0	1	1	0	1	1	4	11	11	28	58	3%
Back	2	0	1	0	3	3	18	21	35	58	141	7%
Crossing	19	14	5	0	15	15	89	186	349	713	1405	74%
Others	9	4	1	2	9	11	50	71	67	66	290	15%
Sub total	30	19	8	2	28	30	161	289	462	865	1894	100%
Frequency	2%	1%	0%	0%	1%	2%	9%	15%	24%	46%	100%	100%

Table 1.7
Fatalities and Severe Injuries Occurred as a Result of Traffic Accidents of Pedestrians in Japan; Adapted from ITARDA (2008)

Age	0-6	7-12	13-15	16-18	19-24	25-29	30-49	50-64	65-74	75-	Sub total	Frequency
Facing	176	364	125	130	256	275	1120	870	610	547	4473	6%
Back	142	335	189	190	507	416	1757	1455	1164	1057	7212	10%
Crossing	3435	5664	1003	879	2157	1925	7434	7420	6579	6887	43383	57%
Others	1651	1926	295	353	1322	1289	4768	3731	2737	2557	20629	27%
Sub total	5404	8289	1612	1552	4242	3905	15079	13476	11090	11048	75697	100%
Frequency	7%	11%	2%	2%	6%	5%	20%	18%	15%	15%	100%	100%

The IHRA reported the parts of the body sustaining AIS2+ injuries caused by pedestrian accidents in Japan (see Figure 1.9), (IHRA, 1998). Between 1993 and 1997, it was found that the AIS2+ injuries of the head, face, neck, and lower leg were the dominant injuries caused by pedestrian accidents in Japan. It was also found that the proportion AIS2+ injuries of the femur and knee caused by pedestrian accidents in Japan was less than that of the AIS2+ injuries that occurred between 1987 and 1988. This decrease in the proportion of the AIS2+ injuries of the femur and knee occurred within a span of ten years, suggesting that changes in the stiffness and shape of the front end of a vehicle may have an impact on the frequency distribution of injuries caused by pedestrian accidents.

The National Police Agency reported that in the case of the AIS2+ injuries caused by pedestrian accidents in 2008, the legs, arms, and head of the pedestrians were the most affected, and in the case of fatal injuries caused by pedestrian accidents in 2008,

the head and chest of the pedestrians were the most affected (see Figure 1.10). Changes in the stiffness and shape of the front end of a vehicle may change the frequency distribution of injuries caused by pedestrian accidents. Tests using postmortem human subjects (PMHSs) for reconstructing vehicle-pedestrian accidents published in the 2000s are reviewed to clarify the effects of a change in the frequency distribution of injuries caused by pedestrian accidents.

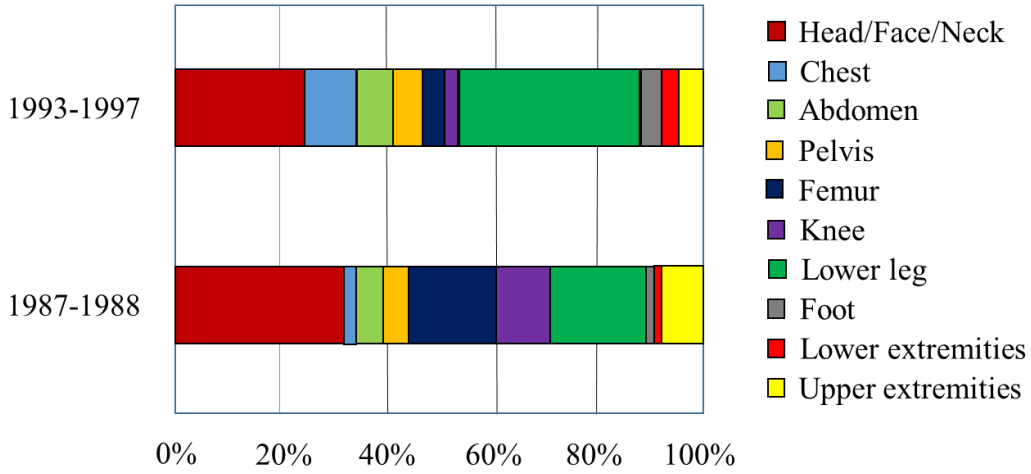

Figure 1.9. Body parts sustaining AIS2+ injuries in pedestrian accidents in Japan (IHRA, 1998).

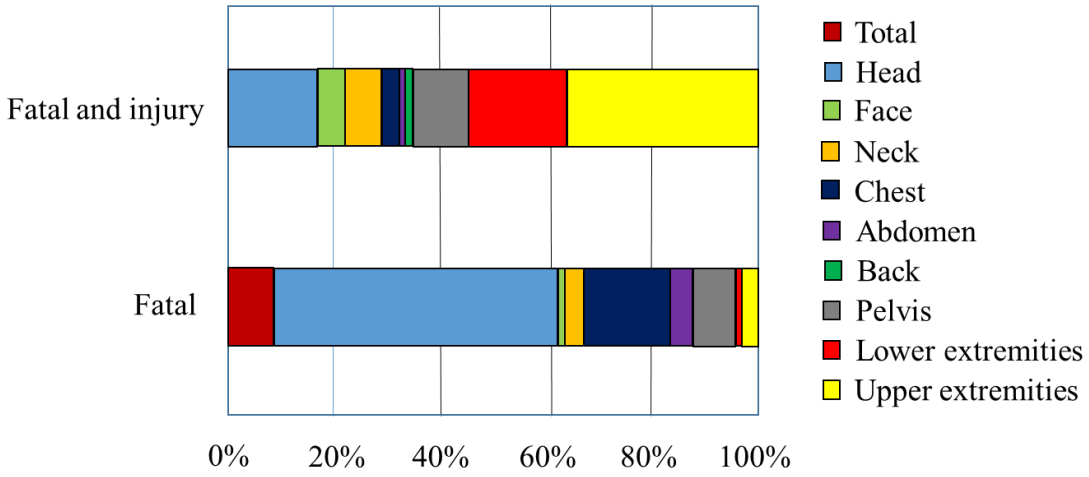

Figure 1.10. Body parts sustaining AIS2+ injuries in pedestrian accidents in Japan in 2008 (National Police Agency, 2009).

1.1.2 Distribution of pedestrian injury by impact test of full-body PMHS

Three technical papers were available for reconstructing vehicle-pedestrian accidents. These papers were written by Snedeker et al. (2005), Schroeder et al. (2008), and Subit et al. (2008) and are currently being reviewed to conduct research on the impact of vehicles sold in the market in the 2000s on the frequency distribution of injuries sustained by pedestrians.

PMHS tests by Snedeker et al. (2005)

Snedeker et al.'s paper (Snedeker et al. , 2005) was reviewed first. From the results of their study, the physical representations of the simulated vehicle shapes were found to have an effect on the PMHSs at 40 km/h. Further, the trials conducted using the PMHSs were referred as to T1, T2, T3, T4, and T5 in their paper (see Figure 1.11). Lower leg fracture occurred in trials T1, T2, T4, and T5 (see Table 1.8). Pelvic injuries occurred in trials T2, T4, and T5. These injuries occurred in similar body parts as those sustaining the AIS2+ injuries occurring in pedestrian accidents in Japan, as reported by the National Police Agency (National Police Agency, 2009), (see Figure 1.10). The physical representations of the simulated vehicle shapes were similar to the vehicles sold in the market in 1996, 1997, and 1998. Further, these representations were not as deformable as were the physical vehicles, and the effects of a low degree of deformation of the front end of a vehicle on the pedestrian injury were not certain in their study.

Figure 1.11. Lateral view of the vehicle geometries and relative postures of the PMHSs; adapted from Snedeker et al. (2005).

Table 1.8
Lower Extremity Injuries Based on the Vehicle Geometry, Age, Pedestrian Stature, and Bone Quality; Adapted from Snedeker et al. (2005)

Test No.	T1	T2	T3	T4	T5
Hood radius (mm)	250	250	50	250	50
Age (Years)	52	76	35	76	78
Hood height (% of hip height)	97	91	83	100	96
Bone quality	Good	Poor	Good	Poor	Poor
Lower leg fracture	Yes	Yes	No	Yes	Yes
Pelvic ramus fracture	No	Yes	No	Yes	Yes
Pelvic acetabulum fracture	No	No	No	Yes	Yes
Femur shaft fracture	No	No	No	No	No

PMHS tests by Schroeder et al. (2008)

Schroeder et al.'s paper (Schroeder et al., 2008) was reviewed next. In their study, impact tests were performed on the entire body of a pedestrian PMHS using a sport-utility vehicle (SUV) and a minivan. The four test trials performed in their study were referred to as HJ1, HJ2, HJ3, and HJ4. Test trials HJ1 and HJ2 involved SUV-to-pedestrian impacts, and test trials HJ3 and HJ4 involved minivan-to-pedestrian impacts (Table 1.9). The kinematics observed in these tests is shown in Figure 1.12. From this figure, it is observed that the lower legs of the pedestrian were the first to come in

contact with the test vehicles. Further, the lower legs remained in contact with the lower bumper absorber for 100 ms. While the knee-joint ligaments ruptured in test trials HJ1, HJ2, and HJ3, the lower leg bone did not fracture in test trials HJ1, HJ2, and HJ4 (see Tables 1.11 and 1.12). The SUV and minivan used in the test trials were purchased in 2005, and the shape and stiffness of their front ends were identical to those of the SUVs and minivans sold in the market in 2005.

Table 1.9
Vehicle Size and Vehicle Weight; Adapted from Schroeder et al.(2008)

Vehicle		SUV	Mini-van
		HJ1, HJ2	HJ3, HJ4
Bumper height ,top (EEVC,1998)	(mm)	658	631
Bumper protrusion	(mm)	163	121
Hood leading edge (EEVC,1998)	(mm)	907	888
Hood length	(mm)	861	493
Hood inclination	(degree)	9	14
Windshield inclination	(degree)	38	40
Vehicle body mass	(kg)	810	803

Table 1.10
Experimental Condition and Subject Information; Adapted from Schroeder et al. (2008)

Test No.		SUV		Mini-Van	
		HJ1	HJ2	HJ3	HJ4
Collision speed	(km/h)	40	40	40	40
PMHS-height	(cm)	165	185	171	171
PMHS-weight	(kg)	60	85	80	61
PMHS-gender		Male	Male	Male	Male
PMHS-age	(years)	80	84	80	70
PMHS-bone mineral density	(BMD)	66	86	49	89

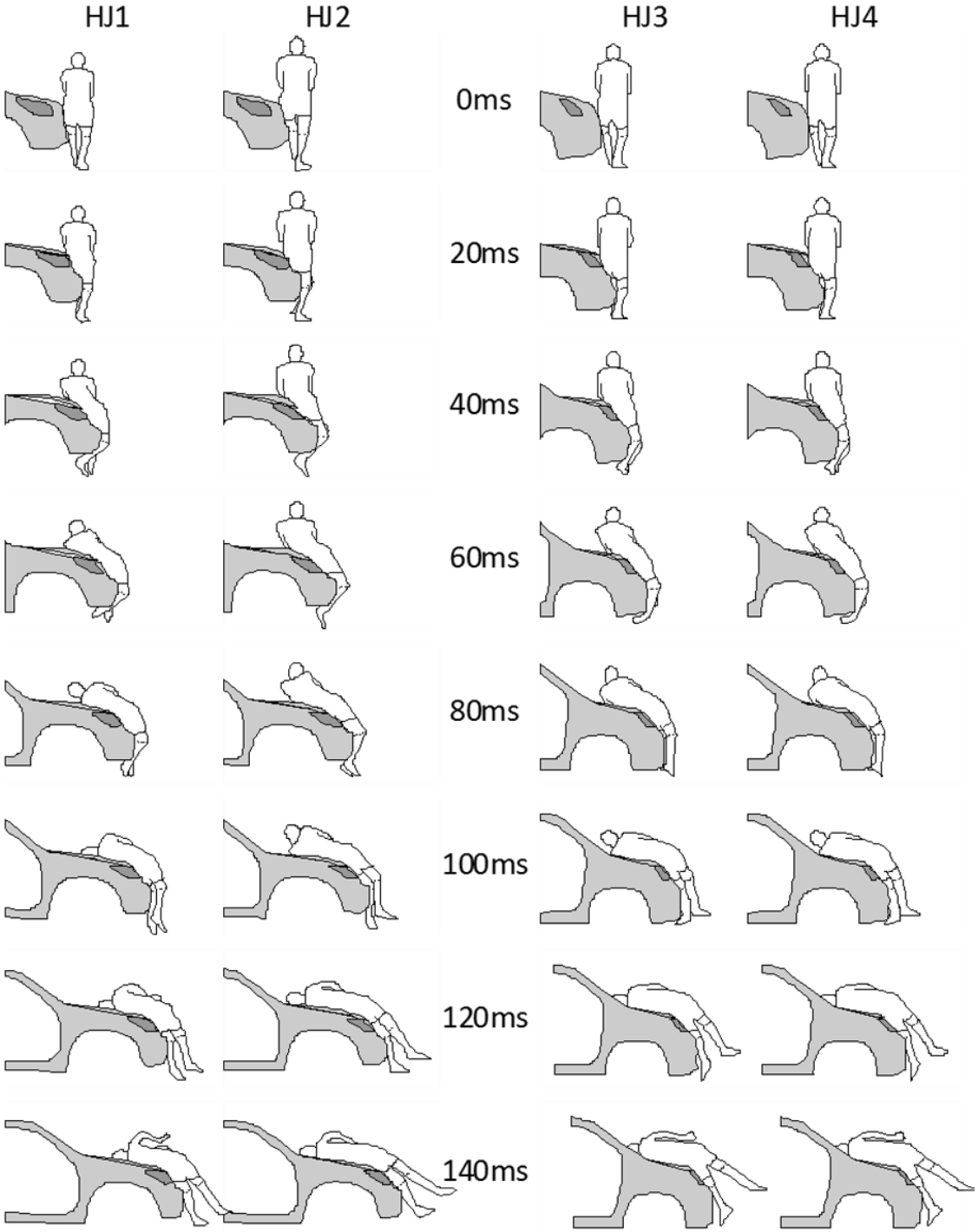

Figure 1.12 Kinematics of the pedestrian PMHS impacted by an SUV (HJ1 and HJ2 test trials) and a minivan (HJ3 and HJ4 test trials); adapted from Schroeder et al. (2008).

Table 1.11
Injuries Sustained by the Pedestrian PMHS after Colliding with an SUV; Adapted from Schroeder et al. (2008)

Test	Part	Detail
HJ1	Left knee	MCL - avulsion of superficial of tibial insertion
		Posterior medial capsule rupture
	Pelvis (left ring)	Anterior pelvic ring fracture including the superior and interior pubic ramus fractures
	Left arm	Abrasion on the forearm
HJ2	Head	Abrasion on the face
	Left knee	Rupture of deep part of the MCL, which is connected to the medial meniscus
		ACL - avulsion of femoral insertion
		MCL - avulsion of tibial insertion
	Pelvis (left ring)	Anterior pelvic ring fracture of inferior pubic ramus
		Anterior pelvic ring fracture of iliopubic eminence
	Left hand	Abrasion on the hand
	Left arm	Abrasion on the forearm
	Rib	Fracture of the 5th and 6th rib at the medio-clavicular line; 120 mm from the center line of the sternum, 130 mm from the center line of the sternum
	Head	Contusion

Table 1.12
Injuries Sustained by the Pedestrian PMHS after Colliding with a Minivan; Adapted from Schroeder et al. (2008)

Test	Part	Detail
HJ3	Left tibia	Tibia wedge fracture
	Left fibula	Fibula transverse fracture
		Fibula transverse fracture below fibula head
	Pelvis (left ring)	Anterior pelvic ring fracture including the superior pubic ramus multi-fragmented fracture and the inferior pubic ramus fracture
	Rib	Fracture of the 5th rib at the medio-clavicular line; 122 mm from the center line of the sternum
	Head	Skull fracture with a length of 15 mm in the vertical direction
HJ4	Right ankle	Elongation of the calcaneofibular ligament
	Left knee	MCL - rupture of superficial layer
		MCL - avulsion of femoral insertion
	Rib	Fracture of the 11th and 12th rib at the middle of the scapula line
	Head	Skull fracture with a length of 75 mm in the vertical direction toward the skull base

PMHS tests by Subit et al. (2008)

Subit et al.'s paper (Subit et al., 2008) was reviewed finally. In their study, impact tests were performed on a pedestrian PMHS using a midsize sedan and a small commuter car. The four test trials performed in their study were referred to as MSS-S, MSS-T, SCC-S, and SCC-T. Test trials MSS-S and MSS-T involved midsize car-to-pedestrian impacts, and test trials SCC-S and SCC-T involved small commuter car-to-pedestrian impacts (see Figures 1.13 and 1.14). Information of the PMHSs are shown in Table 1.13. Bone mineral density of MSS-T is in good condition.

Kinematic of the PMHSs (MSS-T and SCC-T) are shown in Figures 1.14 and 1.15, respectively. The lower legs of MSS-T came in contact with the test cars first as shown in Figure 1.13 (Left) and the thorax and shoulder of MSS-T simultaneously came in contact with the hood of the mid-size sedan as shown in Figure 1.13 (Right). The lower extremities of SCC-T came in contact with the test cars, and the thorax of SCC-T came in contact with impact the windshield glass as shown in Figure 1.14.

While knee injuries occurred in test trials MSS-S, MSS-T, SCC-S, and SCC-T, lower leg injuries occurred in test trials MSS-T and SCC-T (see Tables 1.14 and 1.15). The injuries of the lower extremities are located around the knee joints of the impacted side (Right) and the left knee joint. Injuries of pelvis are mostly multiple lateral compression fracture.

Table 1.13
Experimental Condition and Subject Information; Adopted from Subit et al. (2008)

Test		Mid-size sedan		Small commuter car	
		MSS-S	MSS-T	SCC-S	SCC-T
Collision speed	(km/h)	40	40	40	40
PMHS-height	(cm)	154	183	161	182
PMHS-weight	(kg)	72.6	114	86.2	46.3
PMHS-age	(years)	62	62	64	67
PMHS-bone mineral density	(BMD)	75	98	78	64

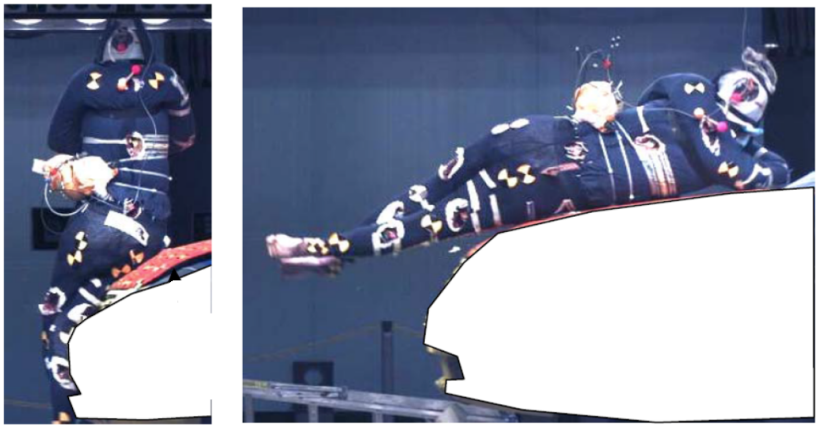

Figure 1.13. Kinematic of the pedestrian PMHS (MSS-T) impacted by the mid-size sedan; adopted from Subit et al. (2008).

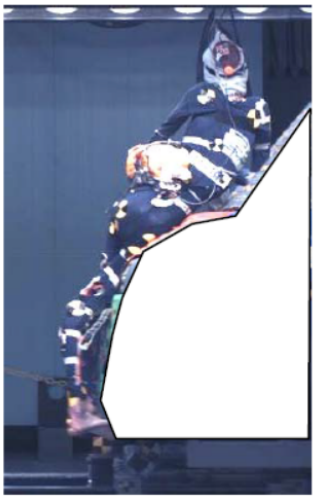

Figure 1.14. Kinematic of the pedestrian PMHS (SCC-T) impacted by the small commuter car, adopted from Subit et al. (2008).

Table 1.14
Injuries of Lower Extremity of the Pedestrian PMHS in the Cases of Mid-size sedan; Adopted from Subit et al. (2008)

Test	Part	Detail
MSS-S	Right knee (Impacted side)	Osteochondral avulsion and fracture of medial tibia plateau
		Tear of insertion of medial collateral ligament and femur
		Osteochondral avulsion and fracture of lateral tibia plateau
		Complete tear of anterior cruciate ligament
	Left knee	Osteochondral avulsion and fracture of lateral tibia plateau
	Pelvis	Multiple lateral compression fracture of pelvis
MSS-T	Left knee	Avulsion and fracture of left lateral tibia plateau
		Comminuted fracture of fibular head
		Avulsion and fracture of fibular insertion of lateral collateral ligament
	Left ankle	Avulsion and fracture of anterior Talo-Fibular from fibula with bone piece
	Pelvis	Multiple lateral compression fracture of pelvis

Table 1.15
Injuries of Lower Extremity of the Pedestrian PMHS in the Cases of the Small City-car; Adopted from Subit et al. (2008)

Test	Part	Detail
SCC-S	Right knee	Rupture of medial collateral ligament at femur insertion
SCC-T	Right knee	Avulsion and rupture of medial collateral ligament at femur insertion
	Right tibia	Complex oblique fracture of tibia
	Right fibula	Comminuted fracture of fibula neck
		Spiral fracture of fibula
	Left knee	Avulsion and fracture of fibula head at lateral collateral ligament insertion
		Incomplete fracture of medial tibia condyle
	Pelvis	Multiple lateral compression fracture of pelvis (Bilateral)

1.2 Differences in the pedestrian injuries based on the statistical database and the full-body PMHS impact test

Differences were observed in the injuries sustained by a pedestrian PMHS, as found from the results of the impact tests performed by Snedeker et al. (2005), Schroeder et al. (2008), and Subit et al. (2008).

In the impact tests performed by Snedeker et al. (2005), the pedestrian PMHS was found to mostly suffer from bone fractures of the lower extremities. However, in the impact tests performed by Schroeder et al. (2008) and by Subit et al. (2008), the pedestrian PMHS was found to mostly suffer from the rupture of the knee-joint ligaments. Snedeker et al. (2005) used physical representations of the simulated vehicle shapes whose degree of deformation was lower than that of a physical vehicle. Schroeder et al. (2008) and Subit et al. (2008) used a physical representation of a simulated vehicle with a body in white along with a bumper and a hood; the deformation of this representation was similar to that of the physical vehicles sold in the market. This difference in the location of injuries in these tests suggests that a low degree of deformation of the front end structure of a vehicle increases the risk of occurrence of a fracture of the lower leg bone and that a high degree of deformation of the front end structure of a vehicle increases the risk of the rupture of the knee joint ligaments.

The statistics of the body parts sustaining AIS2+ injuries in pedestrian accidents, as reported by IHRA (1998), although indicated a low risk of knee injuries, the injuries that occurred during the impact tests performed by Schroeder et al. (2008) and by Subit et al. (2008) were mostly knee injuries. This difference in the location of injuries in these laboratory tests and the statistical data suggest that the deformation of the front end of a vehicle manufactured in 1997 and 2006 may have impacted the change in the frequency distribution of injuries sustained by pedestrians involved in accidents.

From the results of the review of the researches on the tests involving the reconstruction of pedestrian accidents using full-body PMHSs, the knee injuries were found to be the most frequently occurring injuries in all the impact tests performed on pedestrian PMHSs using a physical vehicle sold in the market in around 2005; further, it was found that suitable physical representations with a similar shape and degree of

deformation to the vehicles sold in the market are required to reconstruct a pedestrian accident in order to accurately evaluate the knee joint and lower leg injuries. The relationship between the risk of a knee-joint injury and that of a lower leg injury during a pedestrian accident depends on various factors pertaining to the vehicle involved in the accident, such as the year in which the vehicle was manufactured and the type of vehicle such as a sedan, an SUV, a minivan, and a commuter car. It is essential to develop a new method that can investigate the relationship between injuries such as knee-joint injuries and lower leg injuries and characteristics such as the shape and stiffness of the front end of a vehicle in order to understand the mechanism of occurrence of these injuries in vehicle-pedestrian accidents.

1.3 Methods for reconstructing injuries occurring in pedestrian accidents

Methods for reconstructing injuries occurring in pedestrian accidents, presented in the literatures since 1982, were reviewed; from this review, it was found that six methods in particular, such as a PMHS test, full-scale dummy test, lower legform impactor test, multibody dynamics simulation, a finite element (FE) model of a full scale-dummy, and an FE model of all the pedestrians, were predominantly presented in the literatures. This section discusses the manner in which each of these methods reconstructs injuries occurring in pedestrian accidents.

1.3.1 PMHS tests

Brun-Casssan et al. (1983) performed a PMHS test, the aim of which was to obtain insights into the mechanisms causing injuries in pedestrian accidents by determining the human tolerance and the corresponding safety criteria using dummies. In the reconstruction experiments, the injuries resulting from the actual accidents were compared with the data measured on dummies and the PMHSs.

Backaitis et al. (1983) performed a PMHS test, as well. In their test, seven PMHS specimens in the standing posture were impacted by two vehicles moving at a speed of 40 km/h. One of these vehicles had a steel bumper, and the other vehicle had a plastic bumper. Two mathematical pedestrian models named MVMA-2D and MAC-DAN were employed to simulate pedestrian impacts at 40 km/h by a vehicle with a stylized geometry that was similar to that of the vehicles used in the PMHS tests. A comparison between the results of the simulations and the PMHS tests showed that both the above

mentioned mathematical pedestrian models require further refinement to more accurately simulate the kinematics of the lower legs during impacts with a vehicle bumper.

Cavallero et al. (1983) also performed a PMHS test. In their test, the consequences of the impact of different types of vehicles on PMHSs were compared; here, the vehicles were assumed to move at a constant speed of 32 km/h. Further, the vehicles used in their test were similar. It was difficult to assess the differences in the injury consequences as well as the impact kinematics using vehicles with differences in their mass, profile, bonnet length, and the position and shape of their front bumper.

Kajzer et al. (1997) conducted a study on the shearing and bending effects at the knee joint when it is subjected to high speed lateral loading (see Figures 1.15 and 1.16). The objective of their tests was to determine the damage tolerance and to clarify the damage mechanisms of the extended human knee when it was subjected to lateral impact loads in vehicle-pedestrian accidents occurring at a high velocity of 40 km/h. They also conducted in-vitro experiments using a PMHS, where only the purest possible shearing deformation or the purest possible bending deformation affected the knee region. Further, they performed ten experiments at a velocity of 40 km/h in a shearing and bending setup. The peak values of the shearing force and the bending moment related to the damage of the knee-joint ligaments as well as the bone fractures were calculated at the knee-joint level.

Kajzer et al. (1999) also conducted a study on the shearing and bending effects at the knee joint when it was subjected to low speed lateral loading. The objective of their test was to determine the damage tolerance and to describe the damage mechanisms of the extended human knee when it was subjected to lateral impact loads in vehicle-pedestrian accidents occurring at a low velocity of 20 km/h; the results of this test were compared with those obtained at a high velocity of 40 km/h. They performed five experiments using a shearing and bending setup. The peak values of the shearing force and the bending moment related to the damage of the knee-joint ligaments as well as the bone fractures were calculated at the knee-joint level.

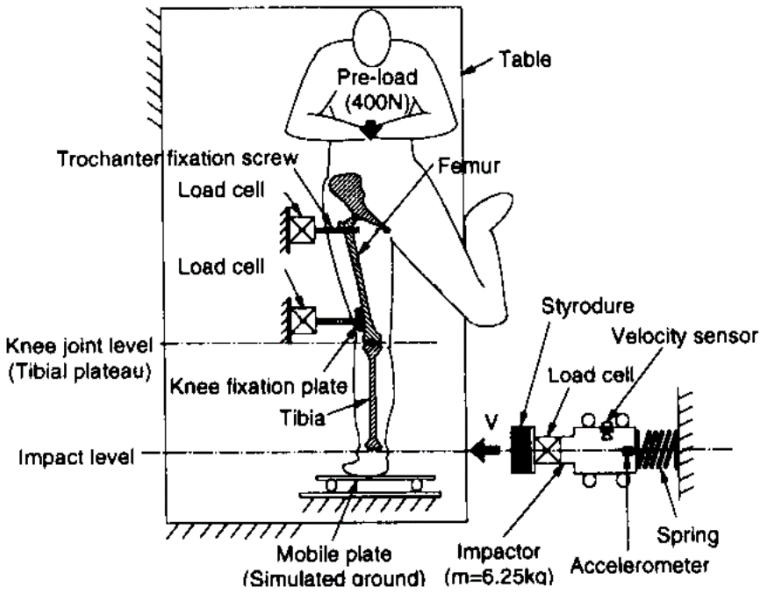

Figure 1.15. Bending test setup using a PMHS; adapted Kajzer et al. (1997).

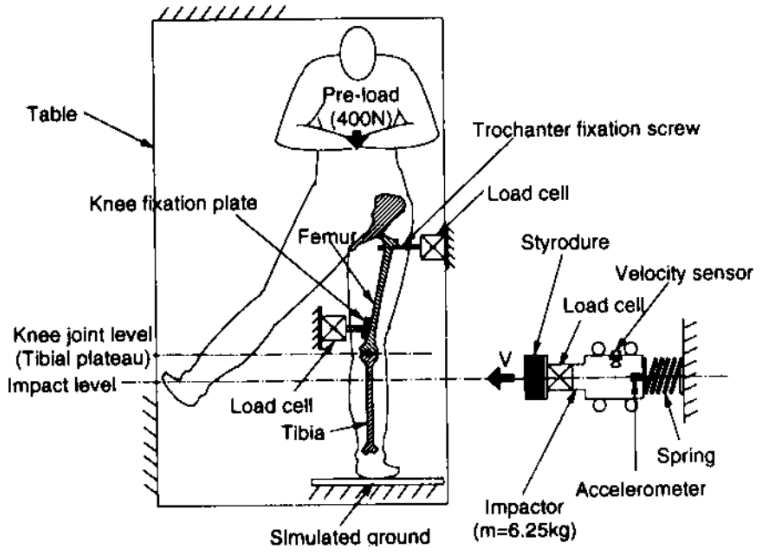

Figure 1.16. Shearing test setup using a PMHS; adapted Kajzer et al. (1997).

Snedeker et al. (2005), Schroeder et al. (2008) and Subit et al. (2008) performed PMHS tests, as described in section 1.1.2.

The PMHS tests reconstructed the kinematics and injuries occurring in vehicle-pedestrians accidents. Although the injury mechanisms and tolerances have been assessed through a PMHS test, the effects of modifying the structure of the front end of

a vehicle for reducing the risk of knee-joint and lower leg injuries sustained by pedestrians could not be examined owing to the lack of repeatability of the test results.

1.3.2 Full-scale dummy tests

A full-scale dummy was developed using Hybrid 3 and EuroSid (Higuchi et al., 1991) for use in pedestrian safety research. This dummy indicated the manner in which the kinematics and the distribution of injuries were affected by the impact velocity, shape of the front end of a vehicle, and pedestrian height. However, a comparison between the responses of a PMHS and the Hybrid 3/EuroSid dummy showed a lack of bio-fidelity of head trajectories. Therefore, a full-scale pedestrian dummy termed Polar was developed by Honda R and D Ltd. and GESAC Inc. (Akiyama et al., 2001), (Okamoto et al., 2003). The kinematics of this dummy was validated with a PMHS test (Takahashi et al., 2005). It was difficult for this dummy to simulate the rupture of the knee-joint ligaments and the fracture of the lower leg bones of a pedestrian (see Figure 1.17).

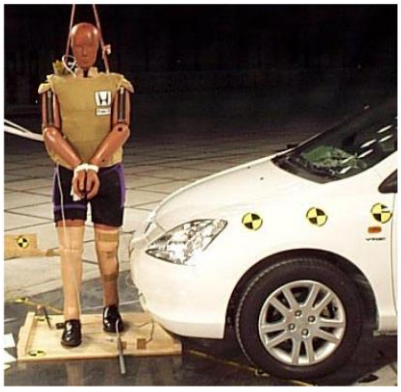

Figure 1.17. Full-scale pedestrian dummy; adapted from Takahashi et al. (2005).

Hood panel and windshield glass sometimes deform a lot in a test by a full-scale pedestrian dummy. This deformation causes consumption of a lot of the testing budget even though for only one test. A full-scale pedestrian dummy was suspended and released just before a vehicle was brought in contact with the full-scale pedestrian dummy. This step sometimes caused insufficient repeatability of the dummy posture at the first impact. To ensure the repeatability of the test procedure, test devices that can assess the risk of injuries to specific human body parts have been developed by researchers (ISO/TC22/SC10/WG2, 1997), (see Figure 1.18).

The Japan New Car Assessment Program (JNCAP) began to assess the pedestrian safety performance in 2003. Initially, only a head safety test was performed; however, another test protocol to assess the lower leg injuries was introduced in 2010. A proposal has also been put forward to integrate a leg test into the Global Technical Regulations (GTR) that is observed as a set of international standards for vehicle safety in various countries around the world (UN/ECE/WP29/GSRP, 2006). This proposal involves the use of a new flexible pedestrian legform impactor (Flex-PLI) that was under development (Konosu et al., 2007). The lower legform impactor used rigid steel components to simulate the femur and the tibia; however, the new impactor used flexible materials to simulate the femur and the tibia (see Figure 1.19). Further, the new impactor used wires to represent the ligaments of the knee joints. The development of the Flex-PLI commenced in 2000 (Wittek et al. , 2001), and a proposal for its final specifications was announced in 2008.

It has also been pointed out that the mass of the pedestrian's upper body has an effect on the leg behavior (Matsui et al. , 2004), which was also thought to be affected by the fact that the legs were inclined inward from the vertical position while walking.

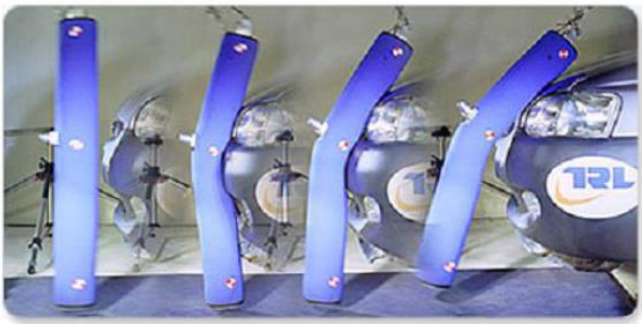

Figure 1.18. Lower legform impactor test.

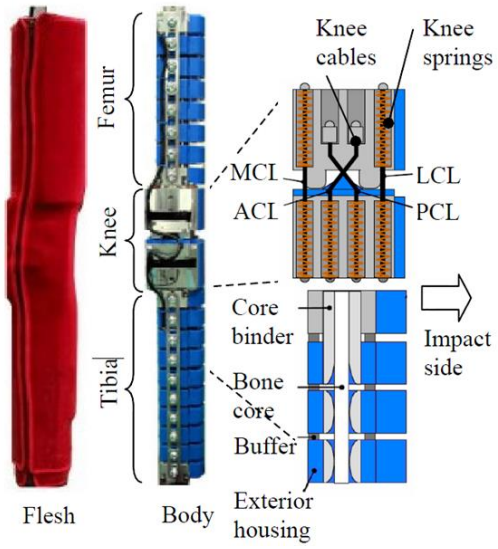

Figure 1.19. Construction of Flex-PLI.

Matsui et al. (2002) impacted Polar with a vehicle and an SUV at a speed of 40 km/h. The results of their experiments using Polar were compared with those obtained using sub-system tests performed according to the EEVC/WG17 procedure. The results of their experiment suggested that the EEVC/WG17 headform and the upper legform test procedures may overestimate the severity of the impact between the front end of a vehicle and the pedestrian's head and pelvis, particularly in the case of SUVs. The lower legform impactor cannot reconstruct the kinematics of a full-scale dummy impacted by a vehicle and can be used only for an American male 50%-ile (AM50%ile) size pedestrian. It is difficult for the lower legform test to simulate ruptures of the knee-joint ligaments and the fracture of the lower leg bones.

1.3.3 Multibody simulations

Research efforts in this field commenced in the 1960s. The most commonly used modeling method during this era was the multibody simulation method which recreated vehicle occupants using rigid body elements with links (McHenry et al., 1963). In the case of a multibody model, major body parts such as the head, torso, and extremities were expressed by ellipsoids, with joints defined from them. Further, a multibody model could simulate the impact behavior of a human body by adjusting the dimensions, mass, and inertia moment of the ellipsoids to those of the relevant body parts, as well by setting the rotational direction and angle of each joint with the same restrictions

applicable to human joints. The multibody model can also be used to predict the mechanical response of an occupant after the model comes in contact with the interior parts or restraint devices when the rigid ellipsoids are replaced with deformable elements. The other advantage of using a multibody model in impact behavior simulations is that it reduces the calculation time. However, a multibody model is not well suited for recreating injuries such as a bone fracture or soft tissue damage.

A wide variety of mathematical models have been applied to the research of pedestrian impact. Out of these models, the most well-known computer program that simulates the multibody dynamics of pedestrians is the mathematical model dynamic model (MADYMO). MADYMO was developed by the Dutch Research Corporation (TNO). The first-published MADYMO pedestrian model was two dimensional (2D) and consisted of two segments (van Wijk et al., 1983).

Yang et al. (1992) developed a three dimensional (3D) pedestrian knee-joint model for computer simulations. This model included the articular surfaces, ligaments, and capsule represented by the ellipsoid and plane elements as well as spring-damping elements, respectively. The mechanical properties of the knee joint were based on the available biomechanical data.

Ishikawa et al. (1993) developed a multibody dynamic simulation model of the entire human body to simulate a pedestrian involved in a road accident with a vehicle. Their objective using this model was to achieve better correlation with the results obtained from the impact tests performed using PMHS specimens by employing the crash victim simulation (CVS) computer program. The responses obtained from their model under various impact scenarios, such as the overall pedestrian behavior, head resultant velocity, and acceleration of the segments, were validated. Konosu reconstructed an actual vehicle-to-pedestrian accident by developing pedestrian and vehicle multibody dynamic numerical models (Konosu, 2002).

Hoof et al. (2003) developed a MADYMO pedestrian model and validated a scalable midsize male pedestrian model. The head kinematics was accurately predicted and indicated with global correlation scores greater than 90%. However, the correlation score for the bumper forces and accelerations of various body parts were lower (47–64%). This difference in the correlation scores was attributed to the limited information available on the vehicle contact characteristics such as its stiffness, damping, and

deformation. This MADYMO pedestrian model could be transformed to that of a 6-year-old (6YO) child pedestrian, an American female 05%-ile (AF05%ile) pedestrian, and an American male 95%-ile(AM95%ile) pedestrian. It was difficult for the MADYMO pedestrian accident simulation to simulate the rupture of the knee-joint ligaments and the fracture of the lower leg bones (Linder et al., 2005), (see Figure 1.20).

Figure 1.20. Simulation of a male pedestrian impacted by a vehicle; adapted from Linder et al. (2005).

1.3.4 Simulations of human FE model

The development of an FE model of a pedestrian has been regarded as the focus of pedestrian impact research for the last ten years. FE models began to be used for the analysis of the vehicle body deformation in the 1980s. It became possible to simulate the deformation modes and force responses accurately by representing the structures of vehicle body panels in an FE model. Moreover, it was also possible to predict whether metal sheets would rupture under the given impact conditions by assuming the stress-strain property up to the rupture point. Despite the fact that the FE simulation generally requires a longer calculation time than the multibody simulation, research using human FE models was an advanced method for predicting the impact behavior and mechanical response. The development of human FE models commenced with the development of component models, such as of FE models of the head or the thorax. Such models were generated on the basis of the commercial databases of human anatomy and anatomical or sectional drawings of the human body. Their material properties were used as input on the basis of the mechanical properties of the body tissues reported in the literature. The validity of a completed model could be verified by comparing the impact response with that of a PMHS.

The full-body human FE models have been developed by combining component models from the head to the lower extremities. Several such models have already been developed, as reported by Choi et al. (1999), Iwamoto et al. (2002), Ruan et al. (2003), Takahashi et al. (2003), and Vezin et al. (2005).

One of these models is the total human model for safety (THUMS), which was jointly developed by Toyota Motor Corporation and Toyota Central Research and Development Laboratory Inc. THUMS has been used in a number of published studies attempting to reproduce injuries occurring in vehicle collisions. THUMS version 1 included a standing pedestrian model and a sitting model of a vehicle occupant, both of which simulated an adult male with an average physique (see Figure 1.21), (Maeno et al., 2001).

Figure 1.21. Pedestrian and occupant of THUMS version 1; adapted from Maeno et al. (2001).

Iwamoto et al. (2002) used THUMS version 1 to simulate an actual traffic accident scenario such as a vehicle colliding with a utility pole and reproduced the injuries suffered by the occupants. Kitagawa et al. (2005) used THUMS version 1 to predict the occupant behavior in a frontal collision in order to study the knee-joint deformation in the case when the knees strike the instrument panel and the effect of airbags in helping to reduce such deformation. Hayashi et al. (2006) and Kuwahara et al. (2008) used THUMS version 1 to simulate vehicle side impact collisions to investigate the mechanism of occurrence of rib fractures and the force-reduction effect of side airbags.

Given that the injuries to the brain and the internal organs generally tend to be more severe than bone fractures or ligament rupture, attempts have also been made to

reproduce such injuries using human FE models. Tamura et al. (2006) used THUMS version 3 featuring a brain to simulate vehicle collisions. This study indicated a high level of strain within the brain immediately before and directly after an impact between the pedestrian's head and the vehicle's hood.

The accuracy of an FE model mainly depends on the geometry description, material law, and contact definition. With regard to the human model geometry, a drastic improvement in medical imaging techniques such as a Visible Human Project (National Library of Medicine, 2008) provided high-definition cross-sectional images of the human body. The geometry description of THUMS version 1 relied on the Visible Human Project. The material law of THUMS version 1 referred static coupon tests data (Yamada, 1970). Only limited test data for determining the dynamic characteristics of the material law were available in the reviewed literatures; additional experimental recording of the tissue strain in human subjects was required for a more detailed validation of the FE models of pedestrians (Maeno et al., 2001). Kinematic joints were generally used in multibody dynamic models; however, the contact definitions of an FE model can cause the contacting surface of the joints of THUMS version 1 to deform while the ligaments and muscle constrain in a manner similar to that applicable to the human body structure.

The kinematics of a pedestrian THUMS version 1 impacted by a vehicle was validated, and the risks of occurrence of bone fractures of the lower legs were evaluated (Maeno et al. , 2001). In their research, the simulation of the rupture of the knee-joint ligaments using THUMS version 1 was not validated. The kinematics of a pedestrian THUMS version 1 impacted by an SUV was also not validated. In this thesis, the knee-joint ligaments of a pedestrian THUMS were modified, and this modified model was used to reconstruct injuries occurring in pedestrian accidents in order to evaluate the relationships between injuries such as the knee-joint and the lower leg injuries and the characteristics of a vehicle such as the shape of its front end and its degree of deformation.

1.4 Objective of the present study

According to a statistical review of the injuries occurring in pedestrian accidents and from the results of the pedestrian PMHS test, it is inferred that the relationships

between the stiffness of the front end of a vehicle and the lower leg injuries should be examined in order to establish means of reducing the number of pedestrian fatalities and the severity of injuries sustained by pedestrians in nonfatal accidents. The objective of the present study is to understand the mechanism of occurrence of the tibia and knee-joint injuries in a pedestrian involved in an accident.

To meet this objective, the following studies are conducted.

Chapter 2 presents a validation of the tibia and knee-joint ligament injuries assessed using an FE model of a human body, with the test data obtained by Schroeder et al. (2008). THUMS version 1 is modified to an accurate size of the PMHS used in the test. The kinematics and the injuries of the modified THUMS version 1 are compared with the test results to validate the accuracies of the kinematics and the injuries.

Chapter 3 presents an assessment of the tibia and knee-joint ligament injuries sustained by a pedestrian impacted by a vehicle. An FE model of the vehicle is established, and the stiffness of this model is compared with the EEVC/WG17 test result to validate the accuracies of the vehicular model. The tibia and knee-joint ligament injuries sustained by an AM50%ile pedestrian, an AF05%ile pedestrian, and a 6YO child pedestrian impacted by a vehicle are assessed by using THUMS version 1. The relationships between the size of a pedestrian and the tibia and knee-joint ligament injuries sustained by the pedestrian are discussed.

Chapter 4 presents a parametric study on the shape and stiffness of a vehicle, as well as discusses their relationships with the tibia and knee-joint ligament injuries sustained by an AM50%ile pedestrian, an AF05%ile pedestrian, and a 6YO child pedestrian. The relationships between injuries such as the tibia and the knee-joint ligament injuries and the shape and stiffness of the front end of the vehicle are examined to minimize the risk of the tibia and knee-joint ligament injuries sustained by an AM50%ile pedestrian, an AF05%ile pedestrian, and a 6YO child pedestrian.

Chapter 5 presents an assessment of the tibia and knee-joint ligament injuries sustained by a pedestrian impacted by an SUV. An FE model of the SUV is established, and the stiffness of this model is compared with the EEVC/WG17 test result to validate the accuracies of the SUV model. The tibia and knee-joint ligament injuries sustained by an AM50%ile pedestrian impacted by the SUV is assessed by using THUMS version

1. The relationships between the kinematics of a pedestrian and the tibia and knee-joint ligament injuries sustained by the pedestrian are discussed.

Chapter 6 presents a parametric study on the shape and the stiffness of the front end of an SUV, as well as discusses their relationships with the tibia and knee-joint ligament injuries sustained by an AM50%ile pedestrian. The relationships between injuries such as the tibia and the knee-joint ligament injuries and the shape and stiffness of the front end of the SUV are discussed to minimize the risk of occurrence of the tibia and knee-joint ligament injuries in an AM50%ile pedestrian.

Chapter 7 compares the leg kinematic behavior of THUMS version 1 with that of the lower legform impactor. The kinematics and the knee-bending angles of the legform impactor are compared with those of THUMS version 1. An interaction between the bending of the tibia and the knee joint of THUMS and the lower legform impactor is discussed. Further, the impact of the bending deformation of the tibia and the femur on the knee-bending angle is clarified.

Chapter 8 presents an analytical study of the leg behavior of the lower legform impactor. The relationships between the knee-bending angle and the position and stiffness the upper bumper absorber are explained by solving an equation of motions of the lower legform impactor. The effect of the lack of bending deformation of the tibia and the femur of the lower legform impactor on the knee-bending angle is discussed.

Chapter 9 presents a general discussion and conclusion on the basis of the results of this thesis.. From the main result of this thesis, the relationships between injuries such as the tibia and the knee-joint ligament injuries and the shape and stiffness of the front end of a vehicle are clarified. The results of this thesis promise to contribute toward the development of new vehicles, with the objective of reducing the number of lower extremity injuries occurring as a result of vehicle-pedestrian accidents across the world.

2 Validation of tibia and knee-joint ligament injuries assessed using human FE model

2.1 Introduction

A human FE model can be used to evaluate the risk of occurrence of a lower leg injury sustained by a pedestrian involved in a vehicle-pedestrian collision. A full-scale pedestrian FE model termed was developed by Toyota Motor Corporation and Toyota Central Research and Development Laboratory and named Total Human Model for Safety (THUMS). THUMS is one of the most well-known human FE models that is used for vehicle safety research in the 2000s.

THUMS is distributed to academic institutes, vehicle manufacturers, and vehicle part suppliers around the world. Provided below is a list of distributors of THUMS for LS-DYNA in 2014:

(1) JSOL Corporation in Japan (http://www.jsol.co.jp/english/)
(2) Livermore Software Technology Corporation in the USA (http://www.lstc.com/)
(3) Ove Arup and Partners in the UK (http://www.oasys-software.com/dyna/en/)
(4) DYNAmore in Germany (http://www.dynamore.de/de/)
(5) DYNAmore Nordic in Sweden (http://www.dynamore.se/)
(6) ALYOTECH TECHNOLOGIES in France (http://www.alyotech.fr/)
(7) Theme Engineering, Inc. in South Korea (http://www.lsdyna.co.kr/)
(8) Korea Simulation Technologies in South Korea (http://www.kostech.co.kr/)

Maeno et al. (2001) validated the kinematics and risk of occurrence of a bone fracture in a pedestrian THUMS version 1 impacted by a vehicle, using the PMHS test results. THUMS version 1 can be used to simulate lower leg injuries such as the rupture of the ligaments of the knee joint and bone fractures in pedestrians impacted by an SUV. It is essential to validate the rupture of the ligaments of the knee joint and the kinematics of a pedestrian by using THUMS version 1 in an SUV-pedestrian collision scenario.

In this chapter, the kinematics and the injuries of the lower extremities of a pedestrian THUMS version 1 impacted by an SUV are validated with a PMHS test. The kinematics of a full-scale pedestrian model and the mechanism of occurrence of injuries

sustained by the lower extremities of pedestrians impacted by an SUV are also discussed.

2.2 Validation of THUMS

THUMS version 1 was modified and validated using the PMHS test result. Hereafter, the modified THUMS version 1 is referred to as "modified THUMS."

2.2.1 Structure of modified THUMS

THUMS version 1 consisted of bones and soft tissues that include skin, muscles, ligaments, and tendons (see Figures 2.1 and 2.2). The lower extremity skeleton consists of a pelvis, femur, tibia, fibula, patella, and foot bones. The femur of the modified THUMS is shown as an example of a skeleton FE model (see Figure 2.3). The bone of this model consists of two layers: the outer hard layer called the cortical bone was modeled using shell elements, and the inner soft layer called the spongy bone was modeled using solid elements (see Figure 2.3). The material properties of each layer were determined on the basis of the test data obtained by Yamada (1970). From the test data, it is found that the ultimate strain of the cortical bone depends on the age (see Figure 2.4). The modified THUMS resembled a forty-year-old pedestrian. In this study, if the plastic strain of the cortical bone element exceeded 3%, the tibia, femur, and fibula of the modified THUMS were considered to be fractured.

Figure 2.1. THUMS version 1; half of the model is displayed without muscles and skin.

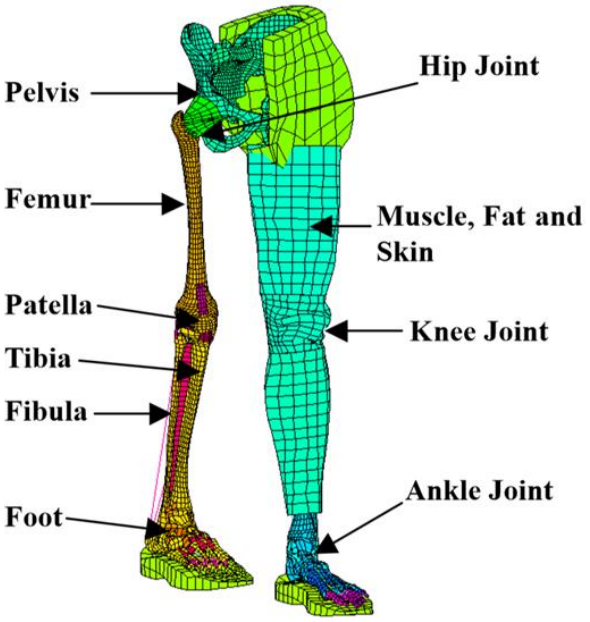

Figure 2.2. Lower extremities and pelvis of THUMS version 1; half of the model is displayed without muscles and skin.

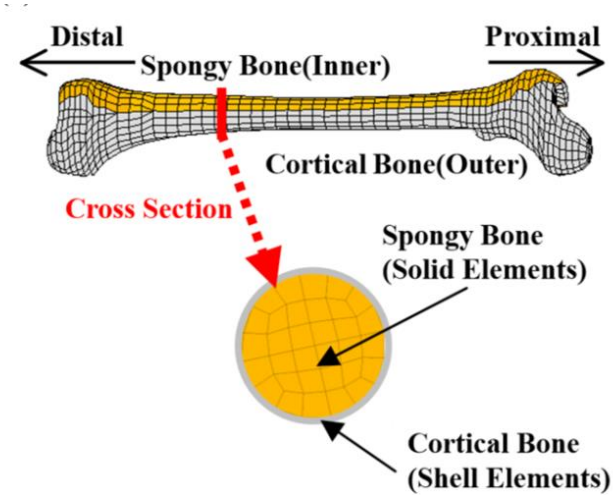

Figure 2.3. Femur of modified THUMS.

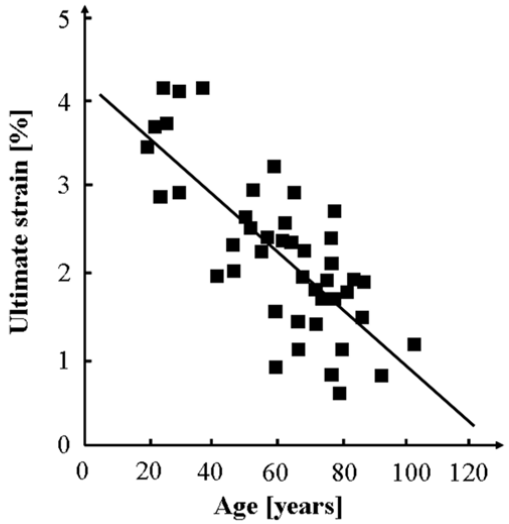

Figure 2.4. Age-related changes in the tensile properties of the cortical bone; adapted from Abe (Eds), (1996).

2.2.2 Stiffness of tibia, femur, and fibula

The bending stiffness of the tibia and femur of the modified THUMS was compared with the results obtained from the PMHS tests performed by Yamada (1970). The relationships between the load and the deflection of the tibia, femur, and fibula of the modified THUMS were similar to those obtained from the PMHS tests (see Figure 2.5).

Further, the knee structure of the modified THUMS is similar to that of a human knee (see Figure 2.6). The elongation of the ligaments of the knee joint generates a knee-bending moment. The anterior cruciate ligament (ACL), lateral collateral ligament (LCL), medial collateral ligament (MCL), and posterior cruciate ligament (PCL) of the modified THUMS were modeled using membrane elements.

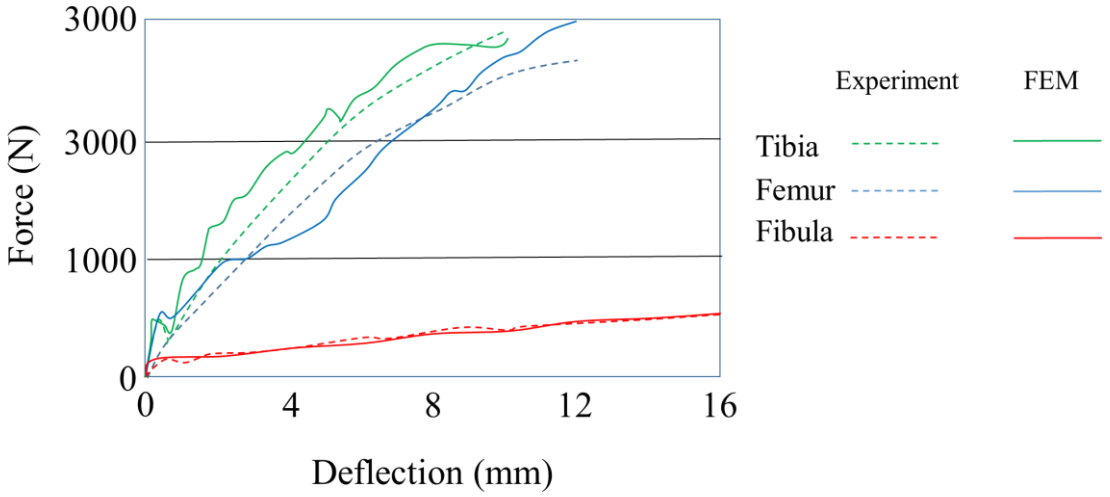

Figure 2.5. Relationships between the load and the deflections of the tibia, femur, and fibula of the modified THUMS obtained from three-point bending tests.

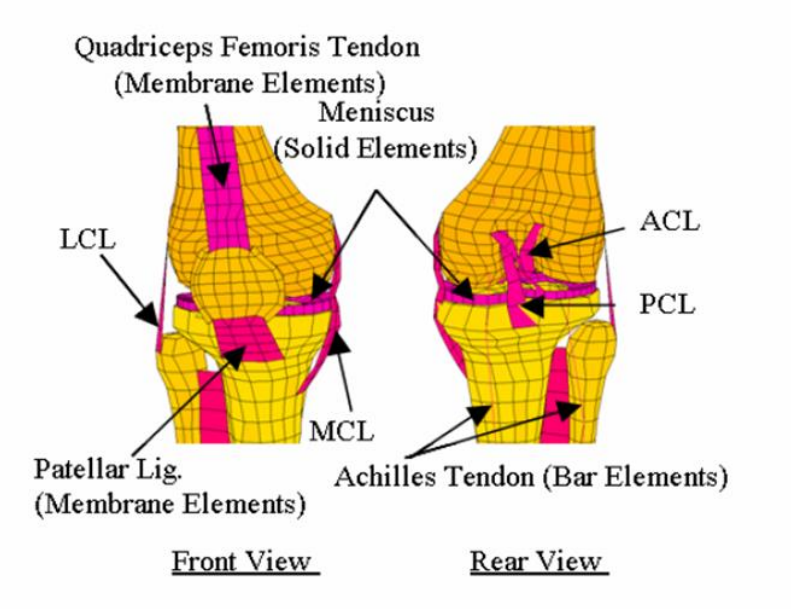

Figure 2.6. Right-hand side of knee joint of the modified THUMS.

2.2.3 Stiffness of knee joints

The MCL of the modified THUMS was 4-mm thick. In this study, the ligaments of the knee joint of the modified THUMS were considered to rupture when the plastic strain of the membrane element of the ligaments exceeded 11%, and the elements whose membrane strain exceeded 11% were eliminated. In the tensile tests, the ligaments of the knee joint ruptured completely at a relative elongation of 20%, whereas the tensile force of the ligaments was almost constant at a relative elongation ranging from 11% to

20% (see Table 2.1). Here, it was assumed that the ligaments of the knee joint began to rupture at a relative elongation of 11%.

The relationship between the knee-bending moment and the bending angle of the knee joint of the modified THUMS was similar to that obtained from the results of the PMHS tests reported by Kajzer et al. (1999); Kajzer et al. (1997); and Levine et al. (1984). The test method employed by Kajzer et al. (1999) is shown in Figure 2.7. A comparison between the knee-bending moment and the bending angle of the knee joint of the modified THUMS, as well as the tests by Levine et al. (1984) are shown in Figure 2.8.

Table 2.1
Overview of Ultimate Strain Levels Recorded for Knee Ligaments; Adopted from Masson et al. (2005)

Author	Collateral tibial	Collateral medial	Posterior cruciate	Anterior cruciate
Viidick (1973)	30%	40%	60%	60%
Kennedy (1976)			24 (±6) %	
Marinozzi (1982)			20 (±5) %	
Prietto (1992)			28 (±9) %	
Race (1994)			18 (±5)	
Arnoux (2000)	24-38%	22-38%	15-23%	18-24%
Kerrigan (2003)	7-10%	11-20%		

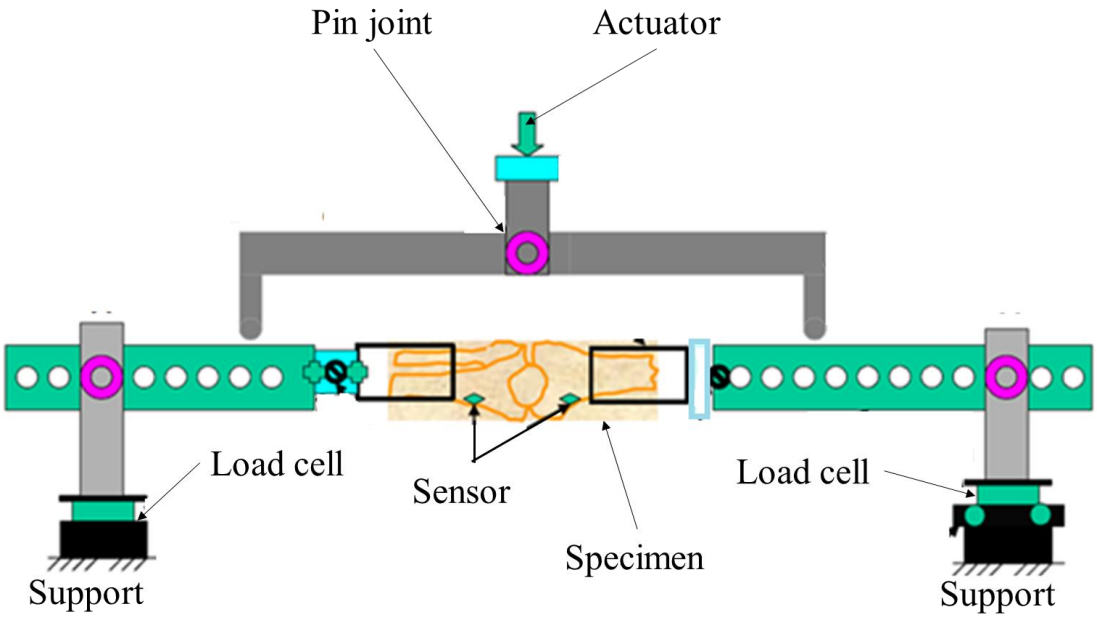

Figure 2.7. Schematic of the knee-bending test; adapted from Kajzer et al. (1999).

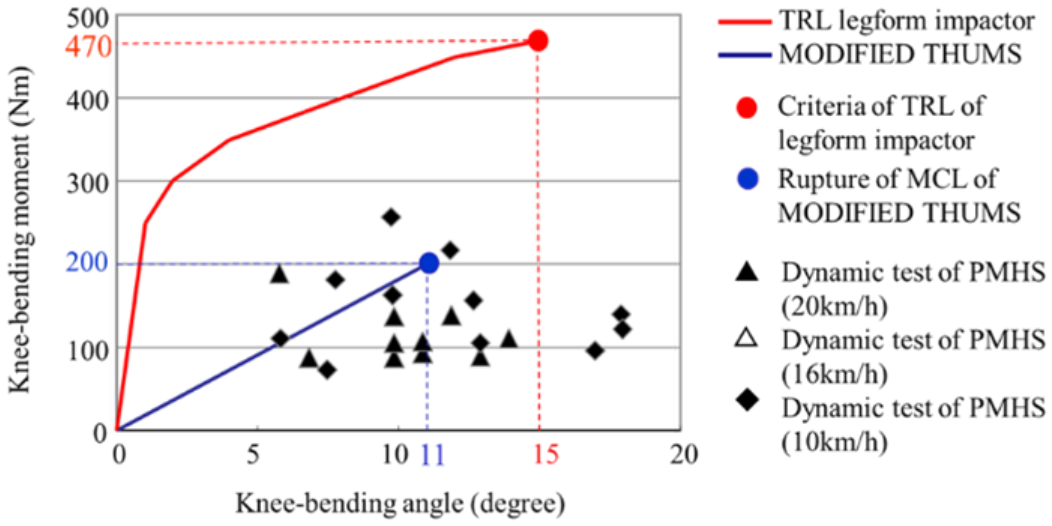

Figure 2.8. Bending moment-angle relationship of knee joint; adopted from Levine et al. (1984), Kajzer et al. (1997), and Kajzer et al. (1999).

The thickness distribution of the cortical bone of the pelvis of the modified THUMS is not uniform, as in the case of humans (see Figure 2.9), whereas that of THUMS version 1 is uniform. The simulation condition for a pelvic lateral impact is shown in Figure 2.10; this condition is identical to that tested by Cesari et al. (1980).

This test shown in Figure 2.10 was performed to investigate the dynamic response in the case of pelvic lateral impacts. Generally, a trend similar to that obtained by Cesari et al. (1980) is observed between the simulation and the test results for peak forces near the upper bound of the test corridor to that obtained by Cesari et al. (1980), (see Figure 2.11).

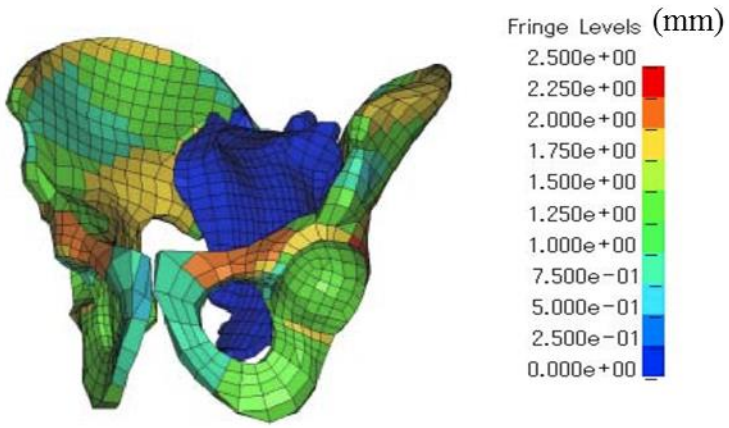

Figure 2.9. Thickness distribution of the cortical bone of the pelvis of the modified THUMS.

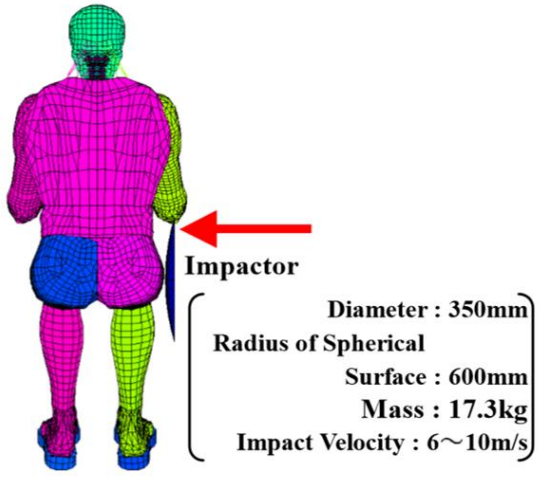

Figure 2.10. Schematic of the test condition of the impacting pelvis.

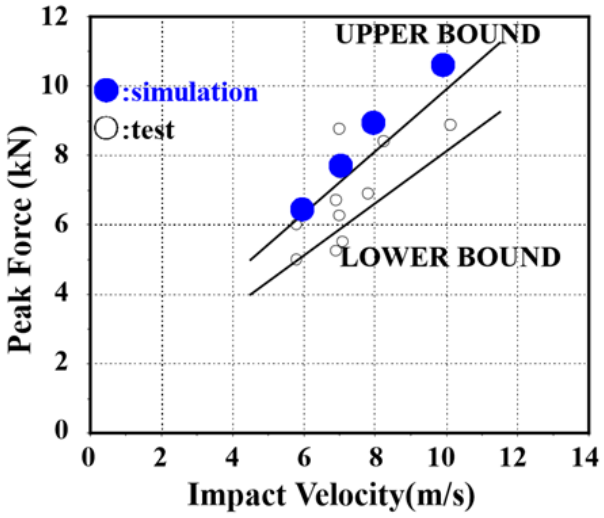

Figure 2.11. Relationships between the peak forces and the impact velocity for lateral pelvic impacts.

2.2.4 Bending and shearing of lower extremity unit

The lower extremity unit model of the modified THUMS was validated through a lower pedestrian impact test performed by Kajzer et al. (1997) and Kajzer et al. (1999). The test condition for applying a shearing force and the bending moment at the knee joint are shown in Figure 2.12. The mass of the impactor was 6.25 kg, and its impact velocity was 20 km/h.

In the case of the shearing test, the peak value of the impact force and the time of its occurrence for the modified THUMS were in good agreement with the test results (see Figure 2.13). The curves of the simulated tibia displacement were also in good agreement with the test results, both qualitatively and quantitatively (see Figure 2.14 and 2.15).

In the case of the bending test, the peak value of the impact force and the time of its occurrence for the modified THUMS are generally in good agreement with the test results (see Figure 2.16). The curve of the simulated lower tibial displacement was also generally in good agreement with the test result, both qualitatively and quantitatively (see Figure 2.17). However, the upper tibial displacement obtained from the bending test simulation tends to be greater than the test result (see Figure 2.18). The lower tibia displacement was measured at a near point from the ground and it is reasonable to

estimate that friction between the ground and the lower leg was underestimated in the bending test simulation.

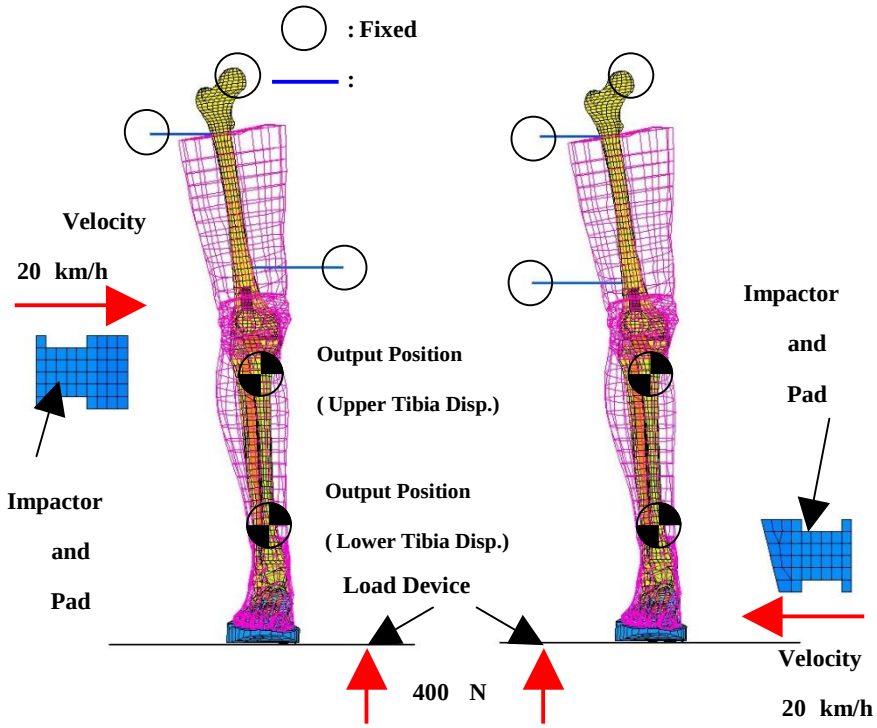

Figure 2.12. Schematic of shearing test (Left) and bending test (Right) of the knee joint.

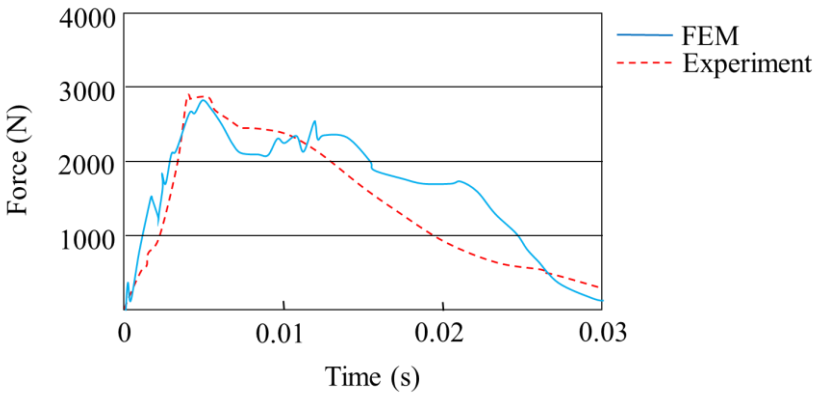

Figure 2.13. Comparison of the impact force curves between the simulation results and the shearing test results.

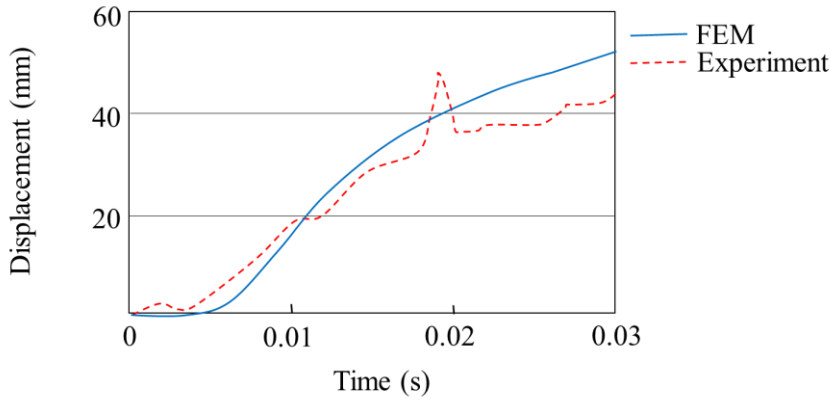

Figure 2.14. Comparison of the lower tibial displacement curves between the simulation results and the shearing test results.

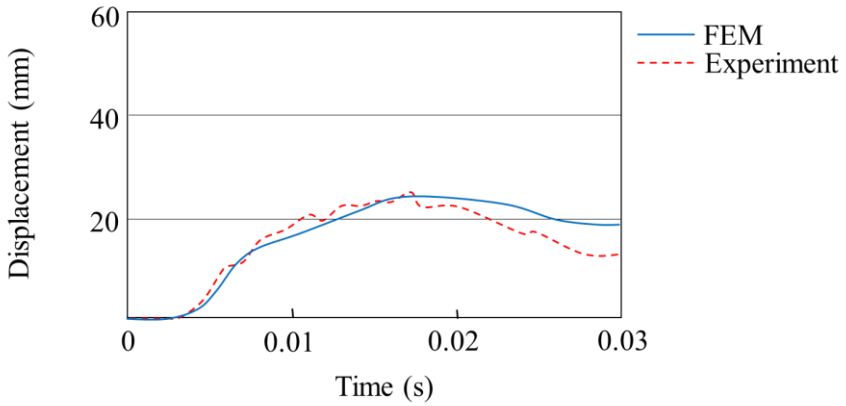

Figure 2.15. Comparison of the upper tibial displacement curves between the simulation results and the shearing test results.

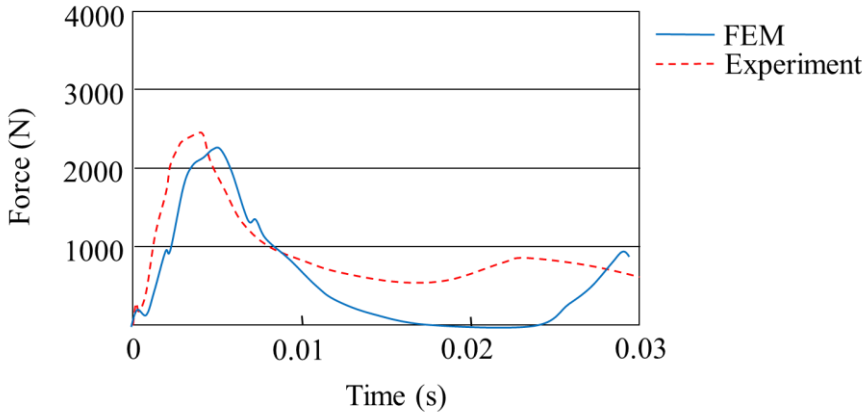

Figure 2.16. Comparison of the impact force curves between the simulation results and the bending test results.

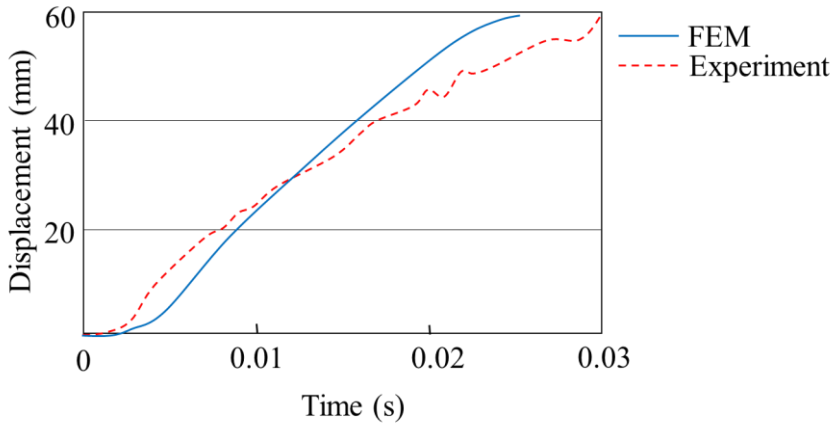

Figure 2.17. Comparison of the lower tibial displacement curves between the simulation results and the bending test results.

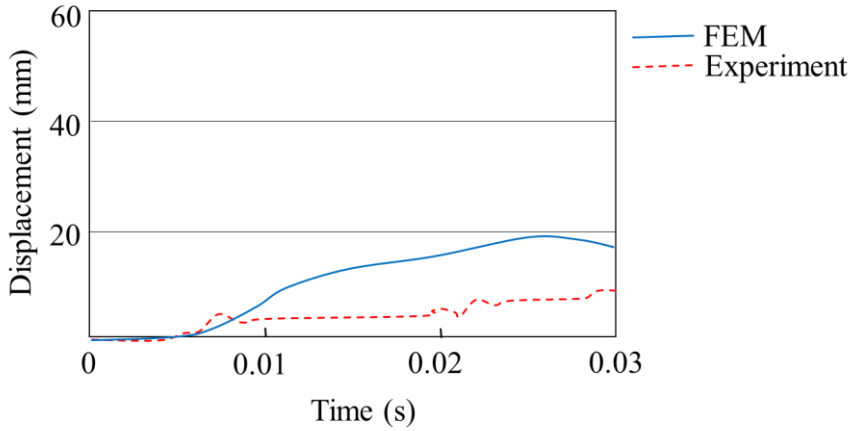

Figure 2.18. Comparison of the upper tibial displacement curves between the simulation results and the bending test results.

2.3 Validation of SUV stiffness

Schroeder et al. (2008) performed vehicle impact-to-pedestrian PMHS tests. Two tests were performed with SUVs, and two tests with minivans. The FE model of an SUV that is identical to that of the vehicle used in the test performed by Schroeder et al. (2008) for the FE crash code LS-DYNA version 960 was established and validated for three test configurations. Two test configurations were employed for the headform impactor of EEVC WG17, and another one was employed for the lower legform impactor of EEVC WG17. Also, two tests for the headform impactor of EEVC WG17 and one for the lower legform impactor of EEVC WG17 were performed using identical vehicle used in the test performed by Schroeder et al. (2008).

The FHWA/NHTSA National Crash Analysis Center (NCAC) provides a similar FE model of an SUV; detail of this model can be downloaded from http://www.ncac.gwu.edu/vml/models.html. Report of the FE model also can be downloaded from http://www.ncac.gwu.edu/vml/archive/ncac/vehicle/rav4-v1.pdf.

2.3.1 Stiffness of hood

The test configurations for the validation of head impacts were similar to the EEVC WG17 procedure. The objective of these validations was to compare the stiffness of the hood of the FE model with that of a physically tested SUV. The mass and initial velocity of the impactor were 2.5 kg and 11 m/s, respectively.

Test configurations of the validation for head impacts were similar to EEVC WG17 procedure. These validations were intended to compare stiffness of the hood of the FE model to that of the tested SUV. The mass of the impactor was 2.5 kg and initial velocity of the impactor was 11 m/s. The mass of the impactor was smaller than the mass of the pedestrian of AM50%ile, but EEVC WG17 procedure is a common test method among many academic institutes and automotive manufacturers in Europe, Japan, and the USA

The first impact position (impacting position 1) was the center of the hood panel (see Figure 2.19). The entire hood panel deformed at 12 ms and the peak value of the resultant acceleration and the time of its occurrence for the impactor were in good agreement with the test results qualitatively and quantitatively (see Figure 2.20). The stiffness of the hood at impacting position 1 of the FE model is similar to that of the physically tested SUV.

The second impact position (impacting position 2) was on the right-hand side of the hood panel (see Figure 2.21). The right half of the hood panel deformed at 12 ms and the peak value of the resultant acceleration and the time of its occurrence for the impactor in good agreement with the test results qualitatively and quantitatively (see Figure 2.22). The stiffness of the hood of the FE model was similar to that of the physical tested SUV.

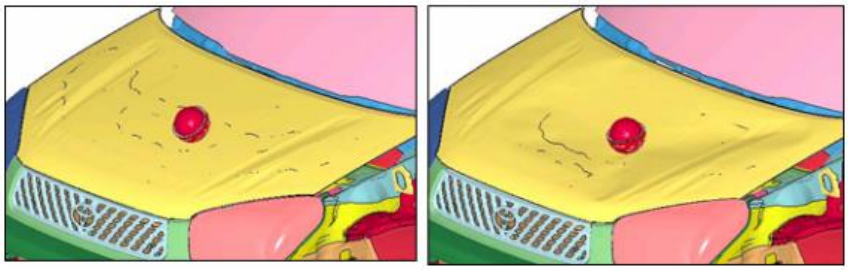

Figure 2.19. Impacting position 1 (Left) and deformation of the hood of the FE model of the SUV at 12 ms (Right).

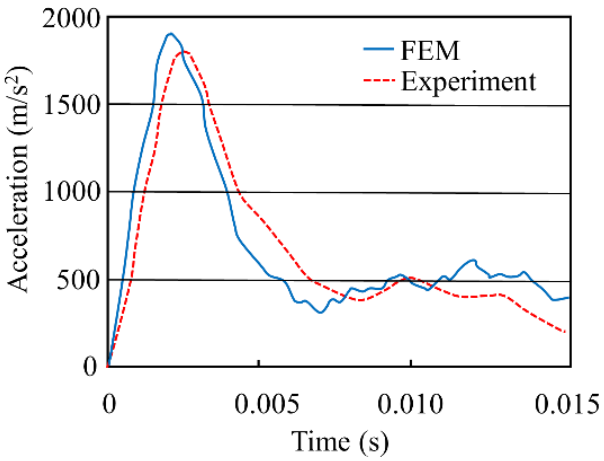

Figure 2.20. Comparison of the resultant acceleration of the impactor at impacting position 1.

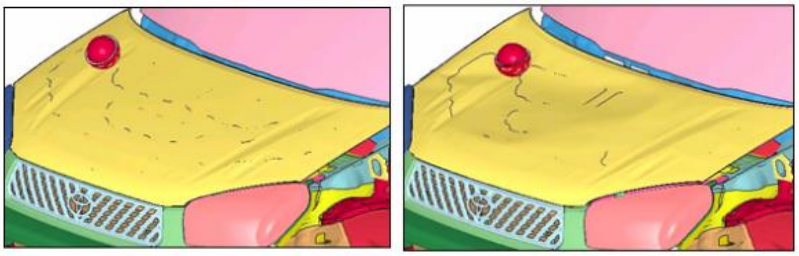

Figure 2.21. Impacting position 2 (Left) and deformation of the hood of the FE model of the SUV at 12ms (Right).

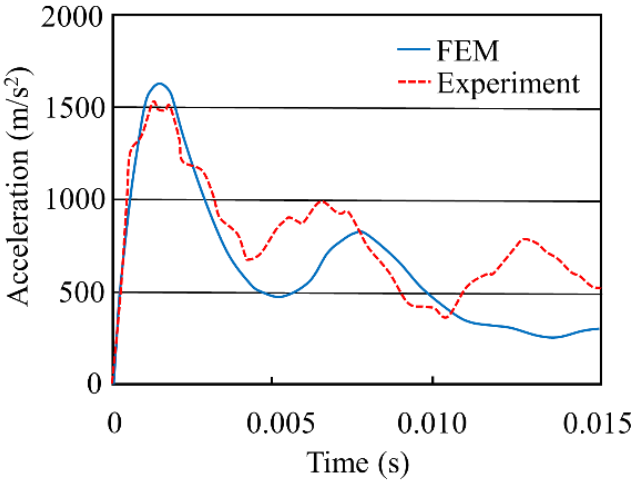

Figure 2.22. Comparison of the resultant acceleration of the impactor at impacting position 2.

2.3.2 Stiffness of bumper

The objective of this validation was to compare the stiffness of the front end of the FE model with that of a physically tested SUV. The initial velocity of the impactor was 11 m/s. The kinematic of FE model of the lower legform impactor showed good correlations with the contacting sequences between the impactor and the front end of the car (see Figure 2.23). The peak value of the resultant acceleration and the time of its occurrence for the lower legform impactor were in good agreement with the test results qualitatively and quantitatively (see Figure 2.24). The resultant acceleration of the lower legform impactor of the test from 10 ms to 20 ms was small and negative, although the resultant acceleration was positive. Rotation of the tibia of the test at 16 ms in counter-clockwise direction in Figure 2.23 was larger than the simulation, and it suggests that the stiffness of the lower bumper of the simulation was higher than the test. The peak value of the knee-bending angle and the time of its occurrence for the FE model of the lower legform impactor were in good agreement with the test results qualitatively and quantitatively (see Figure 2.25). The stiffness of the front end of the FE model was similar to that of the physically tested SUV.

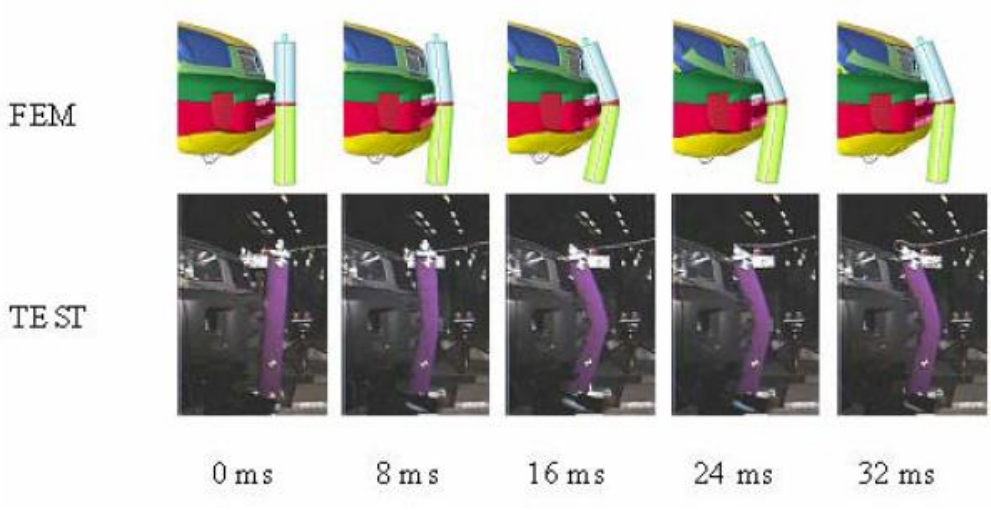

Figure 2.23. Comparison of the kinematics of the lower legform impactor.

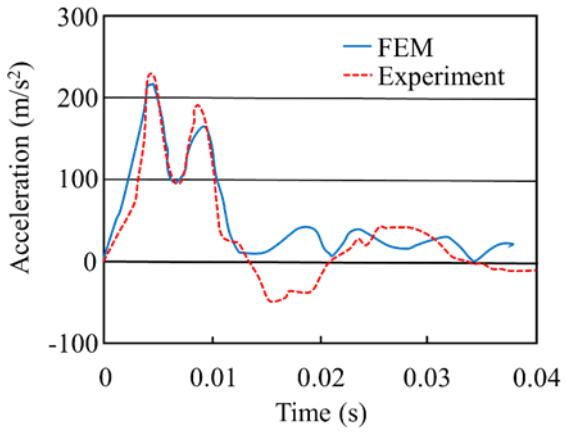

Figure 2.24. Comparison of the resultant acceleration of the lower legform impactor.

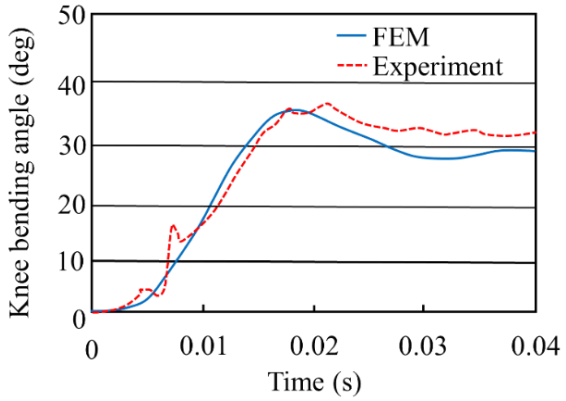

Figure 2.25. Comparison of the knee-bending angle of the lower legform impactor.

2.3.3 Kinematics of full-scale pedestrian model

The kinematics of the full-scale pedestrian model was validated through an SUV-pedestrian impact test performed by Schroeder et al. (2008). Test No. HJ2 in the paper written by Schroeder et al. (2008) was selected for validation (see Table 2.2) because the height and weight of the PMHS used in this test performed by Schroeder et al. (2008) were closer to those of the modified THUMS than those of the PMHS used in test No. HJ1. However, the age of the PMHS used in test No. HJ2 was 84 years, whereas the modified THUMS resembled a forty-year-old male. Further, the PMHS used in test No. HJ2 was bigger than the modified THUMS.

The size and mass of the modified THUMS were modified to match those of the PMHS described in the paper Schroeder et al. (2008). The long bones of the modified THUMS were scaled by referring to the locations of the target marks (see Figures 2.26, 2.27, and Table 2.3). The mass of the modified THUMS was adjusted by reducing its thigh and calf circumference and by increasing its chest, abdominal, and buttock circumferences after scaling the long bones. Hereafter, the modified THUMS scaled to the PMHS used in test NO HJ2 is referred to as HJ2 THUMS.

Table 2.2
Experimental Conditions and Subject Information; Adapted from Schroeder et al. (2008)

Vehicle	SUV		Minivan	
Test No.	HJ1	HJ2	HJ3	HJ4
Collision speed (km/h)	40	40	40	40
PMHS height (cm)	165	185	171	171
PMHS mass (kg)	60	85	80	61
PMHS gender	Male	Male	Male	Male
PMHS age (years)	80	84	80	70
PMHS bone mineral density (BMD)	0.66	0.86	0.49	0.89

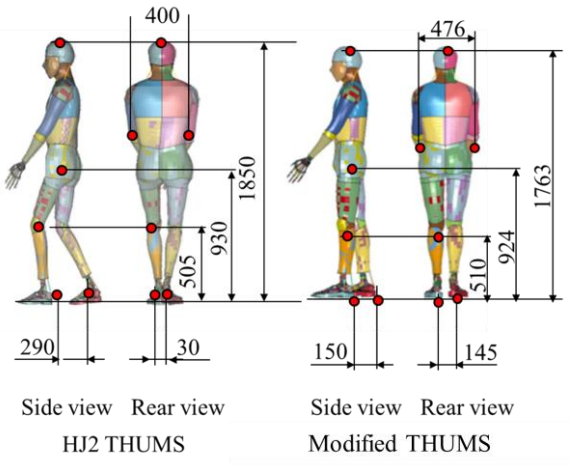

Figure 2.26. Sizes of HJ2 THUMS and Modified THUMS (Unit: mm)

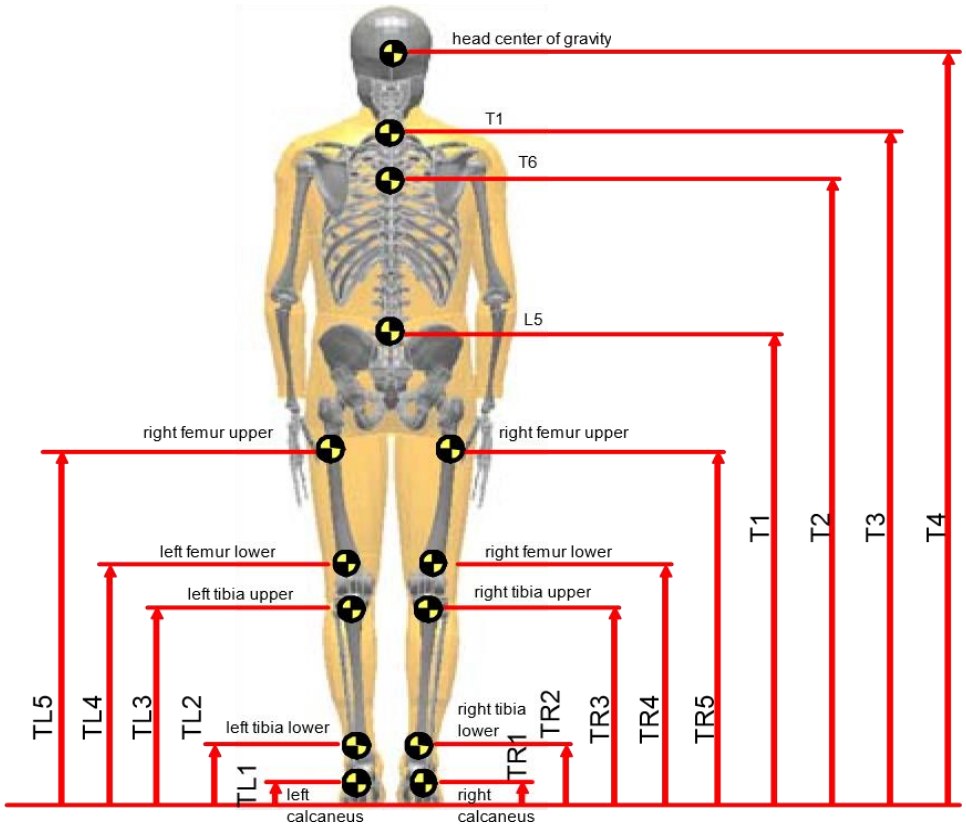

Figure 2.27. Locations of the target marks, adopted from Schroeder et al. (2008).

Table 2.3
Locations of the Target Marks; Adapted from Schroeder et al. (2008)

Location	Value (m)			
	HJ1	HJ2	HJ3	HJ4
T1	0.99	1.18	1.06	0.99
T2	1.27	1.42	1.3	1.25
T3	1.43	1.62	1.51	1.43
T4	1.58	1.77	1.67	1.6
TR1	0.16	0.13	0.15	0.12
TR2	0.26	0.23	0.23	0.21
TR3	0.45	0.49	0.45	0.41
TR4	0.54	0.62	0.54	0.53
TR5	0.75	0.97	0.83	0.7
TL1	0.09	0.08	0.09	0.11
TL2	0.23	0.19	0.18	0.21
TL3	0.46	0.47	0.45	0.42
TL4	0.57	0.61	0.54	0.55
TL5	0.76	0.96	0.83	0.7

It is known that the bone strength is related not only to the age but also to the bone mineral density (BMD), (World Health Organization science group on the assessment of osteoporosis at primary health care level, 2004). The PMHS used in test HJ2 was 84 years old, with a BMD of 86. The BMD of the PMHS was within the corridor and lower than the average BMD for his age (see Figure 2.28). Therefore, the values of the ultimate strength and ultimate strain of the cortical bone of the HJ2 THUMS were assumed to be below the average line at 84 years of age in Figure 2.4, i.e., 1.5% of the ultimate strain. If the plastic strain of the element of the cortical bone exceeded 1.5%, the tibia and the femur of the HJ2 THUMS were considered to fracture, and the elements exceeding a plastic strain of 1.5% were eliminated for the HJ2 THUMS.

The angles of the hip and the legs of the HJ2 THUMS were slightly different from those of the modified THUMS (see Figure 2.29). The initial posture of the HJ2 THUMS was adjusted to that of the PMHS used in the HJ2 test.

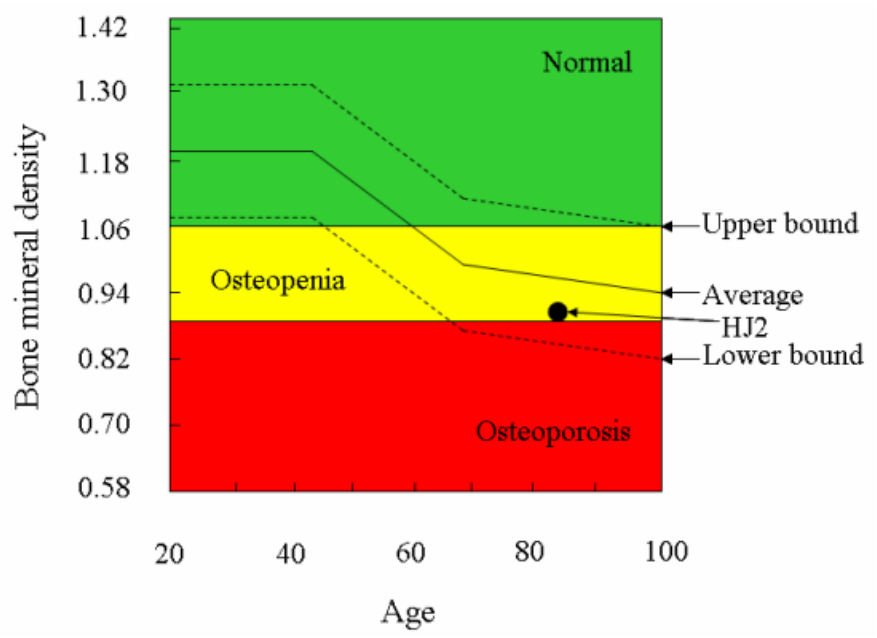

Figure 2.28. Age-related changes in the bone mineral density (BMD) of males.

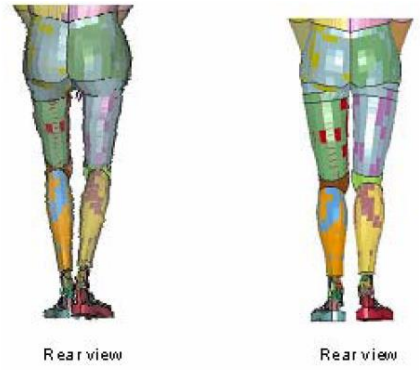

(a) HJ2 THUMS (b) modified THUMS

Figure 2.29. Postures of the HJ2 THUMS and modified THUMS.

The test condition was identical to that described in the paper written by Schroeder et al. (2008). An SUV impacted the PMHS (see Figure 2.30). The mechanism of releasing the suspended PMHS using a solenoid was assumed to be activated 100 ms before the SUV came in contact with the PMHS; it was estimated that the PMHS was moving downwards at a speed of 1.0 m/s owing to gravity, when the vehicle came in

contact with the PMHS. The initial conditions for the simulation of an SUV-pedestrian impact using the HJ2 THUMS are shown in Figure 2.31.

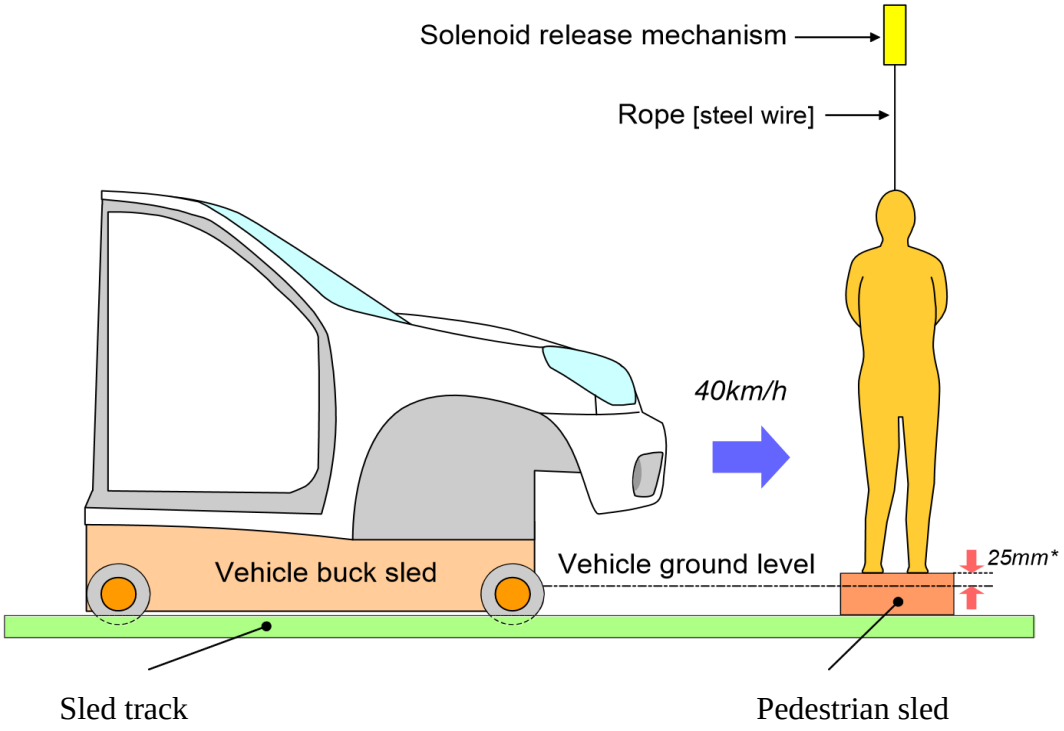

Figure 2.30. Schematic of the experimental setup; adapted from Schroeder et al. (2008).

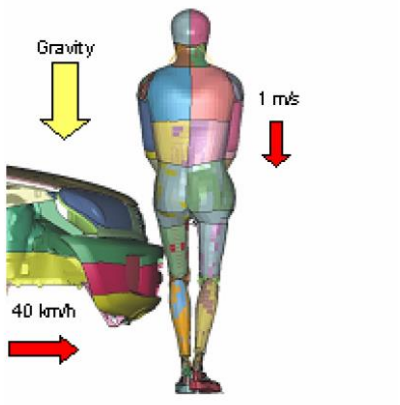

Figure 2.31. Initial condition for the simulation of SUV-pedestrian impact.

The kinematics of the HJ2 THUMS was compared with the test results of HJ2 (see Figure 2.32). The kinematics of the HJ2 THUMS showed good correlations with with those of the PMHS used in the test until 110 ms. The trajectory of the head, L5, left

knee, and left foot of HJ2 THUMS showed fairly good correlations with those of the test until 70 ms (see Figures 2.33 and 2.34). The kinematics of the tibia of the HJ2 THUMS was different from the test result at 110 ms.

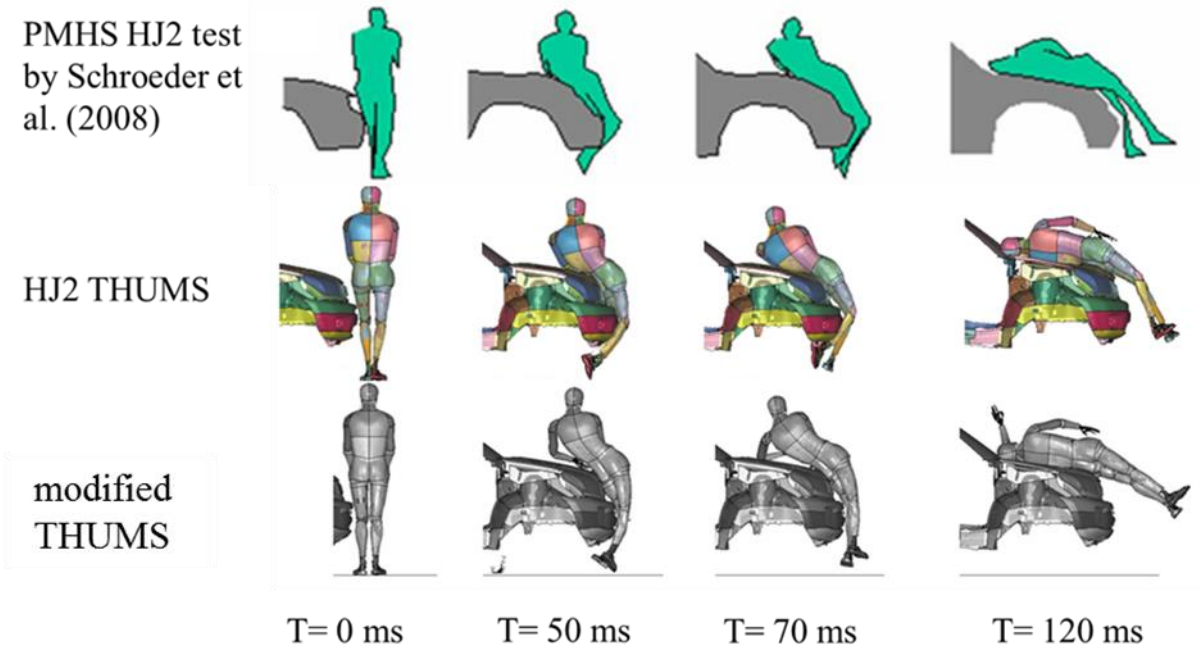

Figure 2.32. Comparison between the kinematics of the PMHS used in the test and HJ2 THUMS.

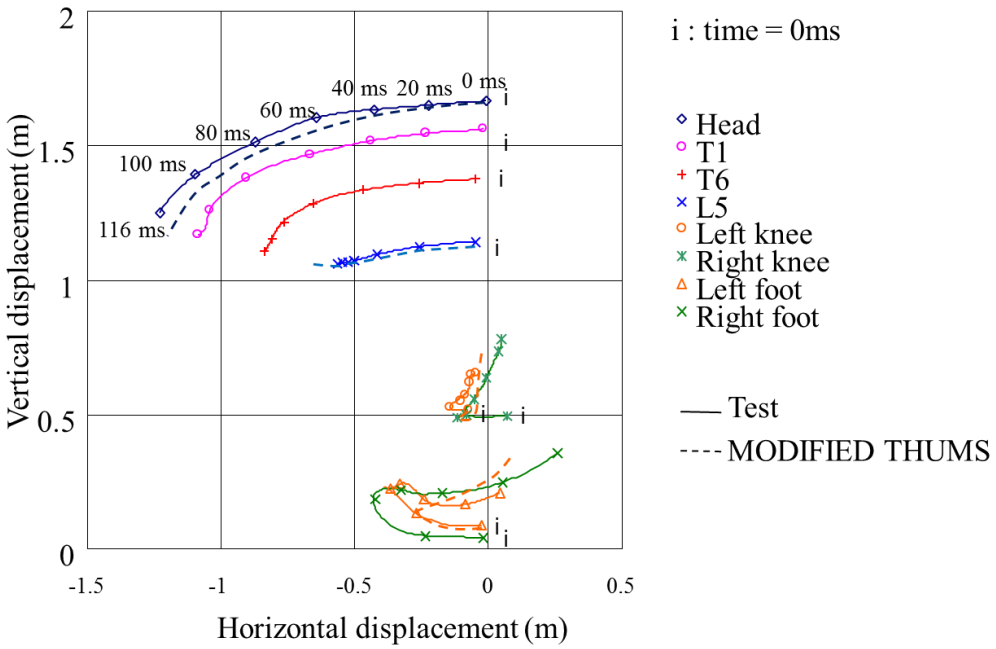

Figure 2.33. Comparison between the trajectories of the modified THUMS and PMHS HJ2; adapted from Schroeder et al. (2008).

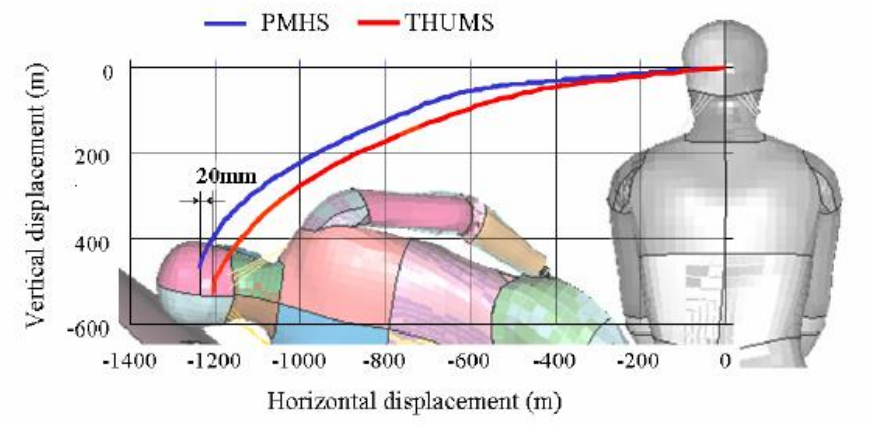

Figure 2.34. Comparison between the head trajectories of the modified THUMS and HJ2 PMHS; adapted from Schroeder et al. (2008).

2.3.4 Injuries sustained by full-scale pedestrian model

The HJ2 PMHS was reported to sustain seven injuries in the test (see Table 2.4). The seven injuries sustained on the head, left arm, left hand, rib, pelvis, and left knee of the HJ2 THUMS were compared with those sustained by the HJ2 PMHS.

Table 2.4
Injuries Sustained by the HJ2 PMHS; Adapted from Schroeder et al. (2008)

Test	Part	Detail
HJ2	Left knee	Rupture of deep part of MCL, which is connected to the medial meniscus
		ACL - avulsion of femoral insertion
		MCL - avulsion of tibial insertion
	Pelvis	Anterior pelvic ring fracture of inferior pubic ramus
		Anterior pelvic ring fracture of iliopubic eminence
	Left hand	Abrasion on the hand
	Left arm	Abrasion on the forearm
	Rib	Fracture of 5th and 6th rib at the medio clavicular line; 120 mm from the center line of the sternum, 130 mm from the center line of the sternum
	Head	Contusion

HJ2 THUMS could not be used to evaluate the contusions and abrasions of the head, arm, and hand. The left hand of the HJ2 THUMS came in contact with the hood panel at 34 ms (see Figure 2.35). The left elbow and lower arm of the HJ2 THUMS came in contact with the hood panel at 52 ms. The left-hand side of the head of the HJ2 THUMS came in contact with the windshield glass at 112 ms. These points of contact of the HJ2 THUMS coincided with the areas of contusion and abrasion of the HJ2 PMHS in the test. The velocity of impact of the head of the HJ2 PMHS against the windshield glass is 12.2 m/s and that of the HJ2 THUMS is 11.9 m/s.

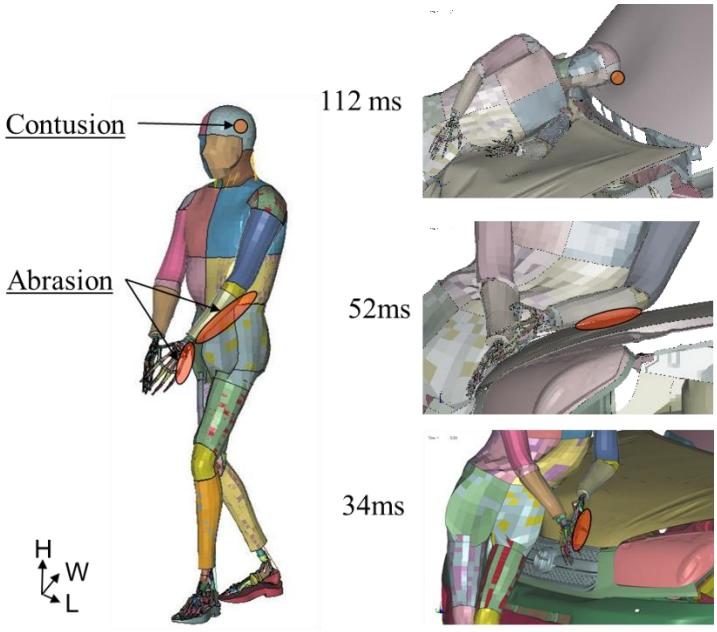

Figure 2.35. Impacted positions at the head, left arm, and left hand of the HJ2 THUMS.

The maximum plastic strain of the ribs of the HJ2 THUMS was observed at 100 ms (see Figure 2.36). The red circles shown in Figure 2.36 indicate the positions of the fractured ribs of the HJ2 PMHS. The plastic strain of the ribs within the dotted area does not exceed 1.5%. These ribs of the HJ2 THUMS are not considered to suffer from fracture during an SUV-to-pedestrian accident.

The maximum plastic strain of the pelvis of the HJ2 THUMS was observed at 30 ms (see Figure 2.37). The red circles shown in Figure 2.37 indicate the positions of the fractured pelvis of the HJ2 PMHS. The plastic strain of the pelvis within the dotted area exceeded 1.5%. Therefore, the pelvis of the HJ2 THUMS was considered to suffer from fracture during an SUV-to-pedestrian impact, as in the case of the HJ2 PMHS.

The MCL of the HJ2 THUMS ruptured at 8.5 ms, and the ACL of the HJ2 THUMS ruptured at 16 ms (see Figure 2.38). These knee injuries were identical to those of the HJ2 PMHS. The tibia and fibula of the HJ2 THUMS were not fractured, as in the case of the HJ2 PMHS.

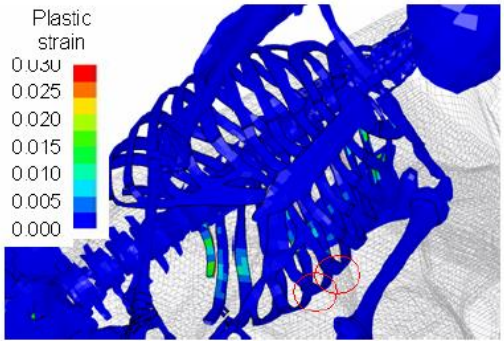

Figure 2.36. Plastic strain distribution of the rib bones of the HJ2 THUMS at 100 ms.

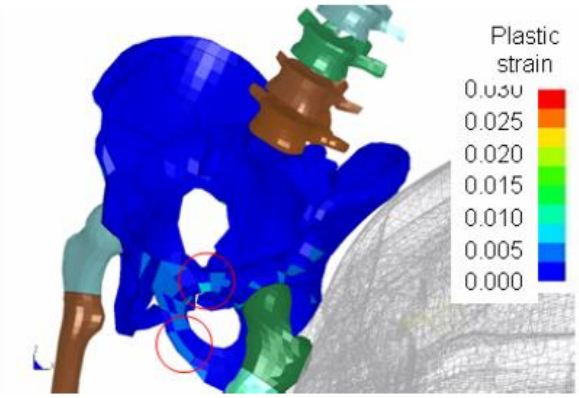

Figure 2.37. Plastic strain distribution of the pelvic bone of the HJ2 THUMS at 30 ms.

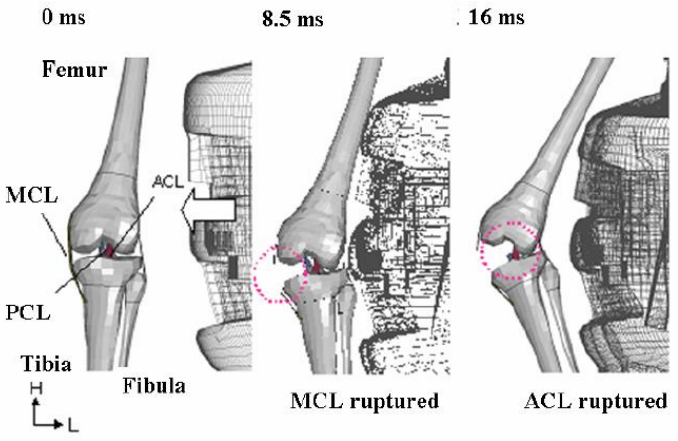

Figure 2.38. Knee-joint ligament rupture of the HJ2 THUMS.

2.4 Discussion

2.4.1 Trajectory of the HJ2 THUMS and contact force of the SUV

The trajectory of the entire HJ2 THUMS consisted of three parts, as observed with its coordinate fixed at an SUV (see Figure 2.39). In the first part, the entire HJ2 THUMS rotated around its knee joint (see point A in Figure 2.39). In the second part, the torso of the HJ2 THUMS rotated around its pelvis (see point B in Figure 2.39). In the third part, the head of the HJ2 THUMS rotated around T1 (see point C in Figure 2.39).

In the first part of the trajectory shown in Figure 2.39, the bumper of the SUV was in contact with the knee joint, and the MCL of the left knee joint ruptured at 8.5 ms and the ACL ruptured at 16 ms (see Figure 2.38). The knee joint is made up of four ligaments; the left knee joint lost its bending moment with the rupture of two of the knee-joint ligaments until 16 ms (see Figure 2.38). The contact point between the HJ2 THUMS and the SUV was that between the femur and/or knee joint and the bumper at 16 ms (see Figure 2.38). Therefore, the contact force between the bumper and the femur and/or the knee joint was responsible for rotating the entire HJ2 THUMS in the first part.

In the second part of the trajectory shown in Figure 2.39, the pelvis was in contact with the hood panel and the thigh bone caput. The maximum contact force between the femur head and the pelvis was 5000 N at 22 ms, and the contact force increased again at 6 ms and remained at the increased value for 140 ms (see Figure 2.40). The pelvis came in contact with the hood panel at point A, as shown in Figure 2.41, and created a dimple. This dimple prevented the pelvis of the HJ2 THUMS from sliding on the hood panel of the SUV. Therefore, the contact force between the hood and the pelvis was responsible for rotating the torso of the HJ2 THUMS in the second part.

In the third part of the trajectory shown in Figure 2.39, the torso was in contact with the hood panel. The first peak of the contact force between the hood panel and the torso showed a value of 1200 N at 83 ms when the elbow was in contact with the hood panel, and the second peak of the contact force showed a value of 2000 N at 120 ms when the ribs were in contact with the hood panel (see Figure 2.42). Therefore, the

contact force between the ribs and the hood panel was responsible for rotating the head of the HJ2 THUMS around T1 in the third part.

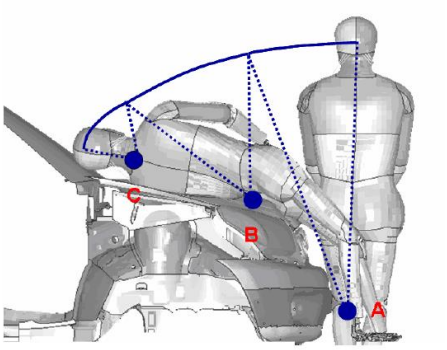

Figure 2.39. Head trajectory of the HJ2 THUMS observed with the coordinate fixed at the SUV.

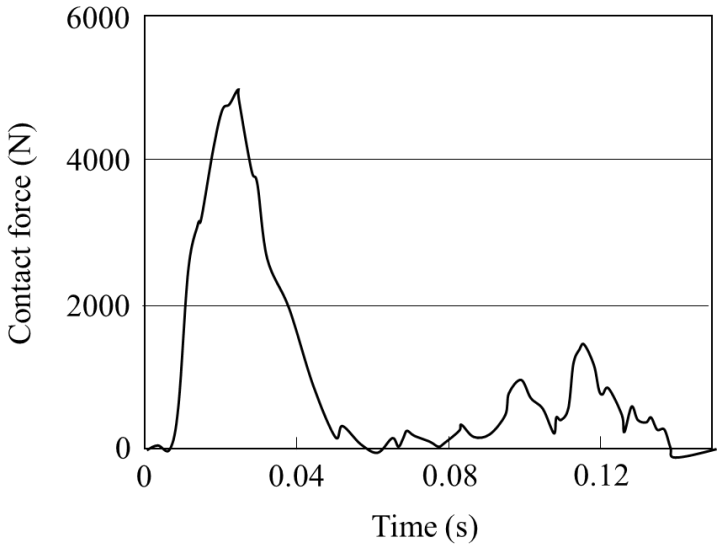

Figure 2.40. Resultant contact force between the thigh bone caput/pelvis of the HJ2 THUMS and the FE model of the SUV.

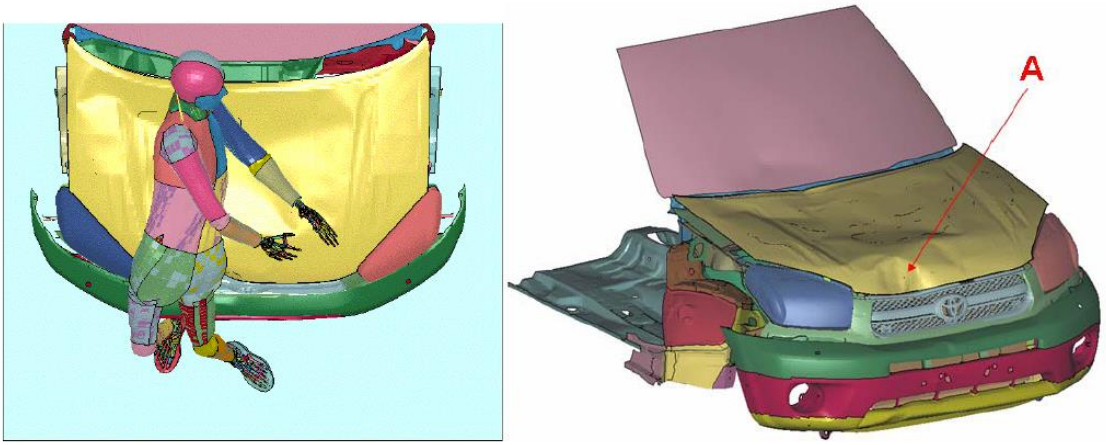

Figure 2.41. Deformed shape of the SUV FE model at 70 ms.

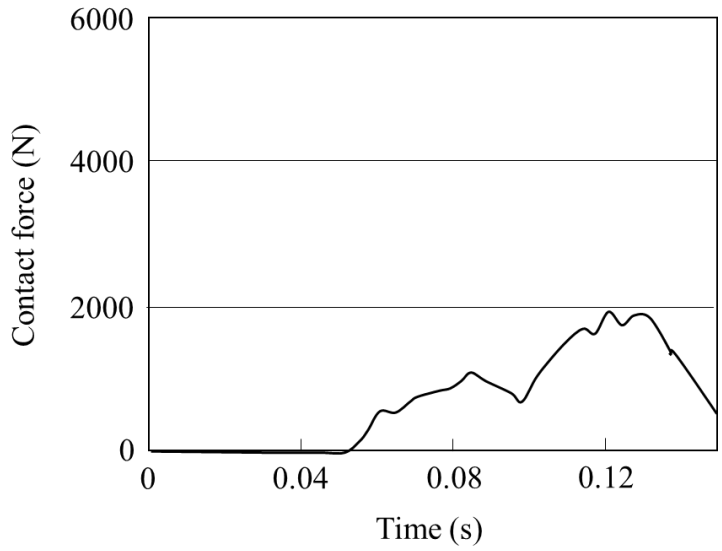

Figure 2.42. Resultant contact force between the torso of the HJ2 THUMS and the hood panel of the SUV FE model.

2.4.2 Injuries sustained by the HJ2 THUMS and contact force of the SUV

The anterior pelvic ring of the inferior pubic ramus and the iliopubic eminence of the HJ2 PMHS fractured in the test (see Table 2.4). The plastic strain of the shell elements of the cortical bone of the anterior pelvic ring of the inferior pubic ramus and the iliopubic eminence of the HJ2 THUMS exceeded 1.5% at 30 ms and were considered to suffer from fracture, as in the case of the HJ2 PMHS. Two possible load passes exist from the hood panel of the FE model of the SUV to the pelvis of the HJ2

THUMS. In the case of the first pass, the iliac crest of the HJ2 THUMS was in contact with the hood panel at 30 ms by way of muscle and skin. In the case of the second pass, the femur head of the HJ2 THUMS was in contact with the hood panel at 30 ms by way of muscle and the skin (see Figure 2.40). From the geometry of the pelvis and the thigh bone caput, it was found that the anterior pelvic ring of the inferior pubic ramus and the iliopubic eminence supported the femur head (see Figure 2.40). The maximum contact force between the femur head and the pelvis was 5000 N at 22 ms (see Figure 2.40). This peak force caused fracture of the anterior pelvic ring of the inferior pubic ramus and the iliopubic eminence of the HJ2 PMHS. The thickness distribution of the cortical bone of the pelvis indicated that the thicknesses of the cortical bone of the anterior pelvic ring of the inferior pubic ramus and the iliopubic eminence were less than the thickness of the iliac crest (see Figure 2.9). It is inferred that the fractures of the anterior pelvic ring of the inferior pubic ramus and the iliopubic eminence of the HJ2 THUMS were caused by the transmission of force through the femur head and thinner cortical bone of the anterior pelvic ring of the inferior pubic ramus and the iliopubic eminence.

The MCL and the ACL of the HJ2 THUMS ruptured at 8.5 ms and 16 ms, respectively. The lower bumper of the SUV did not come in contact with the tibia of the HJ2 THUMS at 16 ms owing to the initial geometry (see Figure 2.38). The upper bumper came in contact with the knee joint, and the shearing and bending deformation of the knee joint caused the MCL to rupture at 8.5 ms (see Figure 2.38). An increase in the bending deformation caused the ACL to rupture at 16 ms (see Figure 2.38). The stiffness of the knee joint was negligible after the rupture of the MCL and the ACL, and the tibia continued to remain in contact with the bumper for 70 ms (see Figure 2.38).

The tibia and the femur of the HJ2 PMHS did not fracture. The plastic strain of the shell elements of these cortical bones of the HJ2 THUMS did not exceed 1.5%. The MCL and the ACL of the HJ2 THUMS ruptured before the tibia came in contact with the bumper; the stiffness of the knee joint at that time was already small when the tibia was in contact with the bumper. A large contact force between the bumper and the tibia was not observed owing to the initial geometry of the SUV. Owing to these reasons, the tibia of the HJ2 THUMS did not fracture. The femur of the HJ2 THUMS did not come in contact with the SUV (see Figures 2.39), whereas the femur head of the HJ2 THUMS came in contact with the hood panel and the knee joint of the HJ2 THUMS came in

contact with the bumper (see Figure 2.38). This was the reason why the femur of the HJ2 THUMS did not fracture. The kinematics of the knee joint of the HJ2 THUMS shown in Figure 2.38 indicated that the height of the knee joint was sensitive to knee-joint injuries. The height of the knee joint is also related to the size of the pedestrian and the initial condition of the test.

2.5 Limitations

The HJ2 THUMS did not show a realistic thickness distribution of the cortical bone of the ribs, and it could not simulate the bone fractures of the HJ2 PMHS. The stiffness of the windshield glass of the FE model of the SUV, which was impacted by the head of the HJ2 THUMS, was not validated, and a more sophisticated material constitutive law for simulating crack propagations should be employed.

2.6 Conclusions

The PMHS test scenario of a pedestrian impacted by an SUV was simulated using the HJ2 THUMS and an FE model of the SUV to validate the kinematics and injuries of the HJ2 THUMS.

THUMS version 1 was validated using PMHS tests in terms of its component levels, and it was modified to match the size of the HJ2 PMHS used in the test performed by Schroeder et al. (2008). This modified THUMS version 1 was referred to as the HJ2 THUMS. The kinematics of the HJ2 THUMS showed fairly good correlations with the PMHS test results. The injuries sustained by the lower extremities of the HJ2 THUMS, such as the knee joint, tibia, femur, and pelvis, showed correlations with the test results.

The result of this FE analysis clarified that the entire kinematics of a pedestrian impacted by an SUV consisted of three parts. In the first part of the kinematics, the entire human body rotated around the knee joint driven by the contact force of the bumper. In the second part of the kinematics, the torso of the human body rotated around the pelvis driven by the contact force of the hood panel. In the third part of the kinematics, the head of the human body rotated around T1 driven by the contact force of the hood panel.

3 Assessment of the tibia and knee-joint ligament injuries sustained by a pedestrian impacted by a vehicle

3.1 Introduction

The tibia and knee-joint ligament injuries sustained by a pedestrian impacted by a vehicle may depend on the size of the pedestrian. For example, the crash configurations of an AM50%ile pedestrian, an AF05%ile pedestrian, and a 6YO child pedestrian differ from each other (see Figure 3.1). The estimated initial contact points of the vehicle include the hood, upper bumper absorber, and lower bumper absorber (see Figure 3.1). The hood panel may come in contact with the upper leg of the AM50%ile pedestrian, the pelvis of the AF05%ile pedestrian, and the abdomen of the 6YO child pedestrian. The upper bumper absorber may come in contact with the upper leg of the AM50%ile pedestrian, the knee joint of the AF05%ile pedestrian, and the upper leg of the 6YO child pedestrian. The lower bumper absorber may come in contact with the lower legs of the AM50%ile pedestrian, the AF05%ile pedestrian, and the 6YO child pedestrian. The crash configurations shown in Figure 3.1 indicate that the mechanism of occurrence of leg injuries depends on the height and stiffness of the hood, upper bumper, and lower bumper of a vehicle.

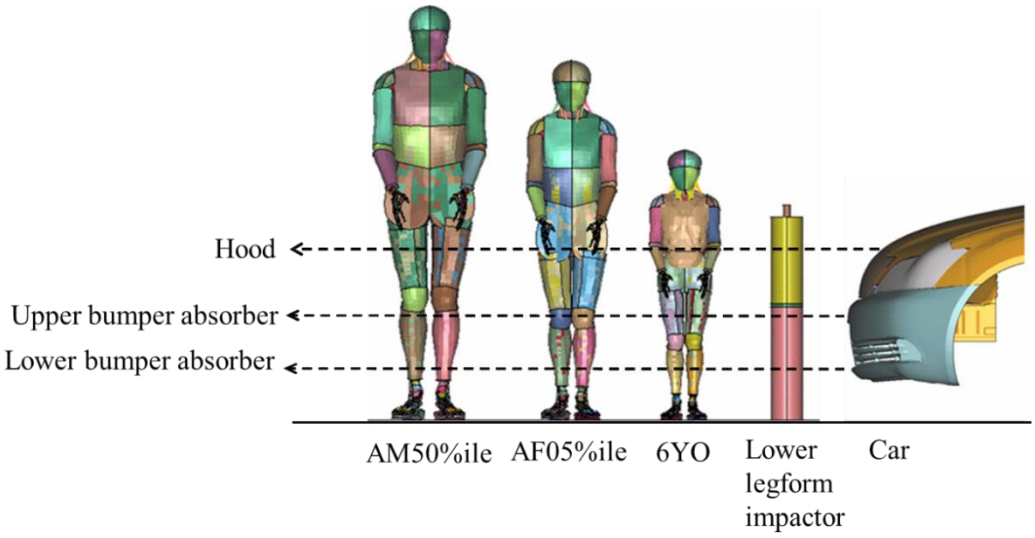

Figure 3.1. Crash configurations of pedestrians and a car.

The objective of this study is to assess the tibia and knee-joint ligament injuries sustained by an AM50%ile pedestrian, an AF05%ile pedestrian, and a 6YO child

pedestrian using impact simulations that precisely simulate the shape and the stiffness of the front end of a vehicle.

3.2 Accident reconstruction methods

In this chapter, four crash configurations were considered. The first crash configuration (case 3.1) involved a collision between a vehicle and the lower legform impactor in order to validate the stiffness of the front end of the vehicle with the test (see Figure 3.2). The second crash configuration (case 3.2) involved a collision between a vehicle and an AM50%ile pedestrian (see Figure 3.3). The third crash configuration (case 3.3) involved a collision between a vehicle and an AF05%ile pedestrian (see Figure 3.4). Finally, the fourth crash configuration (case 3.4) involved a collision between a vehicle and a 6YO child pedestrian (see Figure 3.5).

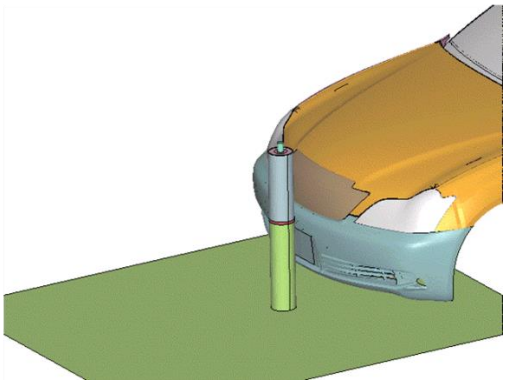

Figure 3.2. Crash configuration of the lower legform impactor (case 3.1).

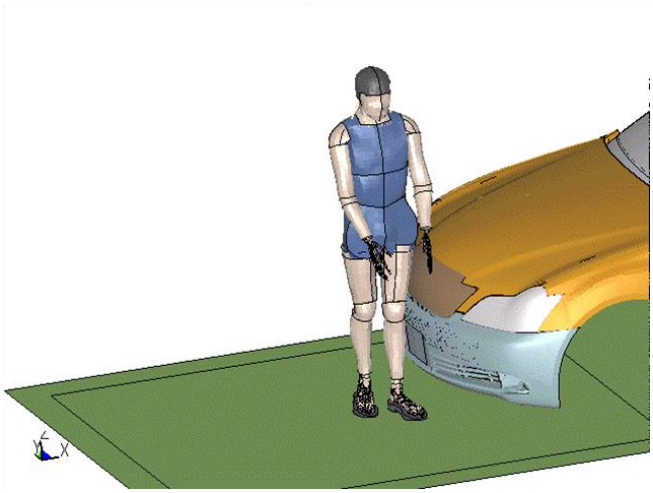

Figure 3.3. Crash configuration of an AM50%ile pedestrian (case 3.2).

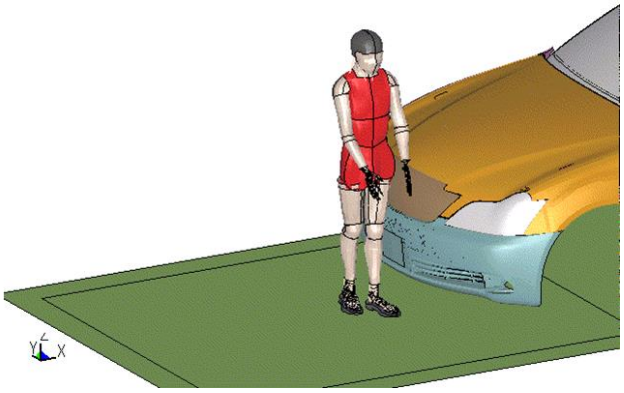

Figure 3.4. Crash configuration of an AF05%ile pedestrian (case 3.3).

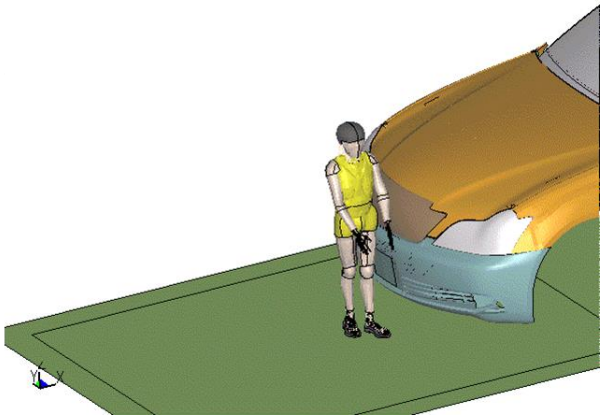

Figure 3.5. Crash configuration of a 6YO child pedestrian (case 3.4).

The modified THUMS—described in chapter 2—was used for an AM50%ile pedestrian. The height and the mass of the modified THUMS were 175.1 cm and 76.6 kg, respectively. Further, the modified THUMS was transformed to match the size and mass of AF05%ile pedestrians. Hereafter, the modified THUMS that is transformed to exhibit the size of an AF05%ile pedestrian is referred to as THUMS AF05. The height and mass of THUMS AF05 were 151.3 cm and 46.9 kg, respectively. The material properties of THUMS AF05 are identical to those of the modified THUMS. A human FE model of a 6YO child pedestrian was developed by (Nishimura and Hasegawa, 2002), which is hereafter referred to as THUMS 6YO. The height and mass of THUMS 6YO were 113.5 cm and 21.2 kg, respectively. The material properties of THUMS 6YO were identical to those of the modified THUMS, except for the elastic modulus and ultimate strain of the cortical bone of the tibia and the femur. The elastic modulus of

THUMS 6YO was 66.7% that of the modified THUMS, as inferred from the scale factors of the elastic modulus of the parietal bone determined by McPherson et al. (1978) and Irwin et al. (1997). The scale factors of the elastic modulus of the parietal bone determined by Irwin et al. (1997) are shown in Figure 3.6 for reference.

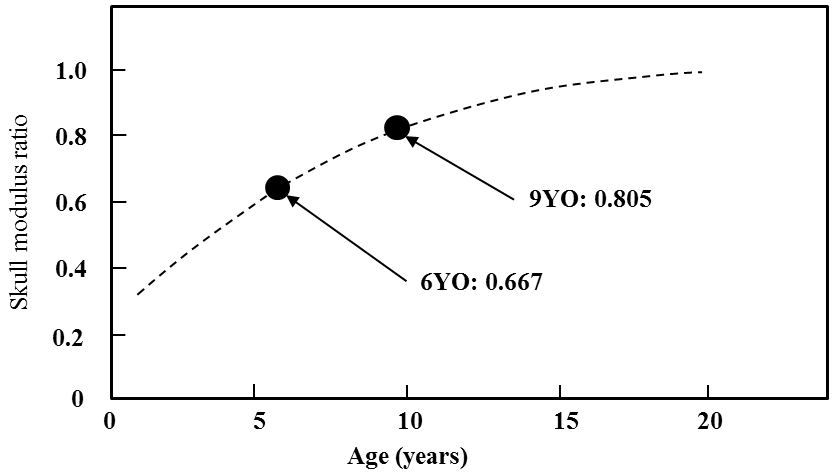

Figure 3.6. Scale factors of the elastic modulus of the parietal bone determined by Irwin et al. (1997).

The ultimate strain of the tibia and the femur of THUMS 6YO was 4%, as inferred on the basis of age-related changes in the tensile properties of the cortical bone of the femur determined by McCalden et al. (1993). McCalden et al. (1993) proposed the fracture strain of the femur cortical bone as a function of age (see Equation (3.1)).

$$\varepsilon_f = 4.235 - 0.03265x \tag{3.1}$$

$$\varepsilon_f : \textbf{Fracture strain}\ (\%)\ , \qquad x : \textbf{Age}\ (\textbf{Years})$$

This equation was applied to the cortical bone of the tibia of a 6YO child whose fracture strain was assumed to be 4%. In this paper, the tibia and the femur of THUMS 6YO fractured when the plastic strain of the element of the cortical bone exceeded 4%. The kinematics and injuries assessed using THUMS AF05 and THUMS 6YO were not validated with the test data owing to the lack of test data obtained using a PMHS in the published literatures.

3.2.1 FE model of a sedan

An FE model of a sedan was generated (see Figure 3.7). A lower legform impact test following the EEVC WG17 test protocol (European Enhanced Vehicle-Safety Committee, 1996) was performed to validate the stiffness of the developed FE model. The kinematics, upper tibia acceleration, and knee-bending angle showed fairly good correlation with the test results (see Figures 3.8, 3.9, and 3.10).

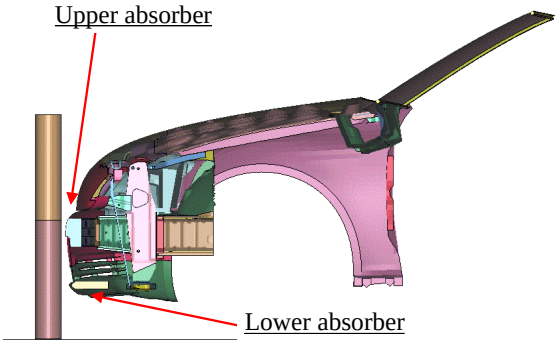

Figure 3.7. FE model of the lower legform impactor and sedan.

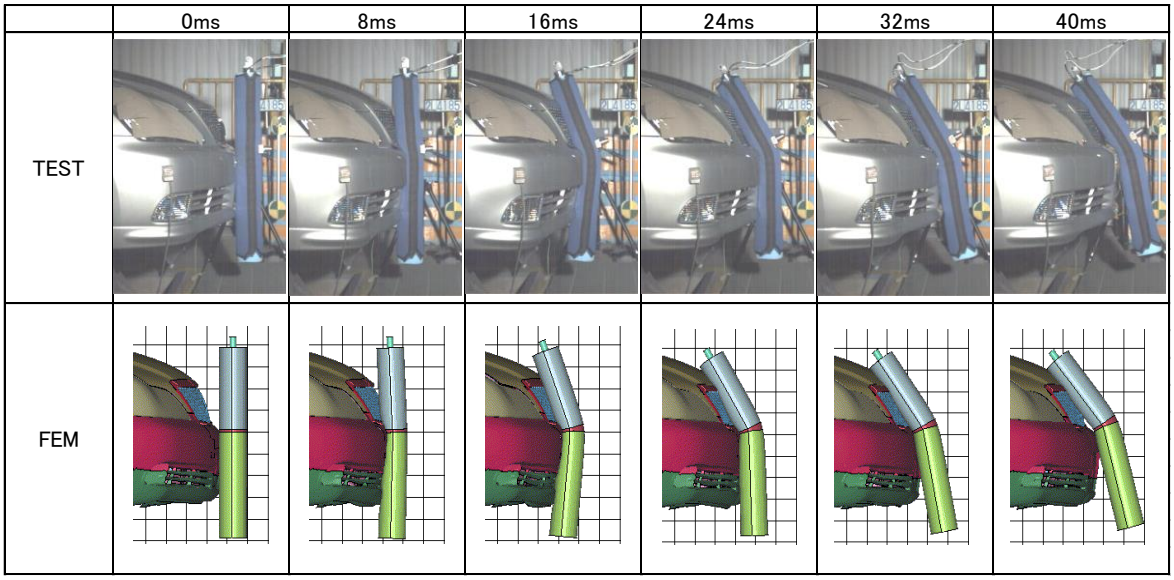

Figure 3.8. Comparison of the kinematics of the lower legform impactor through the test and an FE simulation.

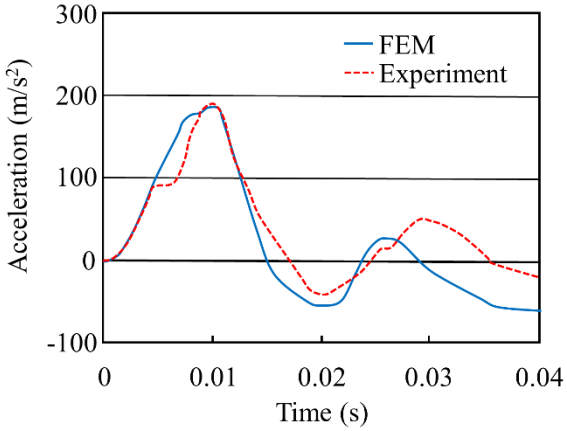

Figure 3.9. Comparison of the tibial acceleration of the lower legform impactor through the test and an FE simulation.

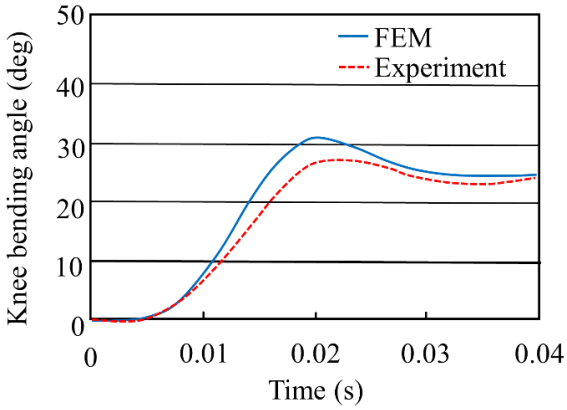

Figure 3.10. Comparison of the knee-bending angle of the lower legform impactor through the test and an FE simulation.

3.2.2 Boundary and initial conditions

The modified THUMS, THUMS AF05, and THUMS 6YO were made to stand stationary in front of the FE model of the sedan, with their left legs forward. The knee joints of the left leg of the modified THUMS, THUMS AF05, and THUMS 6YO were precisely located at the central section of the FE model of the sedan. The FE model of the sedan collided with the modified THUMS, THUMS AF05, and THUMS 6YO at 40 km/h. The objective of the simulations presented in this chapter was to reconstruct pedestrian accidents using three combinations of ages and genders. Therefore, the initial vertical velocities of the modified THUMS, THUMS AF05, and THUMS 6YO were assumed to be 0 m/s.

3.3 Results

3.3.1 Kinematics

The kinematics of the modified THUMS, THUMS AF05, THUMS 6YO, and the lower legform impactor observed relatively close to the fixed coordinate system on the vehicle in cases 3.1, 3.2, 3.3, and 3.4 are shown in Figure 3.11. The kinematics of the lower legform impactor was similar to that of the modified THUMS at 20 ms; however, the bumper fascia bent the tibia of the modified THUMS. The tibia of the lower legform impactor was already detached from the bumper fascia, whereas the tibia of the modified THUMS was still in contact with the bumper fascia at 40 ms (see Figure 3.11).

The kinematics of the lower legform impactor was similar to that of THUMS AF05 at 20 ms; however, the bumper fascia bent the tibia of THUMS AF05. The tibia of the lower legform impactor was already detached from the bumper fascia, whereas the tibia of THUMS AF05 was still in contact with the bumper fascia at 40 ms (see Figure3.11).

The kinematics of the lower legform impactor was similar to that of THUMS 6YO at 20 ms; however, the bumper fascia bent the tibia of THUMS 6YO. The tibia of the lower legform impactor was already detached from the bumper fascia, whereas the tibia of THUMS 6YO was still in contact with the bumper fascia at 30 ms (see Figure 3.11).

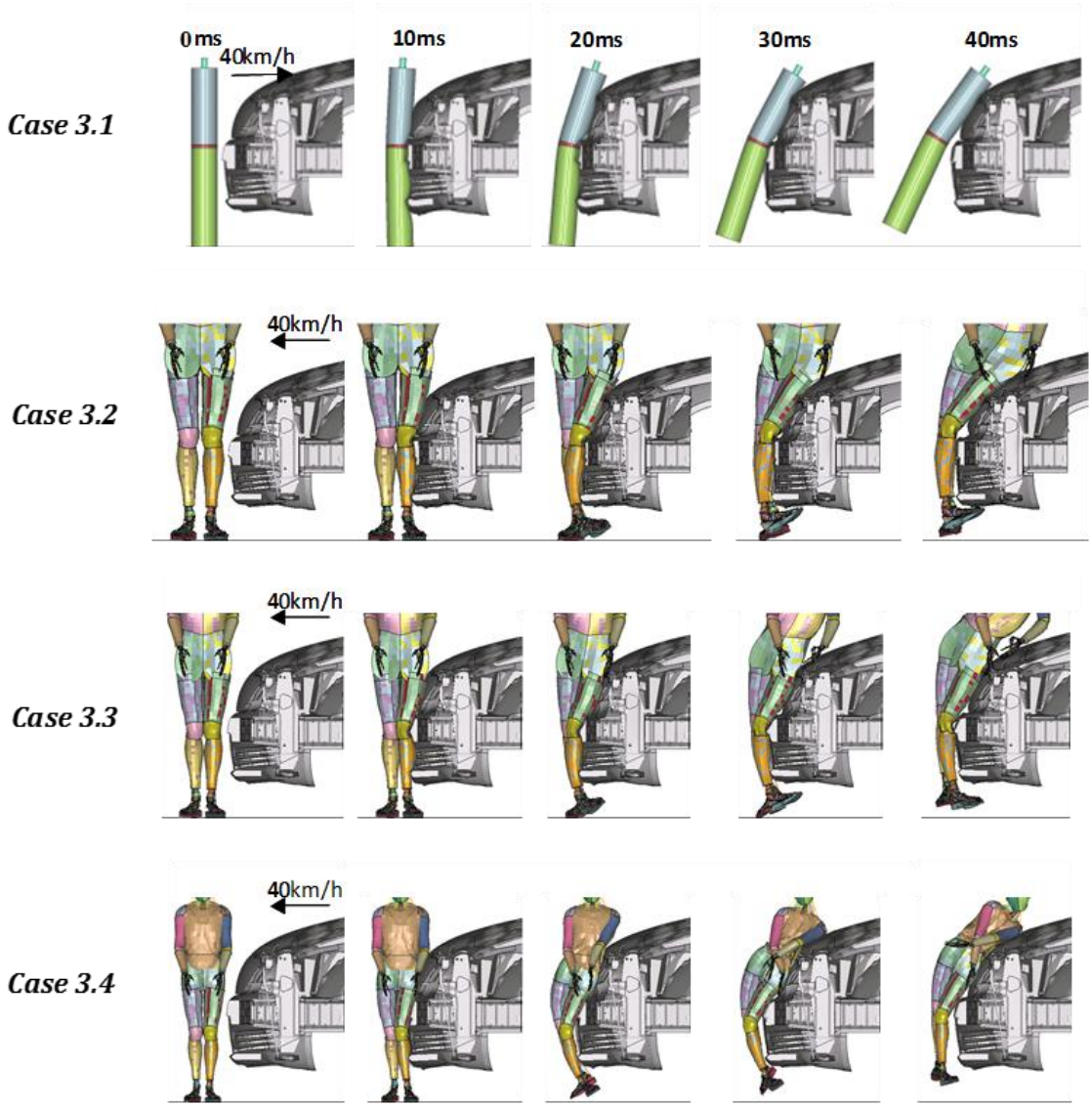

Figure 3.11. Kinematics of the lower legform impactor, modified THUMS, THUMS AF05, and THUMS 6YO.

3.3.2 Knee-bending angle and rupture of knee-joint ligaments

The knee-bending angle of the modified THUMS and the contact force acting on the left lower leg of the modified THUMS in case 3.2 are shown in Figure 3.12. First, the upper absorber came in contact with the knee joint and the upper tibia, and the knee-bending angle increased for 12 ms (see Figures 3.12). Next, the lower absorber came in contact with the tibia (see Figures 3.12). The tibia began to bend, while the knee-bending angle remained almost constant for 22 ms. The MCL of the modified THUMS ruptured at 27 ms. According to the time history of the contact forces acting on the lower leg shown in Figure 3.12, the risk of the occurrence of the fracture of the tibia

was high before 22 ms and the risk of the rupture of the MCL was high after 22 ms. If the stiffness of the lower absorber was considerably higher than that of the FE model of the vehicle in case 3.2, the tibia of the modified THUMS fractured before 22 ms. The tibia did not fracture in case 3.2 because the lower absorber shown in Figure 3.12 limited the contact force acting on the tibia to less than 3 kN.

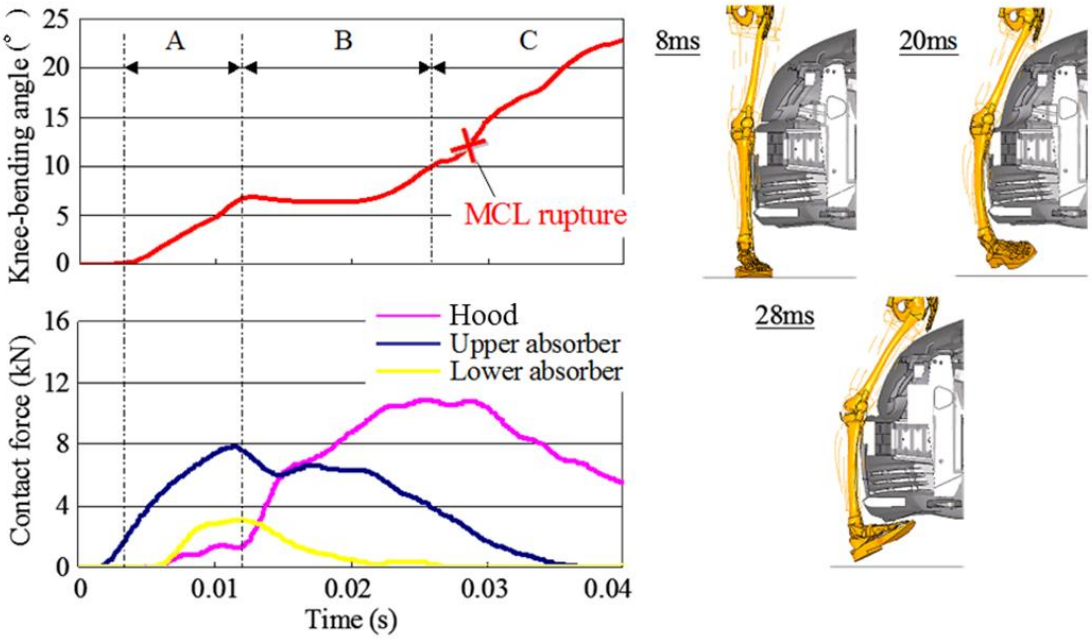

Figure 3.12. Knee-bending angles and contact forces of the modified THUMS.

3.3.3 Injury of knee joint

The injury measures of the lower legform impactor in case 3.1 are in marginal level for adults as shown in Table 3.1. However, injuries sustained in cases 3.2, 3.3, and 3.4 are the ruptures of the MCL of the modified THUMS, THUMS AF05, and THUMS 6YO (see Table 3.2). In case 3.4, THUMS 6YO sustained the rupture of ACL. No fracture of tibia sustained in all cases. It is important to recall that the locations of injuries sustained by the PMHS tests by Subit et al. (2008) as listed in Table 1.14 for cases of MSS-S and MSS-T (AM50%ile to sedan) are the knee joints and the pelvis, and are identical with those of case 3.2. Also, the locations of injuries sustained in case 3.2 (AM50%ile) are identical with those in cases 3.3 (AF05%ile) and 3.4 (6YO). Injuries sustained in case 3.3 and 3.4 suggest that the knee joint injuries are frequent for AF05% ile and 6YO pedestrians as well as AM50%ile pedestrians.

The deformation of the knee joint occurring in case 3.2 is shown in Figure 3.13. Bending and shearing of the knee joint of the modified THUMS seems to cause the rupture of MCL. The ligaments of the knee joint cannot transfer compression loads but tension loads. When the tibia and the thigh contact each other by lateral bending of the knee joint in Figure 3.13, the MCL, the ACL, and the PCL transfer the knee-bending moment of the knee joint. This load transfer at the knee joint in Figure 3.13 is coincident with the mechanism of the damage of the knee-joint ligaments by Kajzer et al. (1999) that the peak values of the shearing force and the bending moment related to the damage of the knee-joint ligaments.

Table 3.1
Injury Scales of the Lower Legform Impactor in Cases Involving Collision with a Vehicle

Knee-bending angle (deg)	14.8
Shear displacement (mm)	1.9
Upper tibia acceleration (G)	148

Table 3.2
Injuries Sustained by the Modified THUMS, THUMS AF05, and THUMS 6YO in Cases Involving Collision with a Vehicle

	Case 3.2	Case 3.3	Case 3.4
	modified THUMS	THUMS AF05	THUMS 6YO
MCL	Ruptured at 27 ms	Ruptured at 23 ms	Ruptured at 21 ms
ACL	Not ruptured	Not ruptured	Ruptured at 23 ms
PCL	Not ruptured	Not ruptured	Not ruptured
Tibia	Not fractured	Not fractured	Not fractured

MCL: Medial Collateral Ligament
ACL: Anterior Cruciate Ligament
PCL: Posterior Cruciate Ligament

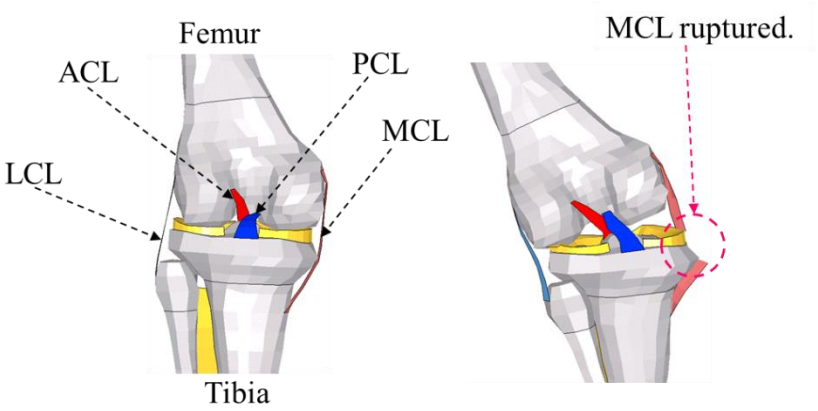

Figure 3.13. Ruptured knee-joint ligament of the modified THUMS.

3.4 Discussion

As reported by Subit et al. (2008), the injuries sustained by the lower leg of a PMHS impacted by a vehicle were mostly knee-joint injuries including the rupture of the ligaments of the knee joint (see Tables 1.14 and 1.15). The MCLs of the modified THUMS, THUMS AF05, and THUMS 6YO also ruptured (see Table 3.2).

In case 3.2, the MCL ruptured owing to the bending and shearing of the knee joint (see Figure 3.13). The knee-bending angle increased almost proportionally with the contact force generated by the upper absorber, for 12 ms (see Figures 3.12), whereas the upper absorber came in contact with the top of the tibia of the modified THUMS. One of the root causes of an increase in the knee-bending angle for 12 ms was the contact force generated by the upper absorber. The knee-bending angle in case 3.2 remained almost constant from 12 ms to 24 ms (see Figure 3.12), whereas the tibia of the modified THUMS was bent (see Figures 3.12). The knee-bending angle increased again from 24 ms, and the MCL ruptured at 27 ms (see Figures 3.12). The contact force generated by the upper absorber increased the knee-bending angle, the contact force generated by the lower absorber decreased the knee-bending angle, and the tibia-bending seems to interact with the knee-bending angle.

The upper absorber came in contact with the knee joint of THUMS AF05, and the injuries and kinematics of the lower legs of THUMS AF05 were similar to those of the modified THUMS in case 3.3. The upper absorber came in contact with the upper leg of THUMS 6YO, and the injuries and kinematics of the lower legs of THUMS 6YO were similar to those of the modified THUMS in case 3.4. The contact force generated by the

upper absorber affected the knee-bending angle in the case when the upper absorber came in contact with the thigh or the tibia within a certain distance from the knee joint.

3.5 Conclusions

Vehicular accidents involving pedestrians of various sizes and genders were reconstructed by using the human FE models of the modified THUMS, THUMS AF05, and THUMS 6YO. Ruptures of the ligaments of the knee joint were observed in each reconstructed accident, as in the case of a PMHS test reported by Subit et al. (2008) wherein a PMHS was impacted with a vehicle.

The rupture of the MCL of the knee joints of the modified THUMS was caused by the bending and shearing of the knee joint. An increase in the contact force generated by the upper absorber and a decrease in the contact force generated by the lower absorber were considered to be the possible factors responsible for causing an increase in the knee-bending angle.

4 Relationships between the shape and stiffness of a vehicle and the tibia and knee-joint ligament injuries

4.1 Introduction

Vehicular accidents involving pedestrians of various sizes and genders were reconstructed by using the human FE model described in chapter 3. The result of chapter 3 indicated that the contact forces generated by the upper bumper absorber and the lower bumper absorber are considered to be the possible factors responsible for causing an increase or decrease in the occurrence of injuries such as the fracture of the tibia and the rupture of the knee-joint ligaments. The objective of this chapter is to clarify the relationships between the characteristics of a vehicle such as its shape and stiffness and various injuries such as the fracture of the tibia and the rupture of the knee-joint ligaments through parametric studies using an FE model of urethane blocks, resembling the shape of the central section of a vehicle.

The kinematics of the human FE model impacted by the FE model of the urethane blocks is compared with the kinematics of the human FE model impacted by the FE model of a vehicle in order to validate the consistencies in the tibia and knee-joint ligament injuries. The position and stiffness of the FE model of the urethane blocks are modified, and the human FE model is impacted by the FE model of the urethane blocks. Parametric studies involving a change in the position and stiffness of the FE model of the urethane blocks are conducted, and the relationship between the parameters such as the position and stiffness of the FE model and the tibia and knee-joint ligament injuries is discussed.

4.2 Methods of parametric study

The FE model consisting of four urethane blocks resembles the shape of the central section of a vehicle. The modified THUMS, THUMS AF05, and THUMS 6YO used in cases 3.2, 3.3, and 3.4 in chapter 3 were again employed in the parametric studies (see Figure 4.1).

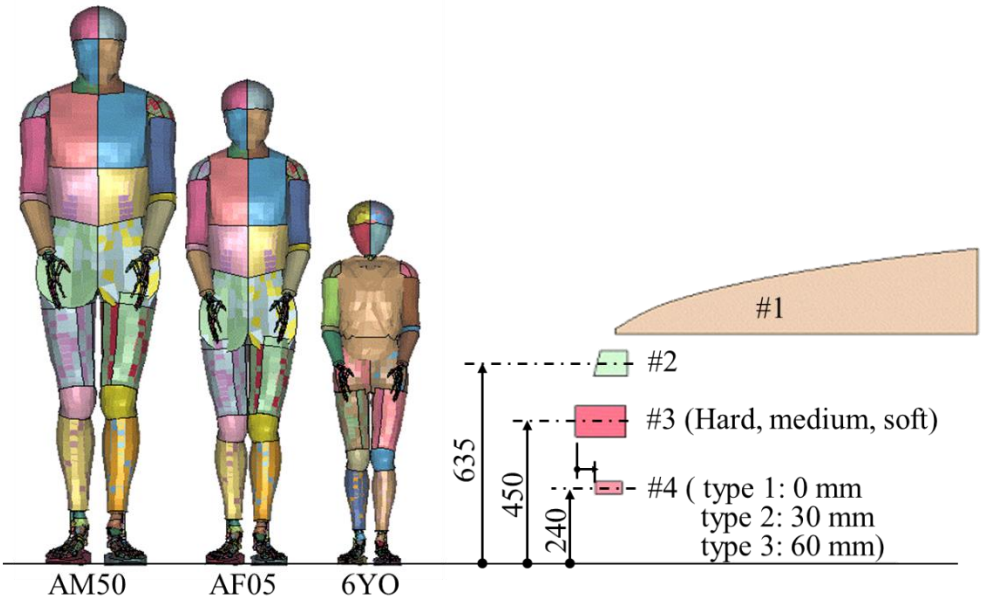

Figure 4.1. Urethane blocks resembling the central section of the front end of a vehicle and the human FE models of pedestrians.

4.2.1 FE model of urethane blocks

Urethane blocks included four blocks i.e., blocks #1, #2, #3, and #4, and fixed to the sled, as shown in Figure 4.1. These blocks represented the shape and stiffness of the hood panel, radiator grill, absorber of upper bumper, and absorber of lower bumper of a vehicle, respectively. The stiffness of these blocks was modeled using a solid element and material-type 181 (MAT_SIMPLIFIED_RUBBER) of LS-DYNA. This rubber model was defined by a single uniaxial load curve. The load curve is obtained from the contact forces of the modified THUMS in case 3.2 described in chapter 3, acting between the hood, radiator, upper bumper absorber, and lower bumper absorber of the vehicle.

In order to evaluate the stiffness of blocks #1, #2, #3, and #4, the blocks were made to collide with the modified THUMS at 40 km/h. The initial and boundary conditions for the evaluation were identical to those considered in case 3.2 in chapter 3. The contact forces acting between the four urethane blocks and the modified THUMS were shown as functions of the deformation of the blocks, and the function of deformation of the blocks showed fairly good correlation with case 3.2 described in chapter 3 (see Figures 4.2, 4.3, 4.4 (block #3: hard block), and 4.5). Contact forces acting between the absorber of the upper bumper/urethane block #3 and the modified THUMS are

dependent on the area of contact between them, when the block #3 came in contact with the modified THUMS. The urethane block #3 is more flexible than the upper bumper of the car, and the area of contact are bigger than the car. This difference in the contact is a reason for difference in the curves in Figure 4.4

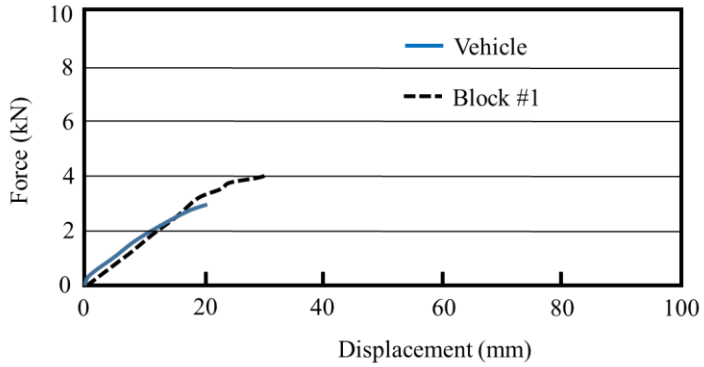

Figure 4.2. Contact forces acting between the hood panel/urethane block #1 and the modified THUMS.

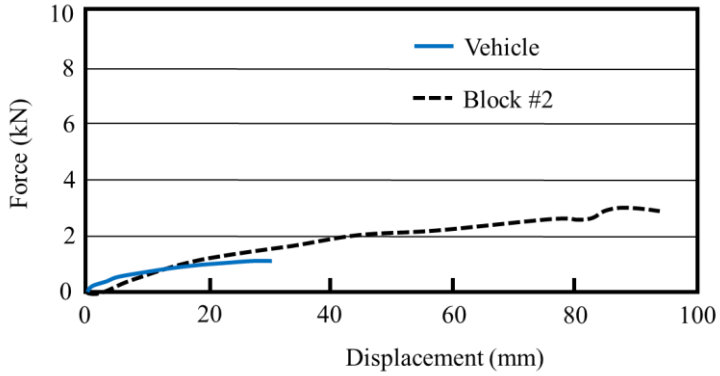

Figure 4.3. Contact forces acting between the radiator grill/urethane block #2 and the modified THUMS.

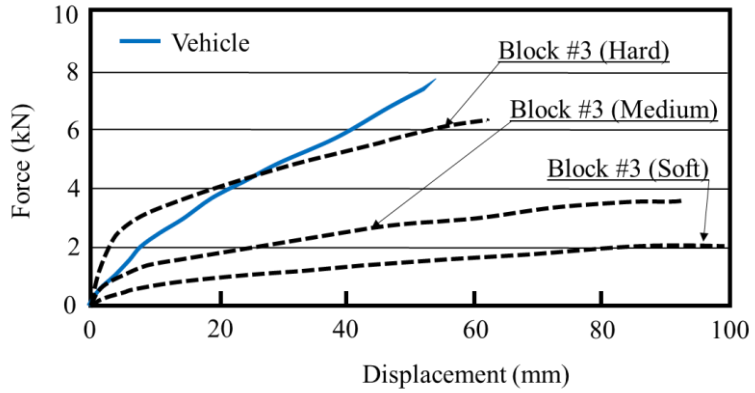

Figure 4.4. Contact forces acting between the absorber of the upper bumper/urethane block #3 and the modified THUMS.

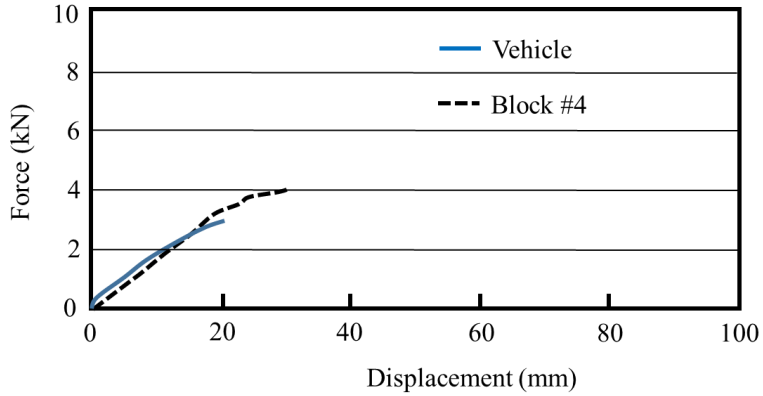

Figure 4.5. Contact forces acting between the absorber of the lower bumper/urethane block #4 and the modified THUMS.

4.2.2 Parametric studies

Two parameters, i.e., the longitudinal position of urethane block #4 (see Figure 4.6) and the contact force of urethane block #3 were studied. In the first longitudinal position of urethane block #4 shown in Figure 4.6, the urethane block was located 30 mm in front of the vehicle. This longitudinal position was expected to reduce the risk of injuries caused to the tibia. In the second longitudinal position of urethane block #4 shown in Figure 4.6, the urethane block was located in the same position as the vehicle. In the third longitudinal position of urethane block #4 shown in Figure 4.6, the urethane block was located 60 mm behind the vehicle.

The solid lines labeled as “Block #3 Medium” and “Block #3 Soft” were expected to reduce the contact force and the risk of occurrence of the knee-joint ligament injuries.

The modified THUMS, THUMS AF05, and THUMS 6YO stood stationary in front of the FE model of the urethane blocks, with their left legs forward. The knee joints of the left legs of the modified THUMS, THUMS AF05, and THUMS 6YO were located precisely at the central section of the FE model of the urethane blocks. The FE model of the urethane blocks collided with the modified THUMS, THUMS AF05, and THUMS 6YO at 40 km/h. Ruptures of ligaments of the knee joint were assumed not to rupture during the parametric studies in order to evaluate sensitivities of strain of the ligament to the parameters.

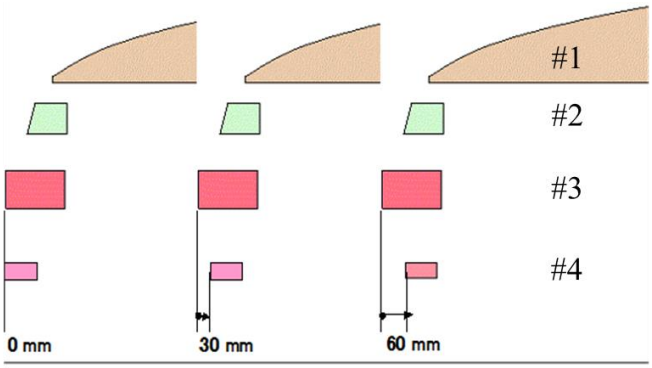

(a) Type 1 (b) Type 2 (c) Type 3

Figure 4.6. Longitudinal positions of urethane block #4.

Table 4.1
Cases of Parametric Study of Urethane Blocks #3 and #4

Case	Block #3	Block #4	THUMS
4.5.1			AM50
4.5.2	Hard	Type 1	AF05
4.5.3			6YO
4.6.1			AM50
4.6.2	Hard	Type 2	AF05
4.6.3			6YO
4.7.1			AM50
4.7.2	Hard	Type 3	AF05
4.7.3			6YO
4.8.1			AM50
4.8.2	Medium	Type 1	AF05
4.8.3			6YO
4.9.1			AM50
4.9.2	Medium	Type 2	AF05
4.9.3			6YO
4.10.1			AM50
4.10.2	Medium	Type 3	AF05
4.10.3			6YO
4.11.1			AM50
4.11.2	Soft	Type 1	AF05
4.11.3			6YO
4.12.1			AM50
4.12.2	Soft	Type 2	AF05
4.12.3			6YO
4.13.1			AM50
4.13.2	Soft	Type 3	AF05
4.13.3			6YO

4.3 Results

4.3.1 Kinematics

The kinematics of the lower leg of the modified THUMS, THUMS AF05, and THUMS 6YO in cases 4.7.1, 4.7.2, and 4.7.3 showed good correlations with those in cases 3.2, 3.3, and 3.4 described in chapter 3 in Figure 3.11, respectively (see Figures 4.7, 4.8, and 4.9). The FE model of the urethane blocks is suitable for use in parametric studies.

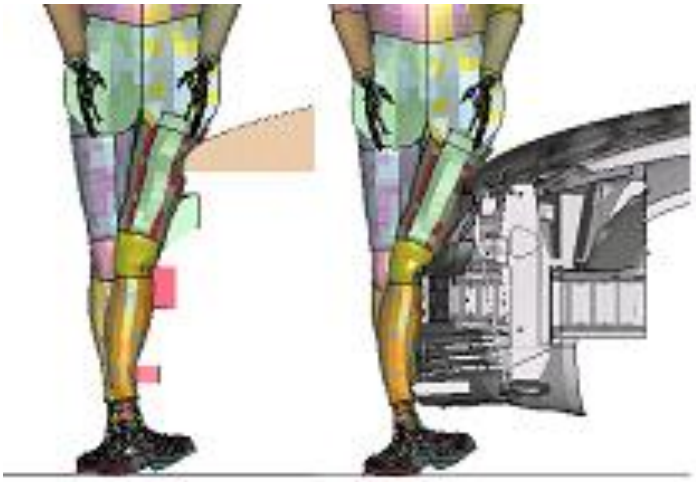

Figure 4.7. Comparison of the lower leg kinematics of the modified THUMS at 20 ms, with the urethane block (left) and the vehicle (right).

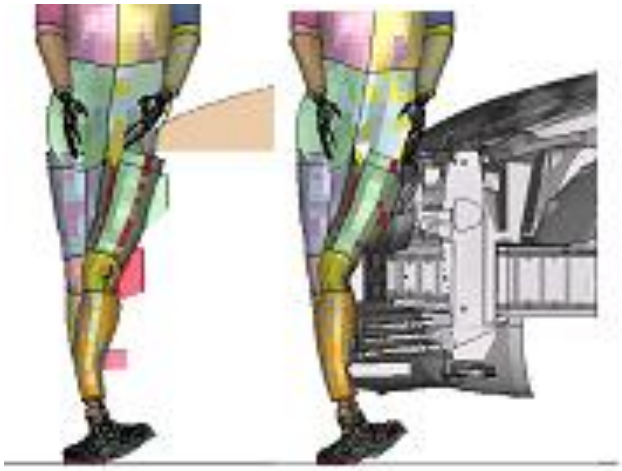

Figure 4.8. Comparison of the lower leg kinematics of THUMS AF05 at 20 ms, with the urethane block (left) and the vehicle (right).

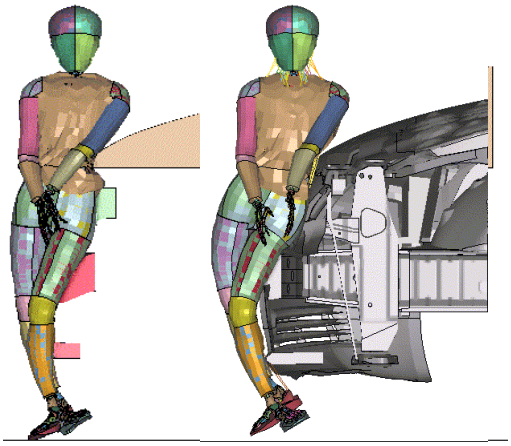

Figure 4.9. Comparison of the lower leg kinematics of THUMS 6YO at 20 ms, with the urethane block (left) and the vehicle (right).

4.3.2 Injury

The results of the lower leg injury sustained by THUMS, the maximum contact force of blocks #3 and #4, and the displacement of block #3 are summarized in Table 4.2. Ligaments of the knee-joint did not rupture in cases 4.8, 4.9, 4.11, 4.12, and 4.13 (see Table 4.2). Kinematics of no injury cases 4.9.1, 4.9.2, and 4.9.3 are shown in Figure 4.10.

Table 4.2
Lower Leg Injury of THUMS, Maximum Contact Force of Blocks #3 and 4, and Displacement of Block #3, (Element eliminations were not activated in all cases)

Case	Block #3	Block #4	THUMS	Lower leg injury		Maximum force (kN)		Displacement (mm)
				Knee-joint ligaments	Bone	Block #3	Block #4	Block #3
4.5.1	Hard	Type 1	AM50	None	None	7.9	4.5	65
4.5.2			AF05	None	None	7.5	4.7	68
4.5.3			6YO	MCL rupture	None	5.0	3.0	69
4.6.1	Hard	Type 2	AM50	None	None	8.5	4.0	71
4.6.2			AF05	None	None	8.4	4.3	76
4.6.3			6YO	MCL, ACL rupture	None	5.6	2.4	73
4.7.1	Hard	Type 3	AM50	MCL rupture	None	9.1	3.2	76
4.7.2			AF05	None	None	8.8	3.3	82
4.7.3			6YO	MCL rupture	None	5.9	1.6	76
4.8.1	Medium	Type 1	AM50	None	None	4.2	5.3	95
4.8.2			AF05	None	None	4.1	5.5	103
4.8.3			6YO	None	None	2.9	3.9	91
4.9.1	Medium	Type 2	AM50	None	None	4.8	5.2	102
4.9.2			AF05	None	None	4.8	5.4	112
4.9.3			6YO	None	None	3.2	2.9	102
4.10.1	Medium	Type 3	AM50	MCL rupture	None	5.2	4.8	108
4.10.2			AF05	None	None	5.3	4.9	117
4.10.3			6YO	MCL rupture	None	3.6	2.4	107
4.11.1	Soft	Type 1	AM50	None	None	2.5	6.1	113
4.11.2			AF05	None	None	2.5	5.8	123
4.11.3			6YO	None	None	1.7	4.5	110
4.12.1	Soft	Type 2	AM50	None	None	2.9	5.8	121
4.12.2			AF05	None	None	2.8	6.0	133
4.12.3			6YO	None	None	2.0	3.8	118
4.13.1	Soft	Type 3	AM50	None	None	3.0	5.5	129
4.13.2			AF05	None	None	3.6	5.8	139
4.13.3			6YO	None	None	2.6	3.3	134

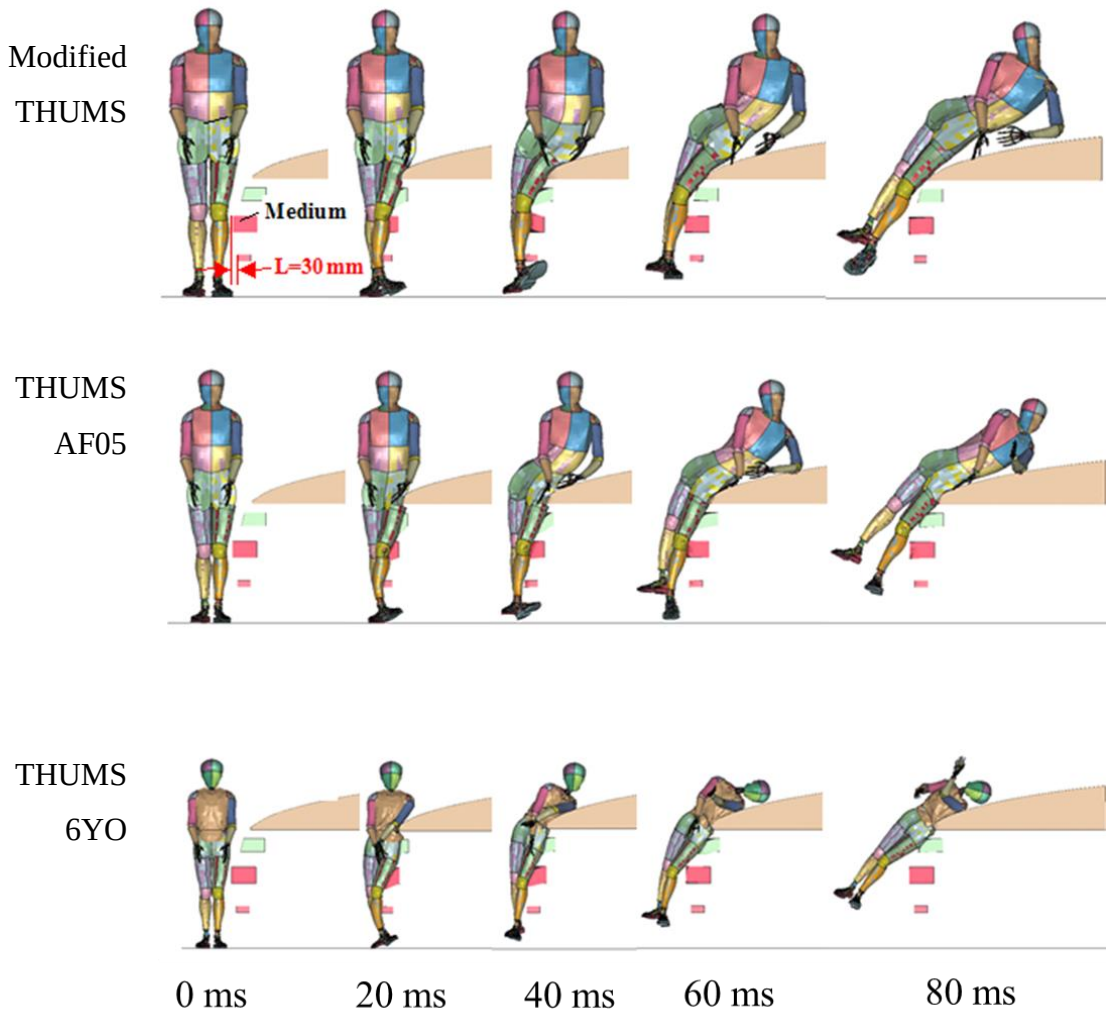

Figure 4.10. Kinematics of the FE model of a pedestrian in cases 4.9.1, 4.9.2, and 4.9.3 (cases in which no lower leg injury was observed).

4.3.3 Relationships between the strain of the MCL and the stiffness of block #3 and position of block #4

The MCL of the modified THUMS began to rupture when the principal plastic strain of the MCL of the knee joint exceeded 11%. Hereafter, the principal plastic strain of the MCL is simply referred to as "strain." The strain distributions of the modified THUMS, THUMS AF05, and THUMS 6YO as functions of the stiffness of block #3 and the position of block #4 are shown in Figures 4.11, 4.12, and 4.13, respectively.

The maximum value of the strain of the modified THUMS depended on the position of block #4 (see Figure 4.11). In these parametric studies, the first and second

longitudinal positions of block #4 could prevent the strain of the modified THUMS from exceeding 11%. The maximum values of the strain of THUMS AF05 depended on the stiffness of block #3 (see Figure 4.12). Further, the stiffness of the soft and medium block #3 could prevent the strain of THUMS AF05 from exceeding 11%. The maximum value of the strain of THUMS 6YO depended on the stiffness of block #3 (see Figure 4.13). The stiffness of the soft and medium block #3 could prevent the strain of THUMS 6YO from exceeding 11%.

The optimum stiffness of block #3 and the position of block #4 for the modified THUMS, THUMS AF05, and THUMS 6YO were determined by superimposing the feasible areas shown in Figures 4.11, 4.12, and 4.13. The feasible area is defined as the area where the strain is less than 11%. The area painted and described “No rupture” in Figure 4.14 indicates the optimum combination of the stiffness of block #3 and the position of block #4. The area in Figure 4.14 indicates the feasible areas only for the modified THUMS, THUMS AF05, and THUMS 6YO.

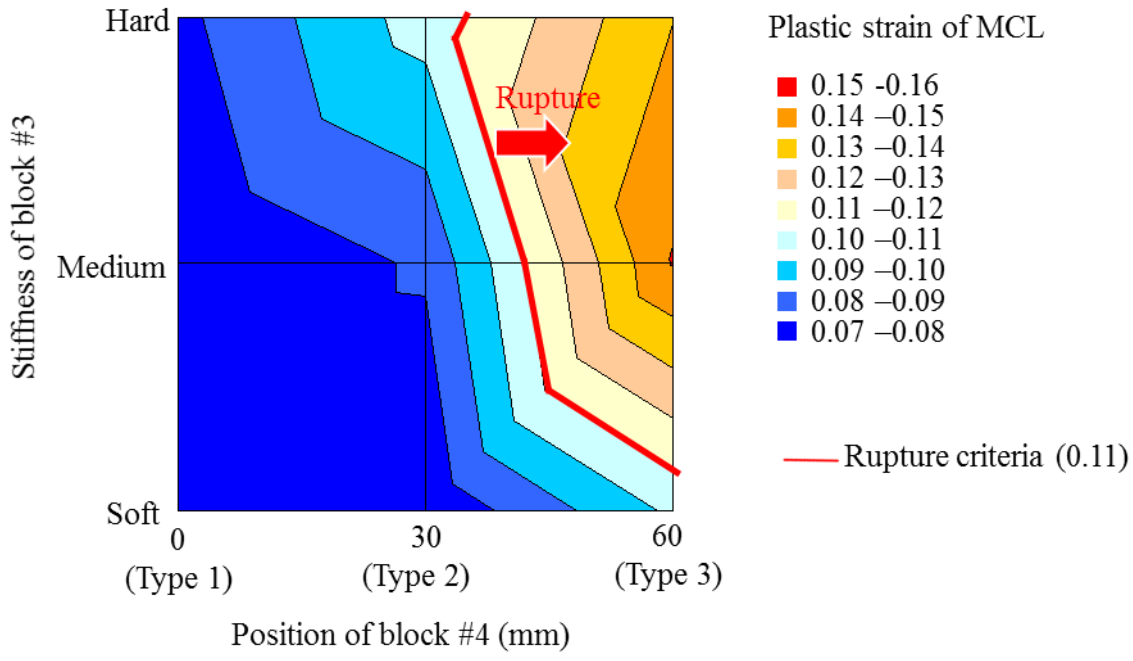

Figure 4.11. Relationships between the MCL strain of the modified THUMS and the stiffness of block #3 and position of block #4.

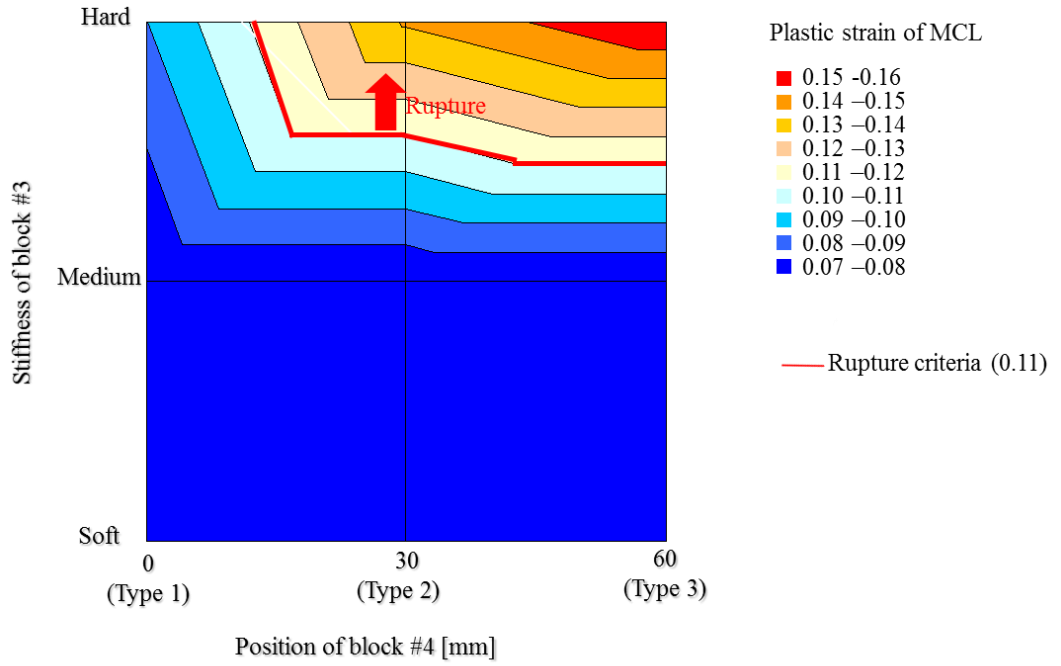

Figure 4.12. Relationships between the MCL strain of THUMS AF05 and blocks #3 and #4.

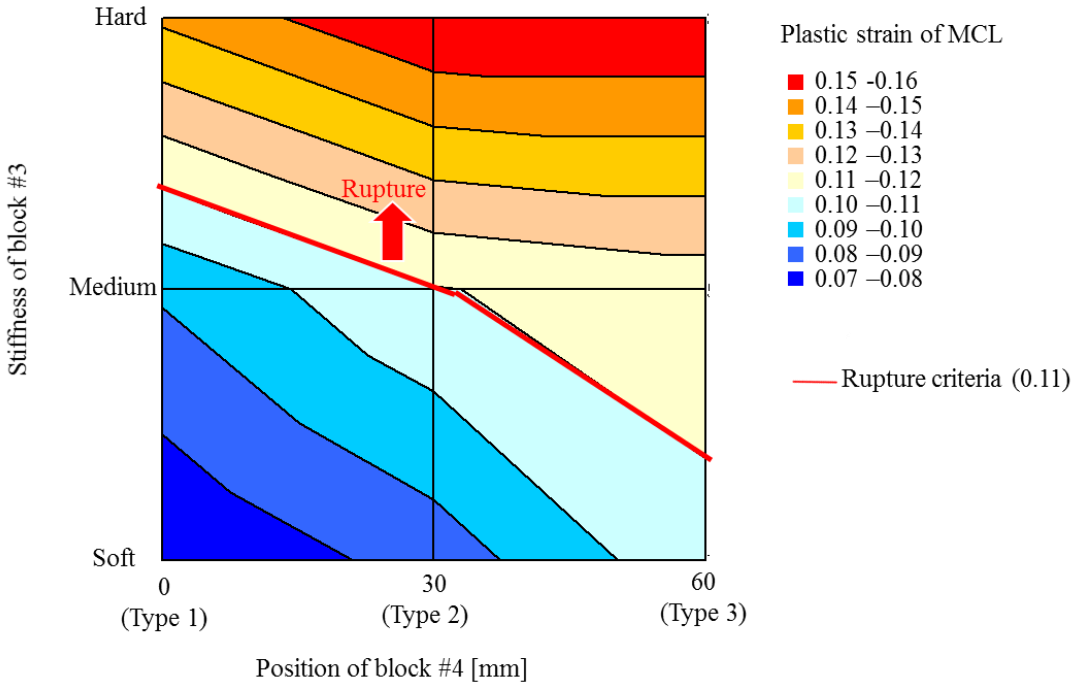

Figure 4.13. Relationships between the MCL strain of THUMS 6YO and blocks #3 and #4.

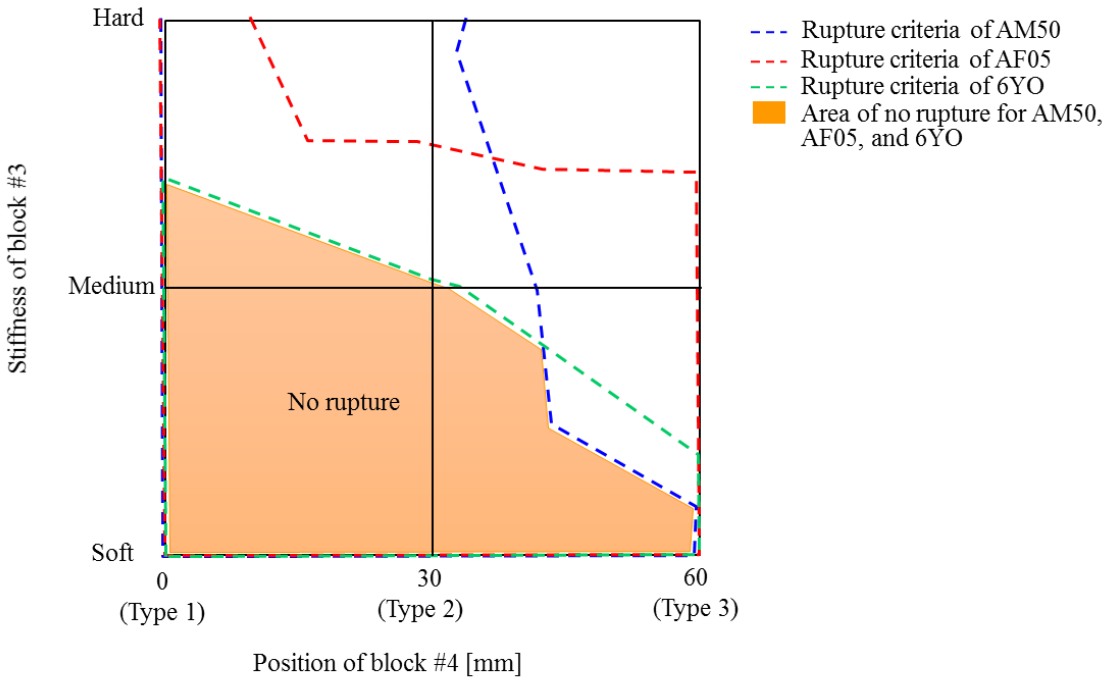

Figure 4.14. Deformation of block #3 and feasible areas that prevent MCL rupture.

4.4 Discussion

The modified THUMS, THUMS AF05, and THUMS 6YO showed different relationships between the strain and the stiffness of block #3 and position of block #4. The maximum values of strain obtained by the parametric studies were observed at around 20 ms. The kinematics of the lower legs of the modified THUMS, THUMS AF05, and THUMS 6YO at 20 ms are shown in Figures 4.7, 4.8, and 4.9, respectively. The tibia of the modified THUMS was in contact with blocks #3 and #4. The tibia of THUMS AF05 was in contact with block #4.The knee joint of THUMS AF05 was in contact with block #3. The tibia of THUMS 6YO was in contact with block #4. The femur of THUMS 6YO was in contact with block #3 (see Figures 4.7, 4.8, and 4.9). These differences in the contact locations may give rise to different relationships between the strain and the stiffness of block #3 and the position of block #4 among the modified THUMS, THUMS AF05, and THUMS 6YO. In another words, it seems that the knee bending angle at 20 ms is sensitive to the contact locations of the bumper to the tibia and the femur. The sensitivities of the knee-bending angle to the contact locations of the bumper to the tibia and the femur are discussed.

The tibia is assumed to be rigid and two dimensional (2D), and the knee joint and the femur are not taken account to simplify the discussion as shown in Figures 4.15. In the first case, the rigid body, which is impacted at the center of the gravity, translates to the left without rotation as indicated by dotted lines in Figure 4.15 (Left). In the second case, the rigid body, which is impacted at below the center of the gravity, translates to the left with rotation as indicated by dotted lines in Figure 4.15 (Right). Larger offset of the external force from the center of gravity causes larger rotation of the rigid body around the center of gravity and less translation of the center of gravity.

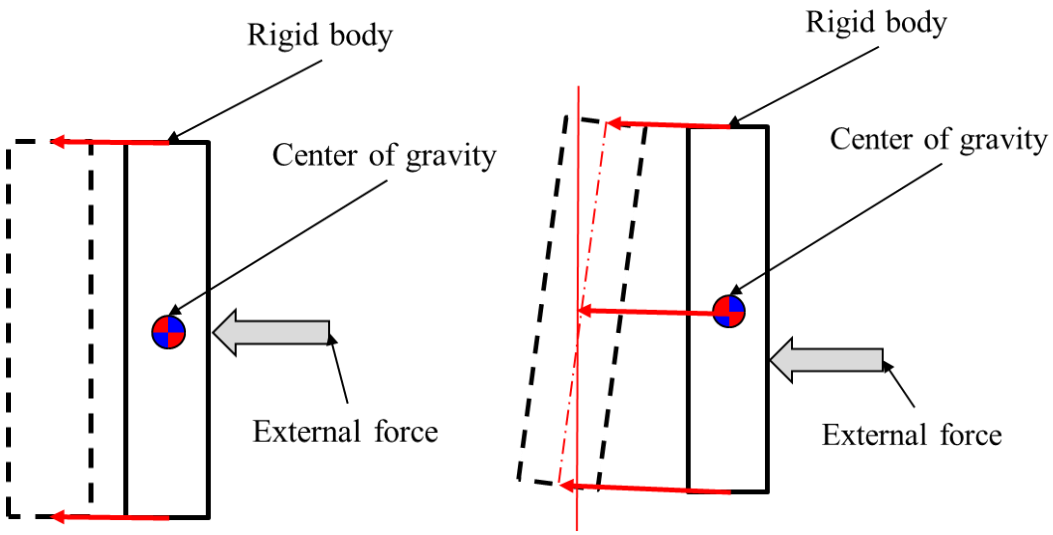

Figure 4.15. Schematic view of the motion of the rigid body impacting at the center of gravity (Left) and below the center of gravity (Right).

In the third case, two rigid bodies, which have the same mass properties and were connected by a rotational joint, are impacted at the mechanical joint as shown in Figure 4.16 (Left). The centers of the gravity of the rigid bodies 1 and 2 translate to the left with clockwise and counter clockwise rotations as indicated by dotted lines in Figure 4.16, respectively. Rotation angle of the mechanical joint (Knee-bending angle) is defined as difference of rotation angles of the rigid body 1 and the rigid body 2 in Figure 4.16. In the fourth case, two rigid bodies, which have the same mass properties and were connected by a rotational joint, are impacted at below the mechanical joint as shown in Figure 4.16 (Right). The translation of the rigid body 1 in the fourth case is larger than the third case, and the rotation translation of the rigid body 1 in the fourth

case is smaller than the third case. These estimations of 2D kinematic of the rigid bodies suggest that the translation and the rotation the rigid body motion are sensitive to the location of the external force. If flexibility of the lower extremities of pedestrians are ignored and assumed to be rigid, the offset of the external forces from the center of gravities of the tibia and the femur is one of root causes of the sensitivities of the knee-bending angle to the contact locations of the bumper to the tibia and the femur.

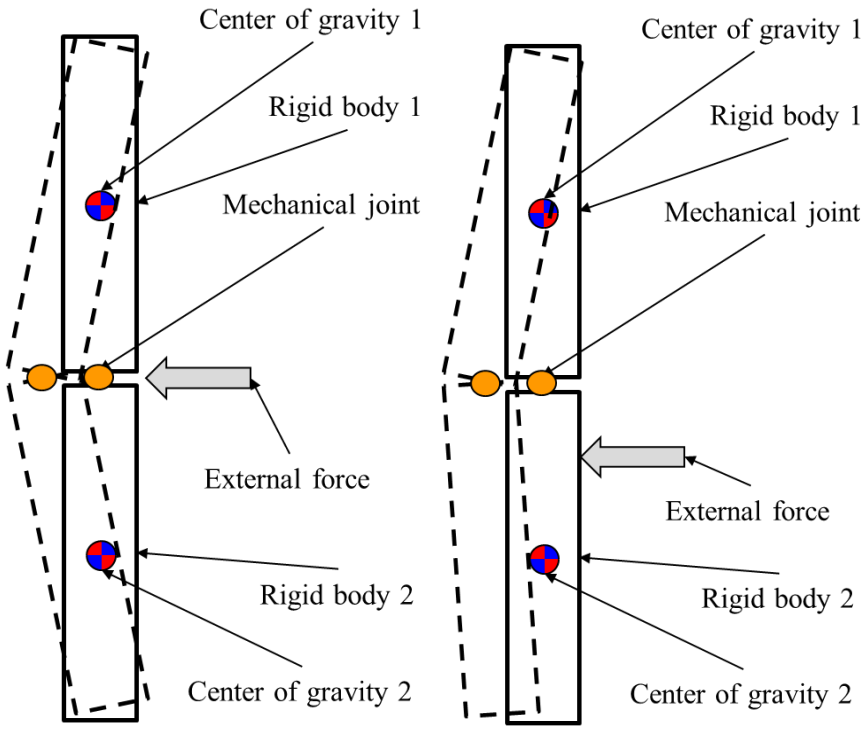

Figure 4.16 Schematic view of the motion of the rigid bodies impacting at the mechanical joint (Left) and below the mechanical joint (Right).

4.5 Conclusions

Vehicular accidents involving pedestrians of different sizes and genders, involving the collision of a pedestrian with a vehicle at 40 km/h were, reconstructed by using the modified THUMS, THUMS AF05, and THUMS 6YO. Rupture of the knee-joint ligaments was observed in each reconstructed accident scenario.

The relationships between the principal plastic strain of the MCL of the knee-joint ligament and the stiffness of the front end of a vehicle were investigated by varying the stiffness of the urethane blocks, whose stiffness is equivalent to that of a vehicle. The

principal plastic strain of the MCL of the knee joint of the modified THUMS mostly depended on the stiffness of the lower bumper absorber. The principal plastic strain of the MCL of the knee joint of THUMS AF05 and THUMS 6YO mostly depended on the stiffness of the upper bumper absorber.

A parametric study was conducted to determine an optimum combination of the stiffness of the upper bumper absorber and the position of the lower bumper absorber that did not cause the MCL rupture. The effects of the mass, center of gravity, and moment of inertia of the pelvis, upper leg, and lower leg on the knee-bending angle are still unknown.

5 Assessment of tibia and knee-joint ligament injuries sustained by a pedestrian impacted by an SUV

5.1 Introduction

The crash configurations of the front end of an SUV and a vehicle impacting AM50%ile pedestrians differ from each other (see Figures 5.1 and 5.2). In Figure 5.2, the hood panel may come in contact with the abdomen of the AM50%ile pedestrian. The upper bumper absorber may come in contact with the femur of the AM50%ile pedestrian. The lower bumper absorber may come in contact with the knee joint of the AM50%ile pedestrian. The crash configurations indicated that the mechanism of occurrence of the tibia and knee-joint ligament injuries sustained by a pedestrian impacted by an SUV differs from that of the occurrence of the tibia and knee-joint ligament injuries sustained by a pedestrian impacted by a sedan.

The objective of the study described in this chapter is to assess the tibia and knee-joint ligament injuries sustained by an AM50%ile pedestrian through numerical accident reconstructions that precisely simulate the shape and the stiffness of the front end of an SUV.

5.2 Method

Two numerical simulations of pedestrian accidents were performed (see Figure 5.1 and 5.2). In case 5.1 (see Figure 5.1), the lower legform impactor collided with the center of the SUV in a still condition following the EEVC WG17 protocol (European Enhanced vehicle-safety Committee, 1996) at 40 km/h. In case 5.2 (see Figure 5.2), the SUV collided with an AM50%ile pedestrian standing still on the ground, at 40 km/h.

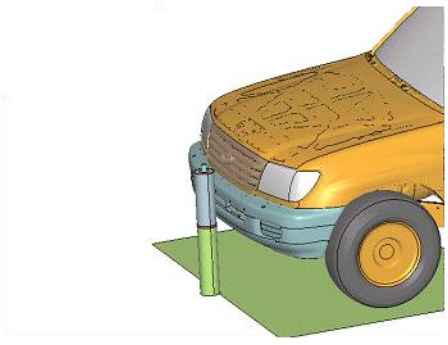

Figure 5.1. Test configuration of the lower legform impactor impacting the SUV.

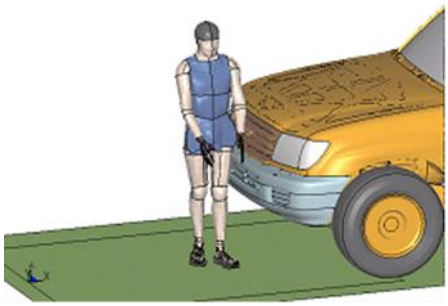

Figure 5.2. Configuration of an accident where a pedestrian was impacted by the SUV.

5.2.1 FE model of the pedestrian

The FE model of the lower legform impactor for case 5.1 was identical to that described in chapter 3. Further, the FE model of the pedestrian for case 5.2 was that of the modified THUMS and identical to that described in chapter 3.

5.2.2 FE model of the SUV

An FE model of the SUV was established (see Figure 5.3). The bumper of the SUV was reinforced at the same height as that of the knee joint of the modified THUMS. A lower legform impactor test following the EURO-NCAP (European Enhanced vehicle-safety Committee, 1996) protocol was performed in order to validate the stiffness of the front end of the FE model of the SUV. The kinematics, upper tibia acceleration, and knee-bending angle of the FE model showed fairly good correlations with those of the test results (see Figures 5.4, 5.5 and 5.6). The lower legform impactor in the test impacted a slightly higher position than in the simulation and the accelerometer measuring the acceleration of the upper tibia seemed to contact the bumper reinforcement at 8 ms and 16 ms (see Figure 5.4). Difference in the impact position is a reason of fairly good correlations of upper tibia acceleration.

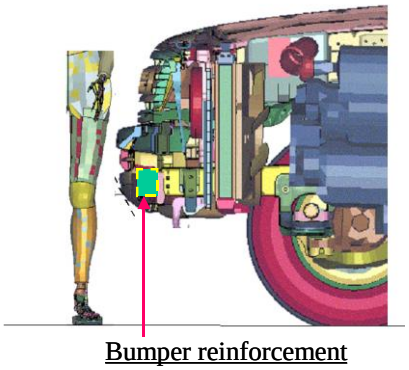

Figure 5.3. FE model of the SUV and the lower extremity of the modified THUMS.

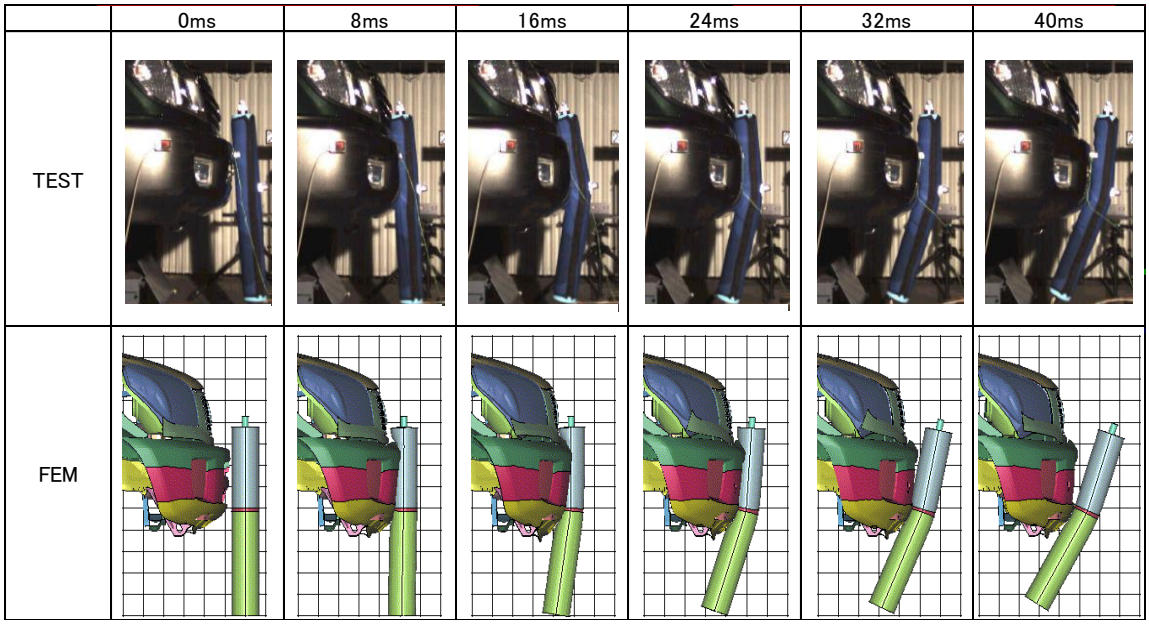

Figure 5.4. Comparison between the kinematics of the lower legform impactor by the test for the lower legform impactor EEVC WG17 protocol and the FE simulation for case 5.1.

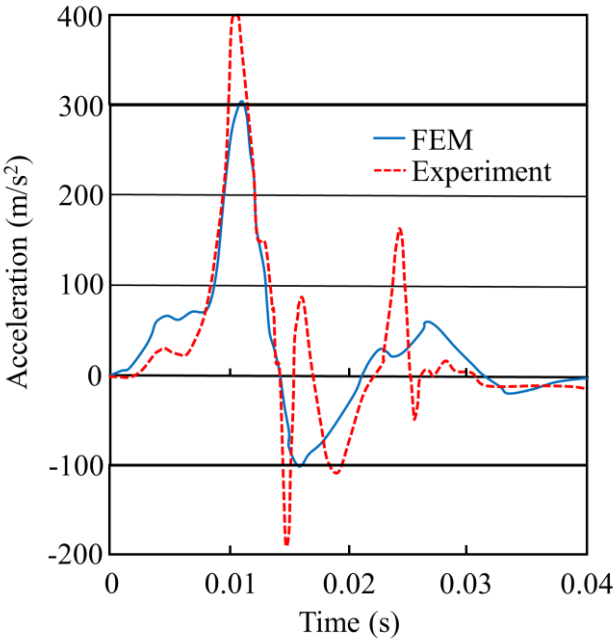

Figure 5.5. Comparison between the acceleration of the upper tibia of the lower legform impactor by the test and the FE simulation for case 5.1.

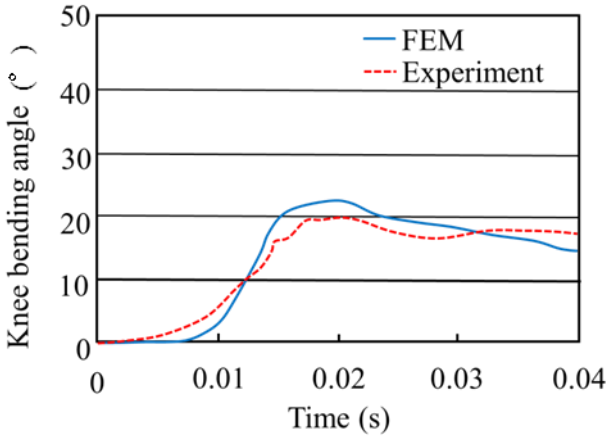

Figure 5.6. Comparison between the knee-bending angle of the lower legform impactor by the test and the FE simulation for case 5.1.

5.2.3 Initial conditions

The modified THUMS stood still in front of the FE model of the SUV, with its left leg forward. The knee joint of the left leg of the modified THUMS was precisely located at the center of the FE model of the SUV. The FE model of the SUV collided with the modified THUMS at a velocity of 40 km/h. Pedestrians involved in the accidents did not have solenoid release systems similar to the test described in chapter 2. Therefore, the initial vertical velocity of the modified THUMS was assumed to be 0 m/s.

5.3 Results

5.3.1 Kinematics

The kinematics of the modified THUMS and the lower legform impactor observed at coordinates fixed on the SUV for cases 5.1 and 5.2 are shown in Figure 5.7. The time histories of the knee-bending angle are shown Figure 5.8. The tibia of the modified THUMS and the lower legform impactor did not come in contact with the bumper and continued to rotate in the anti-clockwise direction, as shown in Figure 5.7. The femur of the modified THUMS continued to remain in contact for 40 ms. The femur of the lower legform impactor continued to remain in contact with the bumper and the radiator grill for 20 ms, and it detached from them at 40 ms (see Figure 5.7). The knee-bending angle of the modified THUMS was coincident with that of the lower legform impactor for 12 ms (see Figure 5.8). The maximum knee-bending angles of the modified THUMS and the lower legform impactor were 25° and 22°, respectively. The knee-bending angle of the lower legform impactor began to decrease at 20 ms (see Figure 5.8).

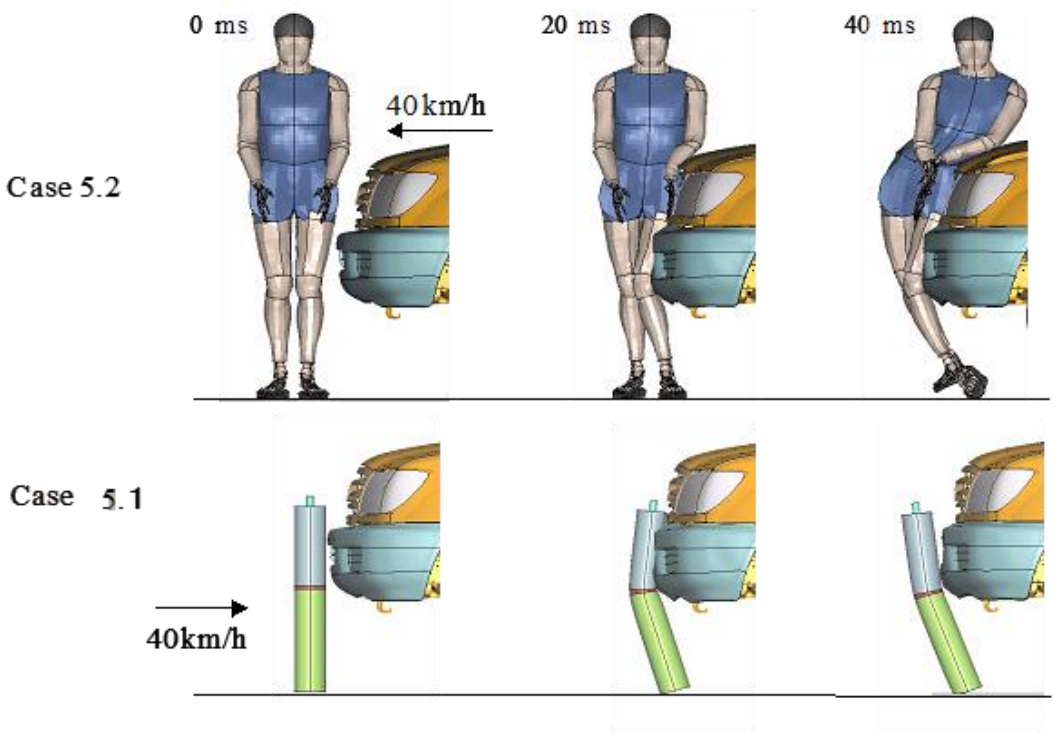

Figure 5.7. Comparison between the kinematics of the modified THUMS for case 5.2 and that of the lower legform impactor for case 5.1.

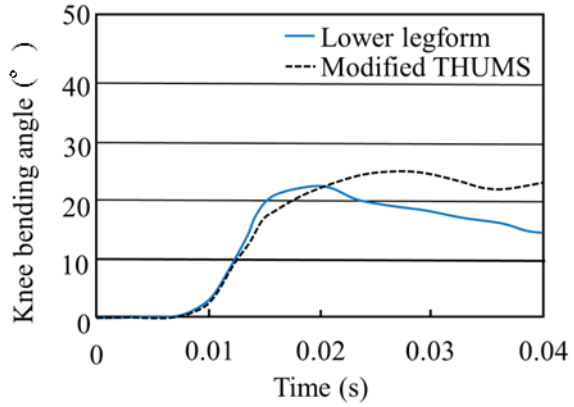

Figure 5.8. Comparison between the time history of the knee-bending angle of the modified THUMS for case 5.2 and that of the knee-bending angle of the lower legform impactor for case 5.1.

5.3.2 Injury

The injury scales for case 5.1 are listed in Table 5.1. The injuries sustained by the modified THUMS for case 5.2 are listed in Table 5.2. The MCL and ACL of the modified THUMS ruptured. The femur bone of the modified THUMS fractured.

Table 5.1
Injury Scales of the Lower Legform Impactor Impacted by the SUV for Case 5.1

	Case 5.1
Injury scales	TRL lower leg subsystem
Knee-bending angle	19.7 [deg]
Shear deformation	5.6 [mm]
Upper tibia acceleration	302 [G]

Table 5.2
Injuries of the Modified THUMS Impacted by the SUV for Case 5.2

	Case 5.2
Location of injury	modified THUMS
MCL	Ruptured
ACL	Ruptured
PCL	Not ruptured
Tibia	Not ruptured
Femur	Fractured

5.4 Discussion

The knee-bending angle of the lower legform impactor is an injury scale for evaluating the knee-joint injuries sustained by pedestrians. The maximum knee-bending angle of the lower legform impactor for case 5.1 was 22° at 20 ms (see Figure 5.8). The tibia and the knee joint of the lower legform impactor were not in contact from 5 ms to 20 ms (see Figure 5.7). Further, the tibia of the lower legform impactor was not subjected to any contact force from 5 ms to 20 ms. Then, the inertia force of the tibia was responsible for increasing the knee-bending angle of the lower legform impactor from 5 ms to 20 ms. The knee-bending angle of the lower legform impactor began to decrease at 20 ms (see Figure 5.8). The femur of the lower legform impactor began to decrease at 20 ms, and it detached from the radiator grill and the bumper at 40 ms. However, the femur of the modified THUMS continued to remain in contact with the radiator grill and the bumper at 40 ms. After 20 ms, the kinematics of the femur of the modified THUMS differed from that of the lower legform impactor; this difference in the kinematics is the root cause of the difference in the knee-bending angle between the modified THUMS and the lower legform impactor. This difference in the kinematics occurred after 20 ms, and the addition of the mass of the pelvis to the top of the lower legform impactor is an estimated countermeasure for reducing this difference.

The MCL and ACL of the modified THUMS ruptured (see Table 5.2). The knee-bending angle of the modified THUMS increased from 5 ms to 27 ms, and the tibia of the modified THUMS was not in contact for 40 ms (see Figures 5.7 and 5.8). The lack of the contact force of the tibia of the modified THUMS caused the tibia of the modified THUMS to rotate for 27 ms. An addition of a lower bumper that enables the contact of the pedestrian’s tibia with the SUV will reduce the knee-bending angle as well as the risk of the rupture of the MCL and the ACL.

5.5 Conclusions

A vehicular accident involving the collision of an AM50%ile pedestrian with an SUV was reconstructed though an FE simulation using the modified THUMS. In this simulation, the knee ligaments ruptured and the femur fractured. The ruptures of the

MCL and the ACL of the knee joints of the modified THUMS were caused by the bending of the knee joint owing to the rotation of the tibia. The lack of the contact force of the tibia was a possible factor responsible for increasing the knee-bending angle. The knee-bending angle of the lower legform impactor was less than that of the modified THUMS, and the addition of the mass of the pelvis was expected to increase the knee-bending angle of the lower legform impactor.

6 Relationships between the stiffness of an SUV and the tibia and knee-joint ligament injuries

6.1 Introduction

In chapter 5, the injury sustained by an AM50%ile pedestrian after colliding with an SUV was simulated using the FE model of a human. The lack of a contact force of the tibia caused the tibia to rotate and was a possible factor responsible for increasing the knee-bending angle. The objective of this chapter is to seek a solution for reducing the knee-bending angle by optimizing the stiffness of the upper bumper absorber of an SUV. An FE model of urethane blocks, which resembled the central section of the SUV, was used in the parametric study instead of an FE model of the SUV.

First, the kinematics of the human FE model impacted by the FE model of the urethane blocks is compared with that of the human FE model impacted by an SUV, in order to validate the consistency of the tibia and knee-joint ligament injuries sustained by a pedestrian between the FE model of the urethane block and the SUV. Next, the stiffness of the urethane blocks was modified, and the tibia and knee-joint ligament injuries sustained by the pedestrian were assessed using the modified THUMS.

6.2 Methods of parametric study

6.2.1 Human FE model

The modified THUMS previously described in chapter 3 was used for the parametric studies in this chapter.

6.2.2 FE model of urethane blocks

The FE model of urethane blocks consisted of six parts fixed to the sled. Hereafter, these blocks are referred to as blocks #1, #2, #3, #4, #5, and #6 (see Figure 6.1). Block #1 resembled the hood of the vehicle in terms of its shape and stiffness. Blocks #2 and #3 resembled the radiator grill in terms of its shape and stiffness. Block #4 resembled the upper bumper in terms of its shape and stiffness. Block #5 resembled the middle bumper in terms of its shape and stiffness. Block #6 resembled the lower bumper in terms of its shape and stiffness (see Figure 6.2). Seven parametric studies were conducted, as shown in Table 6.1, and the material properties of the urethane blocks are listed in Table 6.2. Urethane material causes volumetric change in absorbing energy,

and the material properties of the urethane in this simulation are indicated by pressure and volumetric strain curves (see Figure 6.3). For example, type 10 in Figure 6.3 stands for 10 times foamed in volume material. The stiffness of the six blocks shown in Figure 6.1 was similar to that measured in Figure 5.2 in chapter 5.

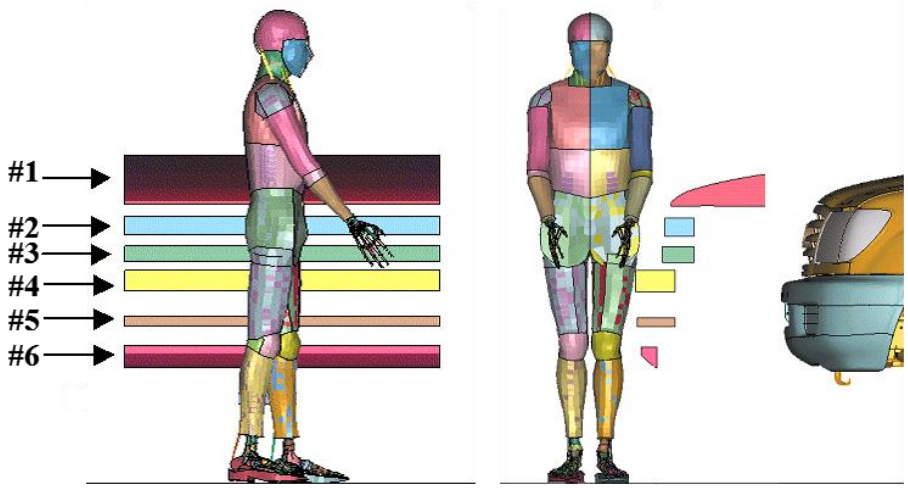

Figure 6.1. Arrangement of urethane blocks and the modified THUMS.

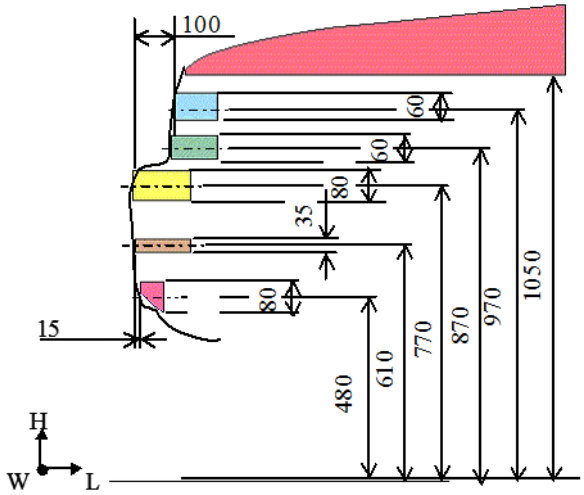

Figure 6.2. Sectional shape of the urethane blocks.

Table 6.1
Type of Urethane Block Used for Parametric Studies

	Type of block					
Case	#1	#2	#3	#4	#5	#6
6.1	10	30	30	10	30	30
6.2	10	30	30	30	30	30
6.3	10	30	30	40	30	30
6.4	50	50	50	50	50	50
6.5	60	60	60	60	60	60
6.6	70	70	70	70	70	70
6.7	100	100	100	100	100	100

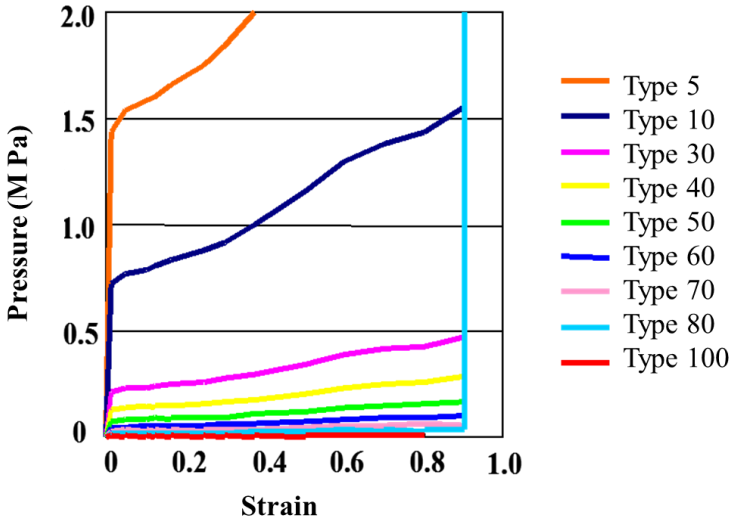

Figure 6.3. Material properties of the urethane blocks used for parametric studies.

The modified THUMS stood still in front of the FE model of the urethane blocks, with its left leg forward. The knee joint of the left leg of the modified THUMS was precisely located at the central section of the FE model of the urethane blocks. The FE model of the urethane blocks collided with the modified THUMS at a velocity of 40 km/h. Ruptures of ligaments of the knee joint were assumed not to rupture during the parametric studies in order to evaluate sensitivities of strain of the ligament to the parameters.

6.3 Results

6.3.1 Kinematics

The kinematics of the modified THUMS observed at fixed coordinates on the SUV for case 5.2 discussed in chapter 5 and Figure 6.1 in this chapter are shown in Figure 6.4. The kinematics of the modified THUMS impacted by the urethane blocks showed fairly good agreement with that of the modified THUMS impacted by the FE model of the SUV. The femur of the modified THUMS came in contact with urethane blocks #4 and #5. The knee joint of the modified THUMS came in contact with urethane block #6. The top of the tibia of the modified THUMS came in contact with urethane block #6 at 40 ms.

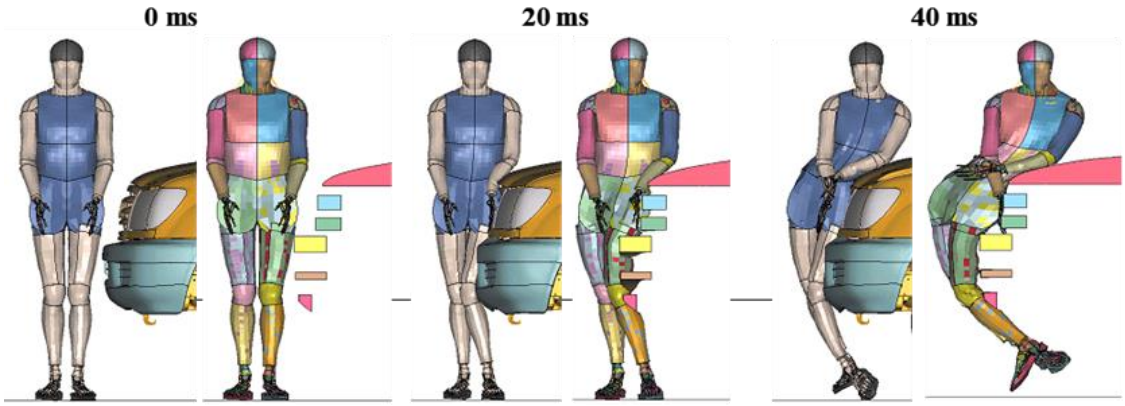

Figure 6.4. Kinematics of the modified THUMS for case 5.2 (SUV, left) and case 6.1(Urethane block, right) at 0 ms, 20 ms, and 40 ms.

6.3.2 Injury

The results of the parametric studies are summarized in Table 6.2. As shown in this table, the femur bone fractured in case 6.1. Further, the femur bone did not fracture in cases 6.2 and 6.3 when the stiffness of urethane block #4 was reduced. The ligaments of the knee joint ruptured in cases 6.1, 6.2, and 6.3.The ligaments of the knee joint also ruptured in cases 6.4, 6.5, and 6.6 when the stiffness of urethane blocks #1, #2, #3, #4, #5, and #6 was reduced. The ligaments of the knee joint did not rupture in case 6.7. The deformation of each urethane block was greater than 480 mm in case 6.7.

Table 6.2
Injuries Sustained by the Modified THUMS, Contact Force of the Urethane Blocks, and Deformation of the Urethane Blocks Observed by the Parametric Studies

	Type of block						Ligament	Bone	Max. force (kN)						Deformation (mm)					
Case	#1	#2	#3	#4	#5	#6	rupture	fracture	#1	#2	#3	#4	#5	#6	#1	#2	#3	#4	#5	#6
6.1	10	30	30	10	30	30	MCL, PCL	Femur	3	3	2	15	1	4	8	25	13	12	17	42
6.2	10	30	30	30	30	30	MCL, PCL	None	4	3	3	9	1	7	10	28	83	83	19	45
6.3	10	30	30	40	30	30	MCL, PCL	None	5	3	3	8	2	4	15	39	92	92	52	32
6.4	50	50	50	50	50	50	MCL	None	3	3	3	5	2	6	97	120	220	220	182	160
6.5	60	60	60	60	60	60	MCL	None	2	3	2	3	2	2	148	174	271	271	241	250
6.6	70	70	70	70	70	70	MCL	None	2	2	2	2	2	2	218	237	326	326	283	270
6.7	100	100	100	100	100	100	None	None	1	2	1	2	3	1	499	480	568	568	534	500

6.4 Discussion

6.4.1 Relationships between the femur fracture and the stiffness of block #4

The femur of the modified THUMS fractured at 10 ms in case 6.1. Urethane block #4 came in contact with the femur of the modified THUMS, and the magnitude of the contact force was 15 kN (see Table 6.2). The femur of the modified THUMS did not fracture in cases 6.2 and 6.3. Urethane block #4 came in contact with the femur of the modified THUMS, and the magnitude of the contact force was 9 kN (see Table 6.2). The static concentrated load that was perpendicularly applied to the bone at the center of the femur caused the bone to fracture at 5 kN (Yamada 1970). The contact forces in cases 6.2 and 6.3 were greater than 8 kN. However, the femur bone of the modified THUMS did not fracture in cases 6.2 and 6.3. Yamada's test included the static loading cases, and the simulation in this chapter included the dynamic loading cases. In this chapter, the manner in which the dynamic loading condition had an effect on the contact force of the femur is discussed.

The average lateral acceleration measured at 8 nodes of the FE model of the femur cortical bone of the modified THUMS at 10 ms in case 6.1 was around 900 m/s^2. The mass of the thigh of the modified THUMS including the femur, muscle, fat, and skin was around 10 kg. Therefore, the inertia force at the thigh at 10 ms in case 6.1 is 9 kN. 14 kN is determined to be the estimated contact force that may cause the femur of the modified THUMS to fracture in case 6.1 when the inertia force is added to the static bone fracture load of the femur at 5 kN. This is the main reason why the femur did not fracture in cases 6.2 and 6.3, although the contact force of the femur exceeded 5 kN,

which is the static loading criteria determined from the three-point bending test performed by Yamada (1979).

6.4.2 Relationships between the stiffness of block #6 and the MCL rupture

Block #6 came in contact with the knee joint of the modified THUMS, and the MCL of the modified THUMS ruptured at 20 ms in case 6.1 (see Figure 6.5). The rupture of the MCL seems to be caused by the knee-bending deformation, and not by the knee shearing deformation shown in Figure 6.5. The tibia of the modified THUMS did not come in contact with any block, and no block prevented the tibia of the modified THUMS from rotating in the anti-clockwise direction before 20 ms, as shown in Figure 6.4. The knee-bending angle increased rapidly in a short time duration from 10 ms to 20 ms (see Figure 5.8). A decrease in the knee-bending angle caused by a decrease in the stiffness of block #6 was expected to enable a decrease in the risk of the rupture of the MCL of the modified THUMS. Then, parametric studies involving a decrease in the stiffness of block #6 were performed in cases 6.4, 6.5, 6.6, and 6.7. The decrease in the stiffness of each block was not effective in reducing the risk of rupture of the MCL of the modified THUMS (see Table 6.2). The MCL of the modified THUMS did not rupture in case 6.7 (see Figure 6.6). The deformation of block #4 in case 6.6 was 326 mm. The deformation of block #4 in case 6.7 was 568 mm. Deformation of block #6 greater than 326 mm was necessary to reduce the risk of rupture of the MCL of the modified THUMS. Further research that takes into account the effects of supporting the tibia of the modified THUMS is required for investigating the rupture mechanism of the MCL of the modified THUMS.

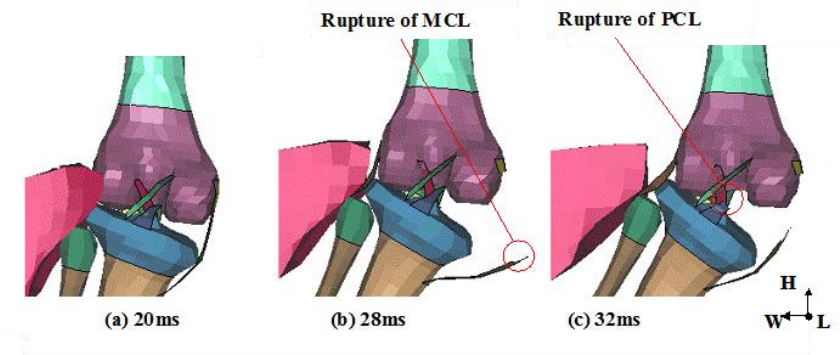

Figure 6.5. Rupture of the knee-joint ligaments of the modified THUMS in case 6.1.

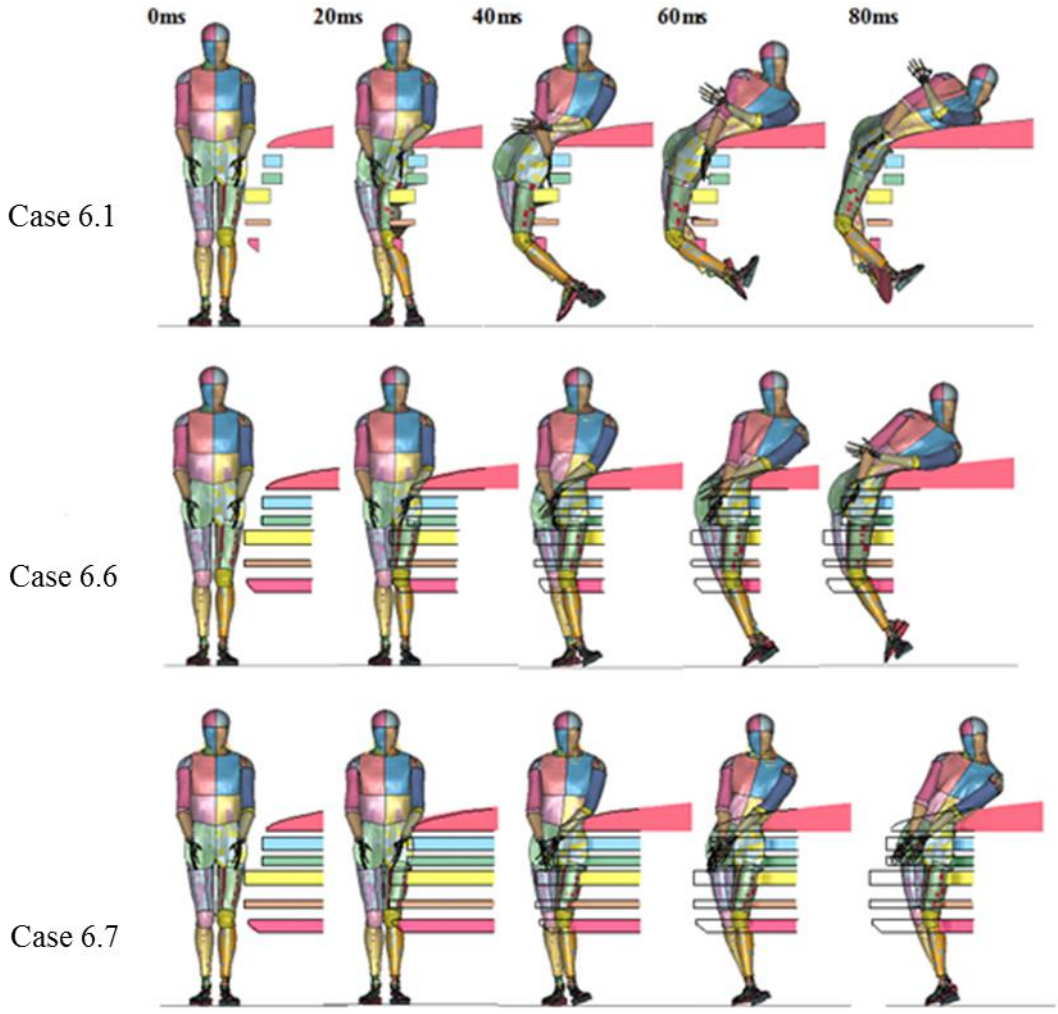

Figure 6.6. Kinematics of the modified THUMS in cases 6.1, 6.6, and 6.7.

6.5 Conclusions

Relationships between stiffness of an SUV and injuries such as the tibia and knee-joint ligament injuries were investigated using the modified THUMS.

An FE model of the urethane blocks, whose shape and stiffness were identical to those of the front end of the SUV, was established. Parametric studies involving a change in the stiffness of the urethane blocks indicated that the femur bone of the modified THUMS fractured when the contact force to the thigh exceeded 15 kN. A decrease in the stiffness of the block at the same height as the femur was effective in reducing the risk of fracture of the femur.

Further, a decrease in the stiffness of each block was not effective in reducing the risk of rupture of the MCL of the modified THUMS. Further research that takes into account the effects of supporting the tibia of the modified THUMS is required for investigating the MCL rupture mechanism of the modified THUMS.

7 Comparative study of the kinematics and injury sustained by the lower leg of the modified THUMS with the lower legform impactor

7.1 Introduction

The kinematics of the modified THUMS and the lower legform impactor were compared, the results of which showed that the kinematics of the lower legform impactor differed from that of the modified THUMS discussed in chapters 3 and 5.

The objective of this chapter is to clarify the cause of the difference in the kinematics of the lower legform impactor and that of the modified THUMS. In this chapter, several mechanical characteristics of the lower legform impactor were compared with those of the modified THUMS in order to identify the biofidelity of the lower legform impactor. Further, the contact forces of the lower legform impactor impacted by a vehicle were compared with those of the modified THUMS in order to identify the effect of different shapes of the lower legform impactor on the modified THUMS. The time history of the knee-bending angle of the lower legform impactor was compared with that of the modified THUMS in order to identify the effects of the bending deformation of the tibia of the modified THUMS on the knee-bending angle.

7.2 Mechanical characteristics of the lower legform impactor

The mechanical characteristics of the lower leg and the knee joint were compared with those of the modified THUMS.

7.2.1 Lower leg

The lower legs of the lower legform impactor and the modified THUMS are shown in Figure 7.1. The lower legs of the lower legform impactor are considerably stiffer than those of the modified THUMS. The tibia of a PMHS and THUMS can deform around 15 mm before fracturing (see Figure 7.2).

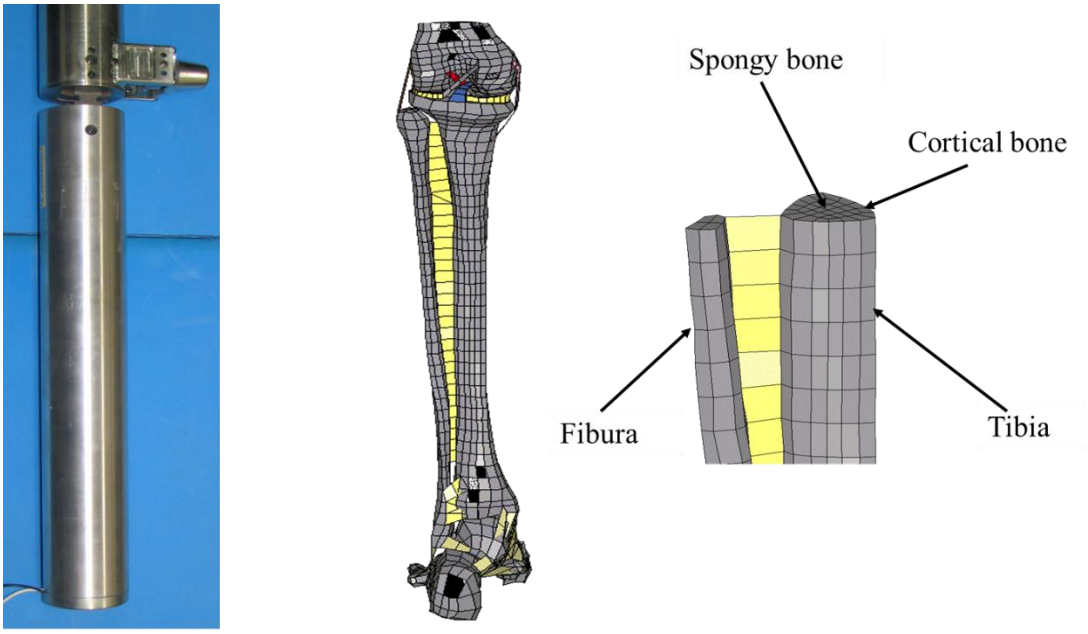

(a) Lower legform impactor (b) Modified THUMS

Figure 7.1. Lower leg of the lower legform impactor and the modified THUMS.

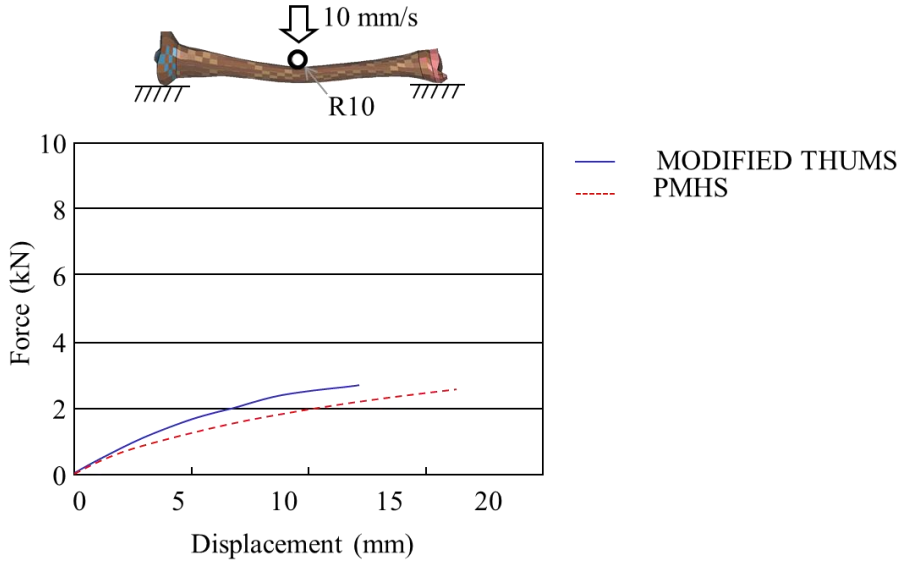

Figure 7.2. Bending stiffness of the tibia bones; adapted from (Yamada 1970).

7.2.2 Knee joint

The knee joints of the lower legform impactor and the modified THUMS are shown Figure 7.3. The knee joint of the lower legform impactor was made of a steel plate, and the plastic deformation of this steel plate simulates the knee-bending

resistance. The knee joint of the modified THUMS consists of the ACL, MCL, PCL, LCL, and the meniscus, and the elongation of the ACL, MCL, PCL, and LCL and the compression of the meniscus generate the knee-bending resistance. The knee joint of the lower legform impactor is stiffer than that of the modified THUMS and that of the PMHS (see Figure 7.4).

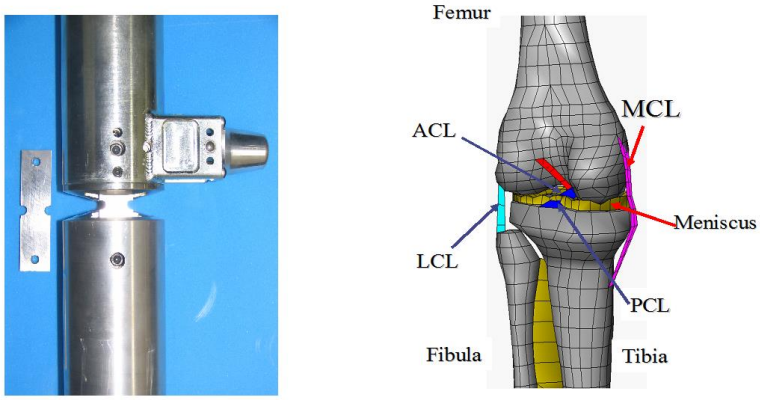

(a) Lower legform impactor (b) Modified THUMS

Figure 7.3. Knee joints of the lower legform impactor and the modified THUMS.

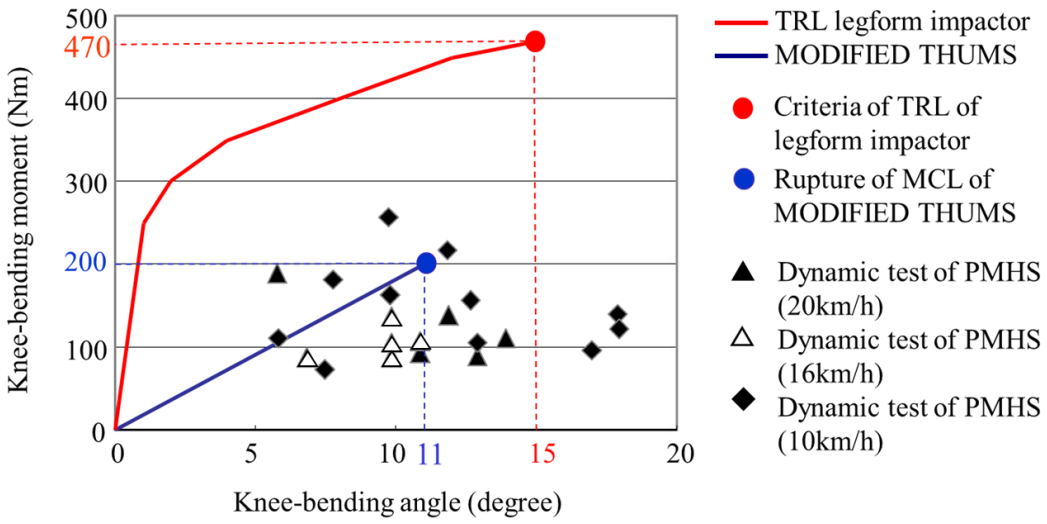

Figure 7.4. Knee-joint bending stiffness; adapted from Kajzer et al. (1997); Kajzer et al. (1999); and Levine et al. (1984).

7.2.3 Kinematics and contact forces

The kinematics of the lower legform impactor differed from that of the modified THUMS. The lower leg of the lower legform impactor rebounded from the vehicle at 40

ms (see Figure 7.5). Possible reasons for this rebounding included the contact forces between the pedestrian and the vehicle.

The contact forces are shown in Figure 7.6. The maximum contact force of the upper bumper absorber to the lower legform impactor was around 9 kN and that to the modified THUMS was around 8 kN. The maximum contact force of the lower bumper absorber to the lower legform impactor was around 5.5 kN and that to the modified THUMS was around 3 kN. The maximum contact force of the hood to the lower legform impactor was around 4 kN and that to the modified THUMS was around 4 kN.

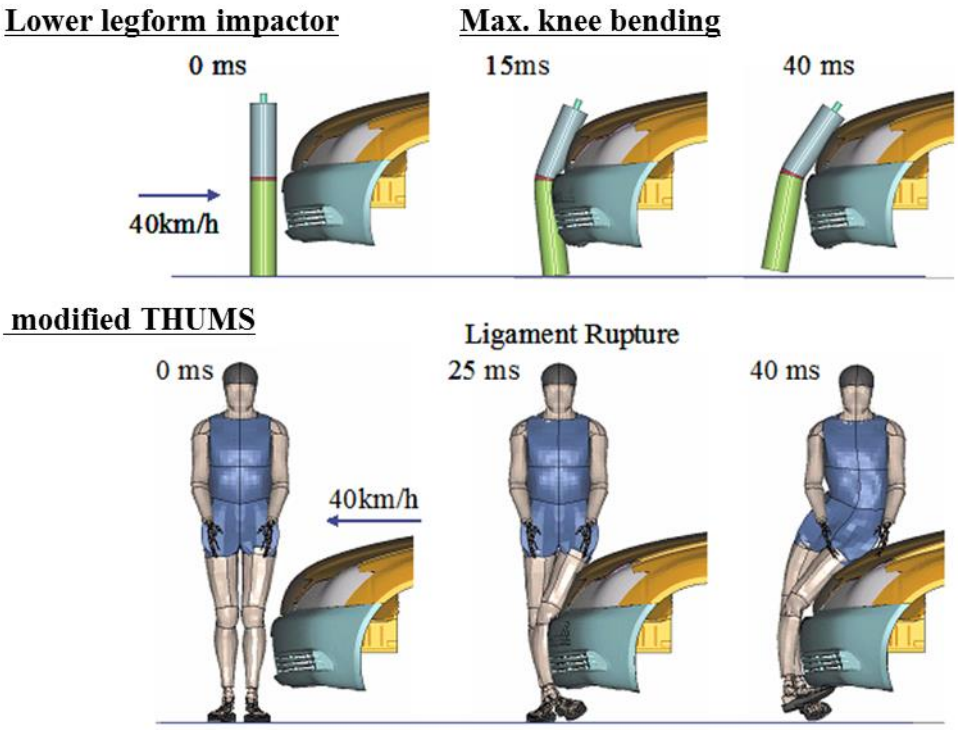

Figure 7.5. Comparison of the kinematics of the modified THUMS with that of the lower legform impactor.

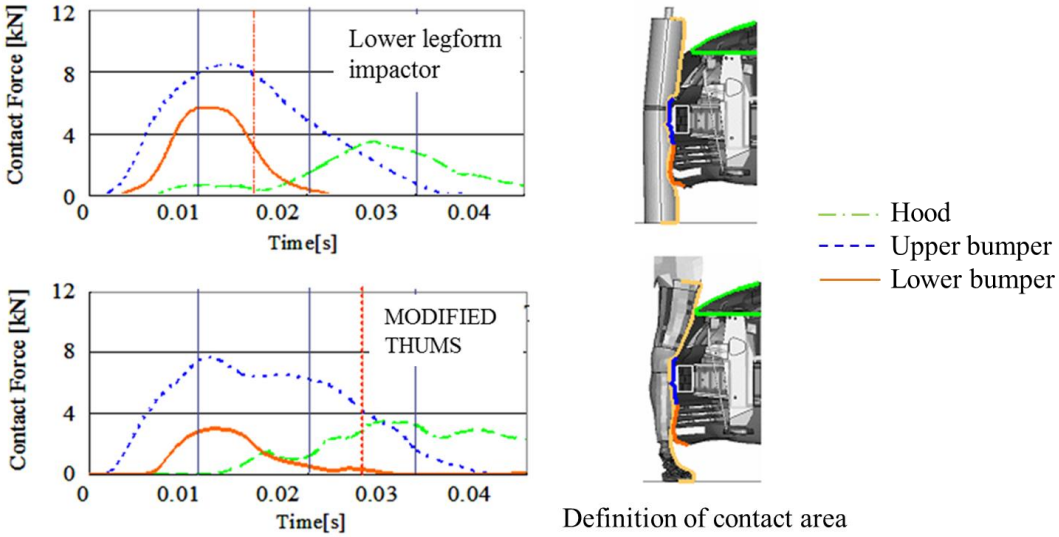

Figure 7.6. Comparison of the contact forces generated by the modified THUMS with those generated by the lower legform impactor.

7.2.4 Knee-bending angle

The knee-bending angle and the tibia-bending angle of the modified THUMS are shown in Figure 7.7. Definitions of the knee-bending angle and the tibia-bending angle of the modified THUMS were identical to those in the case of the lower legform impactor. The knee-bending angle of the modified THUMS remained constant from 10 ms to 22 ms, whereas the tibia-bending angle increased. The knee-bending angle of the modified THUMS increased from 20 ms, whereas the tibia-bending angle decreased. At 27 ms, the MCL of the modified THUMS ruptured.

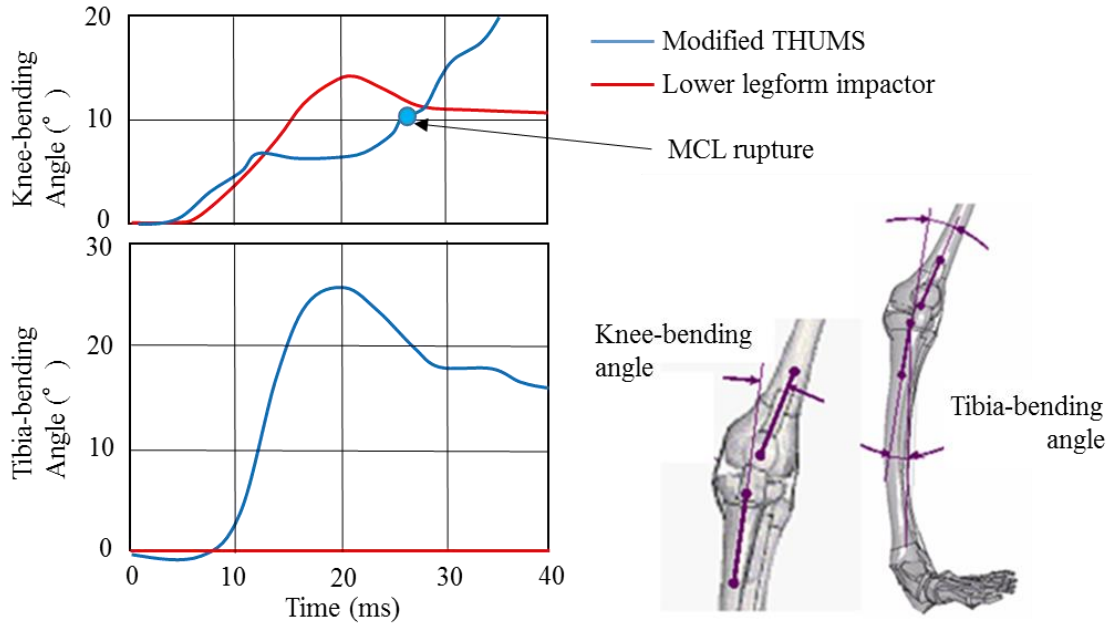

Figure 7.7. Comparison of the knee-bending angles using the modified THUMS and the lower legform impactor.

7.3 Discussion

7.3.1 Potential risk of injuries

The time history of the knee-bending angle and the tibia-bending angle of the modified THUMS was not as straightforward as that of the lower legform impactor (see Figure 7.7). The knee-bending angle and the tibia-bending angle of the modified THUMS increased from 0 ms to 12 ms. It should be noted that the contact force of the upper bumper absorber was responsible for increasing the knee-bending angle and that of the lower bumper absorber was responsible for increasing the tibia-bending angle from 0 ms to 12 ms. The knee-bending angle of the modified THUMS was constant, and the tibia-bending angle of the modified THUMS increased from 12 ms to 22 ms. It should be noted that the contact force of the upper bumper absorber was responsible for increasing the knee-bending angle and that of the lower bumper absorber was responsible for increasing the tibia-bending angle from 12 ms to 22 ms. An increase in the tibia-bending angle reduced the increase in the knee-bending angle owing to the connection of the tibia to the knee joint. The tibia was likely to be fractured from 12 ms to 22 ms. The knee-bending angle of the modified THUMS increased again, and the tibia-bending angle of the modified THUMS decreased from 22 ms to 30 ms. It should

be noted that the contact force of the upper bumper absorber was responsible for increasing the knee-bending angle from 20 ms to 30 ms. The tibia was not likely to be fractured from 20 ms to 30 ms owing to the decrease in the contact force of the lower bumper, whereas the ligaments of the knee joint were likely to be ruptured. Finally, the MCL of the modified THUMS ruptured at 27 ms. The tibia was likely to be fractured before the rupture of the ligaments of the knee joint.

7.3.2 Bio-fidelity of the lower legform impactor

The kinematics of the lower legform impactor was not correlated with that of the modified THUMS (see Figure 7.5). The contact force of the lower bumper absorber of the lower legform impactor was not correlated with that of the modified THUMS (see Figure 7.6). The kinematic of the HJ2 THUMS was validated with a PMHS test performed by Schroeder (2008); the bio-fidelity of the modified THUMS is identical to that of the HJ2 THUMS. Further, the tibia-bending deformation of the lower legform impactor can be further improved. On the basis of the discussion in section 7.3.1, it is inferred that the tibia-bending angle depended on the knee-bending angle. It was preferred for the tibia of the lower legform impactor to be as flexible as that of a human body in order to evaluate the knee-bending angle more precisely.

7.4 Conclusions

The results of an FE simulation performed using the modified THUMS indicated that the knee-bending angle depended on the tibia-bending angle and that the tibia was likely to be fractured before the rupture of the ligaments of the knee joint injury. Further, the flexibility of the tibia was indispensable for evaluating the risk of the rupture of the ligaments of the knee joint, and it was preferred for the tibia of the lower legform impactor to be as flexible as that of a human body.

8 Analytical study of the kinematics and knee-bending angle of the lower legform impactor

8.1 Introduction

Injuries sustained by the tibia and the knee-joint ligaments of a pedestrian impacted by a vehicle and an SUV were assessed by performing a numerical simulation using human FE models such as the modified THUMS, THUMS AF05, and THUMS 6YO in chapters 3 and 5; the rupture of the knee-joint ligaments was found to be one of the most frequently occurring injuries.

The relationships between characteristics such as the shape and stiffness of the front end of a vehicle and an SUV and the injuries sustained by the tibia and the knee-joint ligaments were clarified by performing parametric studies on urethane blocks resembling the central section of the vehicle and the SUV in terms of their shape and stiffness in chapter 4 and 6. The upper and lower bumper absorbers were likely to be responsible for the cause of injuries to the tibia and the knee-joint ligaments.

The kinematics of the lower legform impactor was compared with that of the modified THUMS in chapter 7, and the injuries sustained by the knee-joint ligament of a pedestrian impacted by a vehicle and an SUV depended on the height of the upper absorbers from the ground and the stiffness of the upper and lower bumper absorbers. The upper and the lower bumper absorbers were likely to cause an increase in the knee-bending angle of the lower legform impactor.

The objective of this chapter is to clarify the relationships between the knee-bending angle and the height and stiffness of the upper and lower bumper absorbers of a vehicle by an analytical approach that involves the solving of the equation of motions of the lower legform impactor.

8.2 Development of rigid body and spring model

The kinematics of the lower legform impactor was investigated on the basis of the FE analysis result. The FE models of the lower legform impactor and the vehicle to be investigated were identical to those described in chapter 3. The FE model the lower legform impactor consisted of shell elements and solid elements with fully deformable material properties (see Figure 8.1). The boundary and the initial conditions of the FE

analysis were identical to those used in the lower legform impactor test, which followed the EEVC WG17 test protocol.

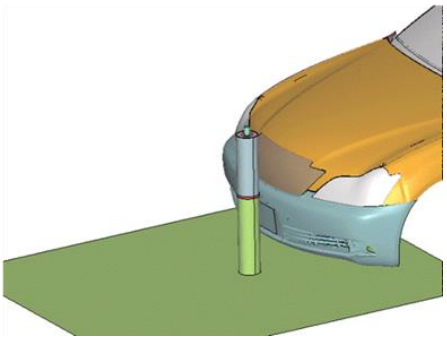

Figure 8.1. FE model of the lower legform impactor and the vehicle.

The kinematics of the lower legform impactor was assumed to be in a plane motion to simplify the constructions of a rigid body and spring model. Hereafter, the rigid body and spring model is simply referred to as “model.” The central sections obtained on the basis of the results of the FE analysis are shown in Figure 8.2.

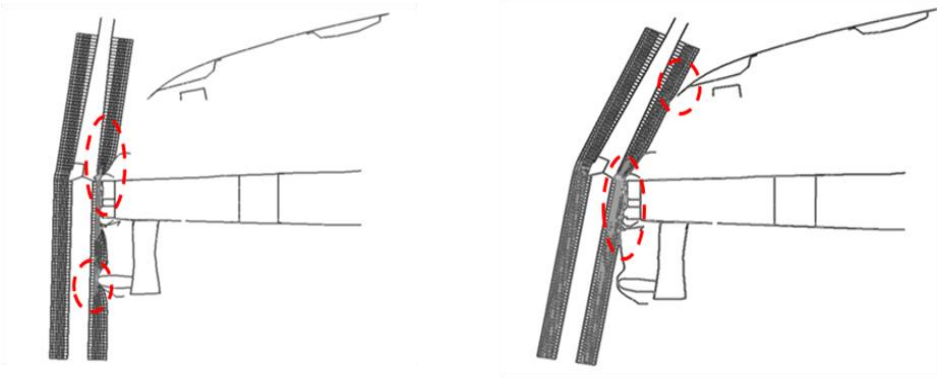

(a) t = 11 ms (b) t = 20 ms

Figure 8.2. Deformed shape of the lower legform impactor and central section of the vehicle.

The kinematics of the lower legform impactor shown in Figure 8.2 is as follows:

(1) The tibia of the lower legform impactor collided with the upper and lower bumpers, and the femur of the lower legform impactor began to rotate in the clockwise direction at 11 ms.

(2) The tibia of the lower legform impactor rebounded from the lower bumper. The femur of the lower legform impactor continued to rotate in the clockwise direction and came in contact with the edge of the hood at 20 ms.

Then, the kinematics of the lower legform impactor shown in Figure 8.2 can be regarded as the motion of two rigid bodies connected by a rotational joint at the knee.

The transmission of forces between the lower legform impactor and a vehicle was determined on the basis of the deformation of the foam materials of the lower legform impactor as follows:

(3) The upper bumper and the edge of the hood of the vehicle came in contact with the lower legform impactor at 20 ms after the knee-bending angle showed maximum values (see Figure 8.2 and 8.3). Forces were transmitted from the vehicle to the lower legform impactor at only three locations, namely, the lower bumper, the upper bumper, and the edge of the hood.

(4) The upper and the lower bumpers of the vehicle came in contact with the lower legform impactor at 11 ms when the upper tibia acceleration showed maximum values (see Figure 8.2 and 8.4).

A rigid body and spring model was established by taking the kinematics, force transmission, and the point of contact of the lower legform impactor into account by performing an FE simulation in chapter 3 (see Figure 8.5).

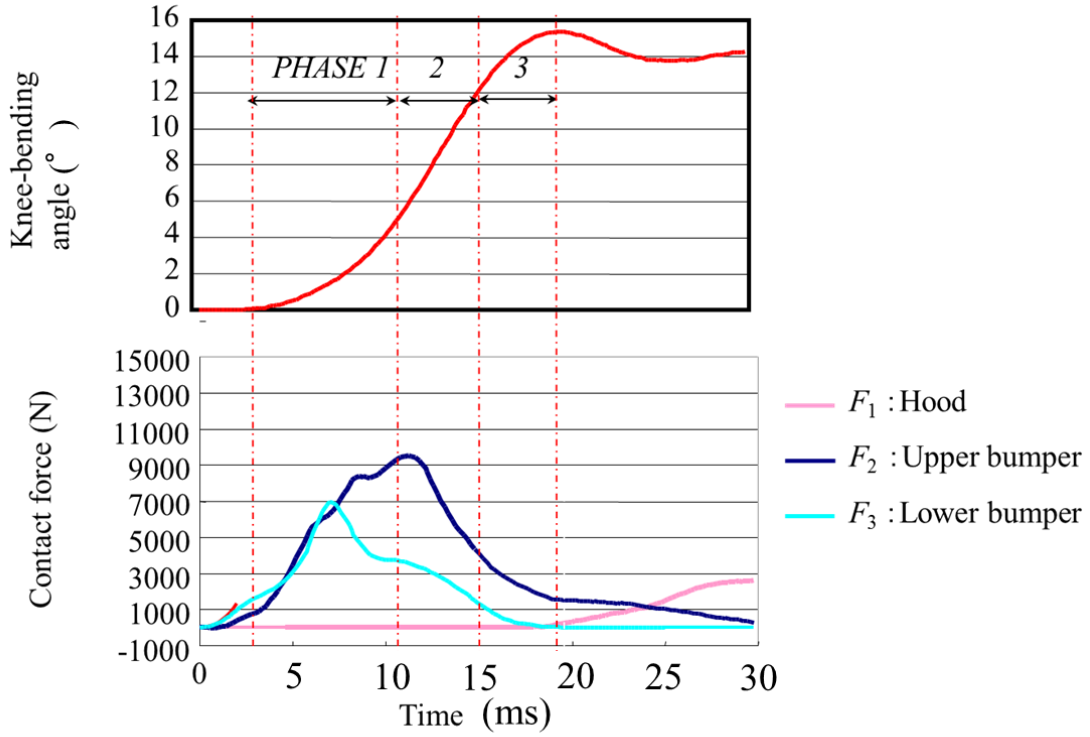

Figure 8.3. Knee-bending angle of the lower legform impactor determined by the FE simulation.

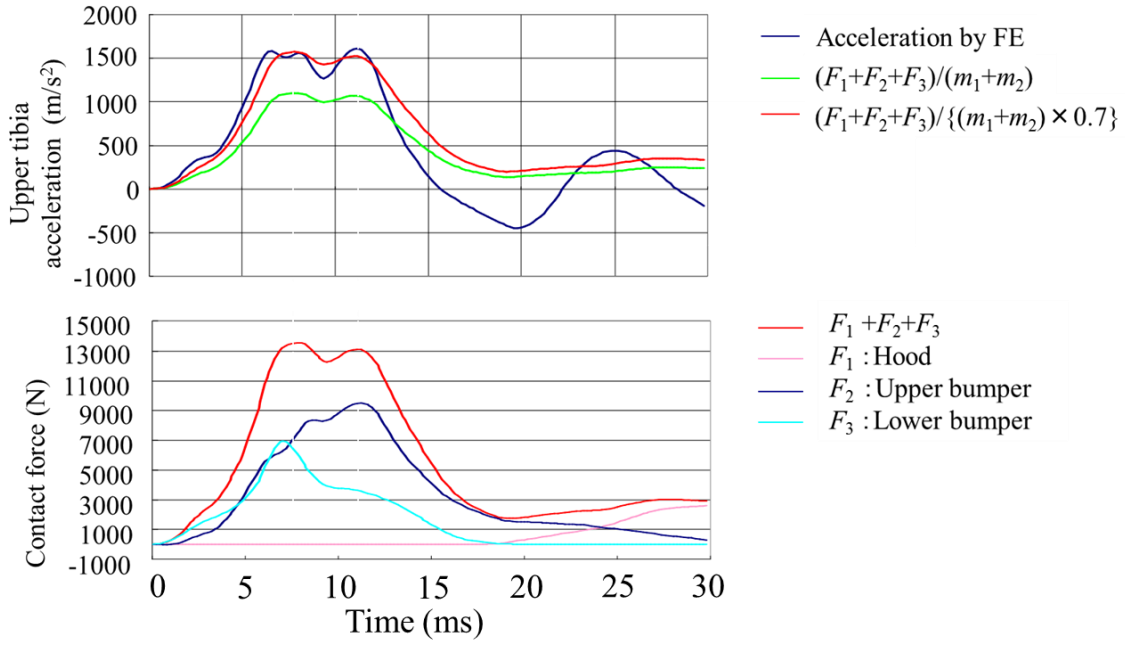

Figure 8.4. Upper tibia acceleration of the lower legform impactor determined by the FE simulation.

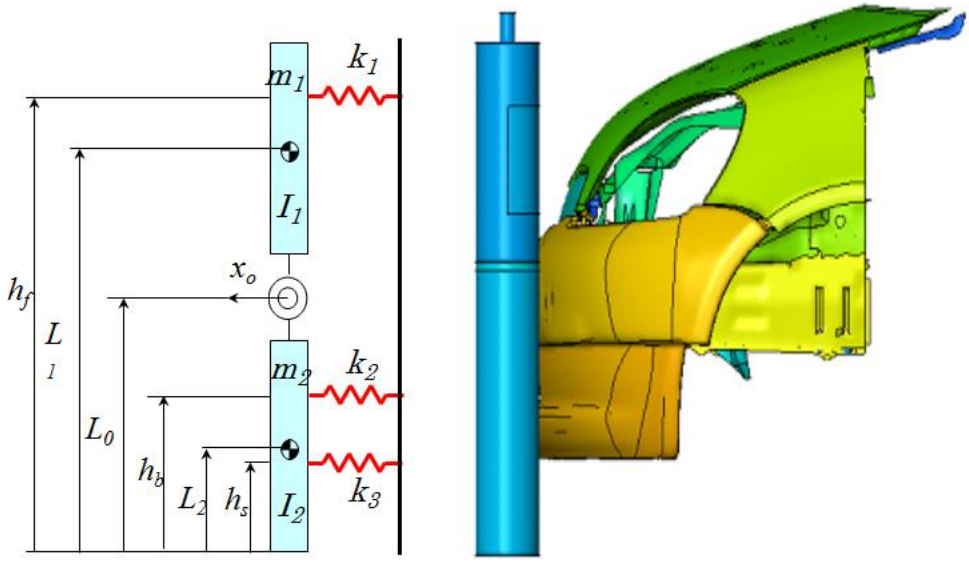

Figure 8.5. Notation of rigid body and spring model (left) and the FE model of the lower legform impactor (right).

The femur and tibia of the lower legform impactor of the model were rigid bodies. The center of gravities, masses, and momentum inertias of the model were determined using the EEVC WG17 test protocol. The knee joint of the model was a mechanical rotational joint, and the relationship between the moment and the bending angle characteristics of the knee joint of the model was determined using the EEVC WG17 test protocol. The shearing stiffness of the knee joint of the model could not be determined (see Figure 8.5).

Forces transmitted from the vehicle to the model were simulated by three nonlinear scalar springs in the x direction (see Figure 8.6). These spring characteristics included the stiffness of the foam material of both the lower legform impactor and the vehicle (see Figure 8.6). The displacements shown in Figure 8.6 were measured between the rear end of the front side rail of the vehicle and the bone of the lower legform impactor. The displacement included the deformation of the foam of both the lower legform impactor and the vehicle.

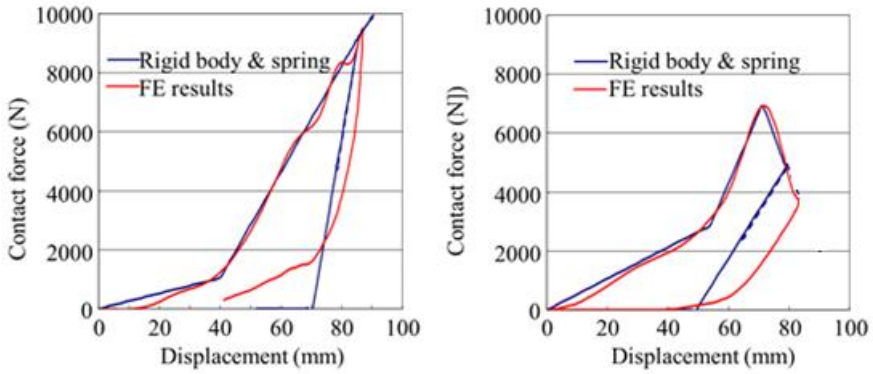

(a) Characteristics of k_2 (b) Characteristics of k_3

Figure 8.6. Plot of the force against the displacement characteristics of the springs of k_2 and k_3.

8.3 Validation of the model

The equations of motion for the model were described as follows by using notations in Figure 8.5.

$$\begin{pmatrix} m_1+m_2 & -m_1(L_1-L_0) & m_2(L_0-L_2) \\ -m_1(L_1-L_0) & I_1+m_1(L_1-L_0)^2 & 0 \\ m_2(L_0-L_2) & 0 & I_2+m_2(L_0-L_2)^2 \end{pmatrix} \begin{Bmatrix} \ddot{x}_0 \\ \ddot{\theta}_1 \\ \ddot{\theta}_2 \end{Bmatrix} + \begin{pmatrix} 0 & 0 & 0 \\ 0 & k & -k \\ 0 & -k & k \end{pmatrix} \begin{Bmatrix} x_0 \\ \theta_1 \\ \theta_2 \end{Bmatrix} = \begin{pmatrix} 1 & 1 & 1 \\ L_0-z_H & 0 & 0 \\ 0 & L_0-z_B & L_0-z_S \end{pmatrix} \begin{Bmatrix} F_1 \\ F_2 \\ F_3 \end{Bmatrix} \tag{8.1}$$

The knee-bending angle of the model θ was described as follows by using the notations in Figure 8.5.

$$\theta = \theta_1 - \theta_2 \tag{8.2}$$

The acceleration of the upper tibia of the model α was described as follows on the basis of the notations shown in Figure 8.5.

$$\alpha = \ddot{x_0} + 0.066 \cdot \ddot{\theta_2} \tag{8.3}$$

where 0.066 (m) is a distance between an accelerometer and top of the tibia.

Equation (8.1) was integrated in the time domain using the Runge-Kutta scheme under the initial and boundary conditions that are identical to those used in the lower

legform impactor test following the EEVC WG17 test protocol. The knee-bending angle and the acceleration of the upper tibia of the model were compared with those obtained from the results of the FE analysis of the lower legform impactor in chapter; the results of this comparison showed that the time histories of the knee-bending angle and the acceleration of the upper tibia of the model were similar to those obtained from the results of the FE analysis (see Figure 8.7 and 8.8). The model can be used to analyze the sensitivity of the contact force to the bending angle of the knee joint and the acceleration of the upper tibia of the lower legform impactor.

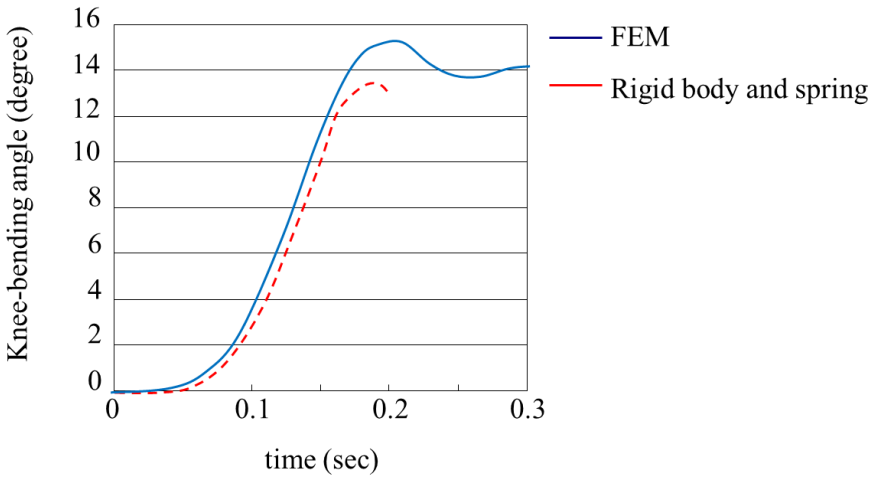

Figure 8.7. Comparison of the knee-bending angle by the FE analysis and the rigid body and spring model.

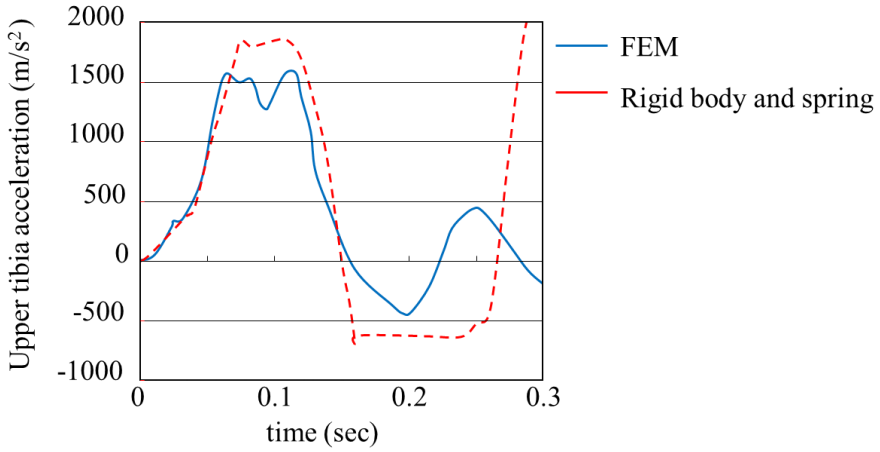

Figure 8.8. Comparison of the Upper tibia acceleration angle by the FE analysis and the rigid body and spring model.

8.4 Results

8.4.1 Knee-bending angle and upper tibia acceleration as functions of contact force

The substitution of Equation (8.3) in the first and the second row of Equations (8.1) eliminates the independent variable x_0, we obtain Equation (8.4). After this equation was integrated twice in the time domain, Equation (8.5) was derived.

$$\begin{aligned}
&[(m_1+m_2)\{m_1(L_1-L_0)^2+I_1\}-m_1(L_1-L_0)\{m_1(L_1-L_0)-m_2(L_0-L_2)\}]\ddot{\theta}_1 \\
&-[(m_1+m_2)\{m_2(L_0-L_2)^2+I_2\}+m_2(L_0-L_2)\{m_1(L_1-L_0)+m_2(L_0-L_2)\}]\ddot{\theta}_2 \\
&=\{-m_1(L_1-L_0)+m_2(L_0-L_2)-(m_1+m_2)(h_f-L_1)\}F_1 \\
&+\{-m_1(L_1-L_0)-m_2(L_0-L_2)-(m_1+m_2)(h_b-L_2)\}F_2 \\
&+\{-m_1(L_1-L_0)-m_2(L_0-L_2)-(m_1+m_2)(L_2-h_s)\}F_3 \\
&-2(m_1+m_2)K(\theta_1-\theta_2)
\end{aligned} \tag{8.4}$$

$$\begin{aligned}
&[(m_1+m_2)\{m_1(L_1-L_0)^2+I_1\}-m_1(L_1-L_0)\{m_1(L_1-L_0)-m_2(L_0-L_2)\}]\theta_1 \\
&-[(m_1+m_2)\{m_2(L_0-L_2)^2+I_2\}+m_2(L_0-L_2)\{m_1(L_1-L_0)+m_2(L_0-L_2)\}]\theta_2 \\
&=\{-m_1(L_1-L_0)+m_2(L_0-L_2)-(m_1+m_2)(h_f-L_1)\}\iint F_1dt^2 \\
&+\{-m_1(L_1-L_0)-m_2(L_0-L_2)-(m_1+m_2)(h_b-L_2)\}\iint F_2dt^2 \\
&+\{-m_1(L_1-L_0)-m_2(L_0-L_2)-(m_1+m_2)(L_2-h_s)\}\iint F_3dt^2 \\
&-2(m_1+m_2)\iint K(\theta_1-\theta_2)dt^2
\end{aligned} \tag{8.5}$$

Further, Equation (8.5) explicitly indicated the relationship between the knee-bending angle of the lower legform impactor and the stiffness of the vehicle. The knee-bending angle of the lower legform impactor is given by $(\theta_1 - \theta_2)$ in Equation (8.5).

$$m_1 = m_2 \tag{8.6}$$

$$I_1 = I_2 = I \tag{8.7}$$

$$L_1 - L_0 = L_0 - L_2 \tag{8.8}$$

$$K(\theta_1 - \theta_2) = M \tag{8.9}$$

where M is a constant.

$$I\theta = (h_b - L_2) \iint F_2 \, dt^2 - (L_2 - h_s) \iint F_3 \, dt^2 - 2 \iint M dt^2 \tag{8.10}$$

where I is the inertia moment of the tibia.

The tibia and the femur of the lower legform impactor exhibit similar shapes and mass properties. The mass properties of the tibia of the lower legform impactor were assumed to be identical to those of the femur of the lower legform impactor (see Equations 8.6, 8.7, and 8.8). Contact force F_1 from the hood to the femur did not affect the maximum knee-bending angle (see Figures 8.3 and 8.4). Further, F_1 was assumed to be zero in Equation 8.5. The knee joint of the model was a mechanical rotational joint, and the moment versus the bending angle characteristic of the knee joint of the model was almost constant, because the knee joint of the lower legform impactor was a solid plate made of mild steel and the plastic bending deformation of the plate was attributed to the resistance of the entire place (see Equation 8.9). Equation 8.10 was obtained by substituting Equations 8.6, 8.7, 8.8, and 8.9 in Equation 8.5.

Equation 8.10 explicitly defined contact forces F_2 and F_3, as well as the knee joint stiffness *M*. The first and second terms of Equation 8.10 indicate the contributions of F_2 and F_3 to the knee-bending angle. The last term of Equation 8.10 indicates the contributions of the knee-joint stiffness *M* to the knee-bending angle.

The contributions of the contact forces to the knee-bending angle, as obtained from Equation 8.10, are shown in Figure 8.9. F_2 between the lower legform impactor and the upper bumper absorber of the vehicle increased the knee-bending angle. F_3 between the lower legform impactor and the lower bumper absorber decreased the knee-bending angle. Further, *M* decreased the knee-bending angle. F_2 between the lower legform

impactor and the upper bumper absorber of the vehicle has a significant effect on the knee-bending angle. Equation (8.10) and Figure 8.9 indicated that the knee-bending angle was dominated by the moment around the center of gravity of the tibia by the contact forces of the upper and lower bumper absorbers. Another investigation is necessary to determine the optimum values of F_2 and F_3 for the lower legform impactor, by taking into account the interactions between F_2 and F_3.

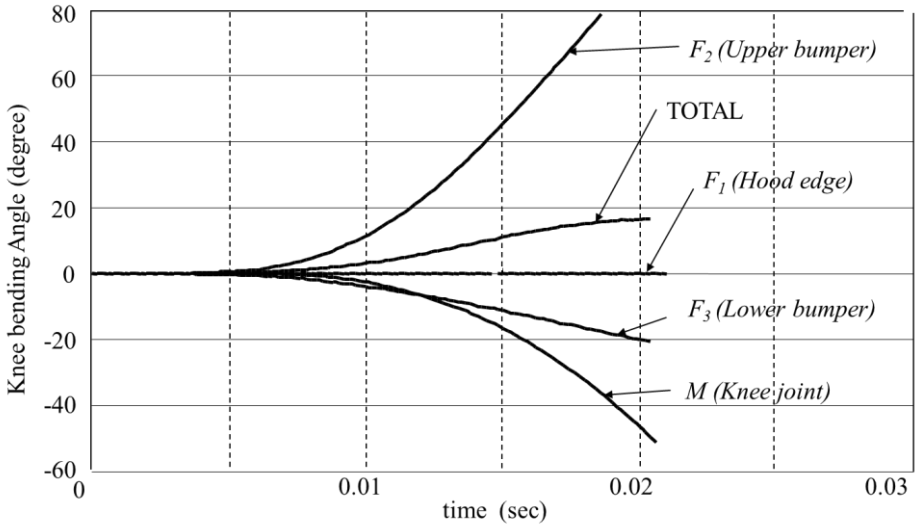

Figure 8.9. Contributions of the contact forces to the knee-bending angle of the lower legform impactor.

8.4.2 Interaction of F_2 and F_3 with the knee-bending angle

Parametric studies involving the change in F_2 and F_3 were conducted to optimize F_2 and F_3 for the lower legform impactor by taking into account the interactions between F_2 and F_3. These parametric studies were conducted by changing the stiffness of the front end of a vehicle. The scalar spring characteristics of k_2 and k_3 were modified, as described in Figure 8.10. Injuries were assumed to occur when the knee-bending angle was more than 15° and the acceleration of the upper tibia was more than 150 G. The knee-bending angle and the acceleration of the upper tibia of the model exceeded the abovementioned assumed injury criteria, and the gradient of curve of the plot of the force against the displacement, where the front end of the vehicle was mostly deformed, was reduced by 12.5%, 25%, 37.5%, and 50% of the original gradient of k_2 and k_3. Twenty-five cases were simulated using the model.

The results of the parametric studies were summarized in Figures 8.11 and 8.12 in terms of the distribution of the knee-bending angle and the acceleration of the upper tibia. The knee-bending angle of the model decreased with an increase in k_2, and the knee-bending angle mostly did not depend on k_3 (see Figure 8.11). The acceleration of the upper tibia depended on k_2 and k_3. Further, the acceleration of the upper tibia was controlled on the basis of the maximum contact forces of the upper and lower bumper absorbers (see Figure 8.12).

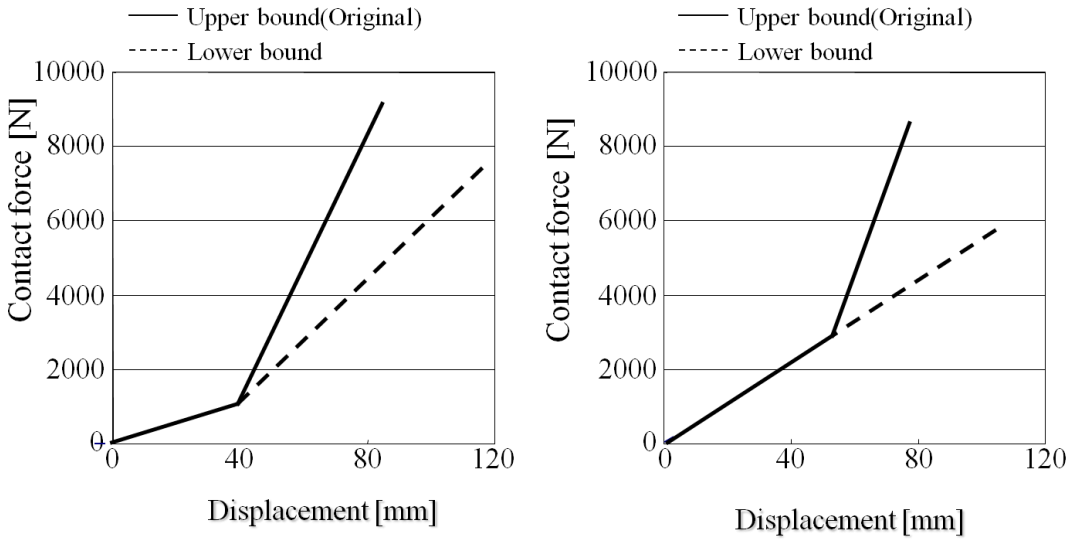

(a) k_2 (b) k_3

Figure 8.10. Plot showing the force against the displacement characteristics of k_2 and k_3.

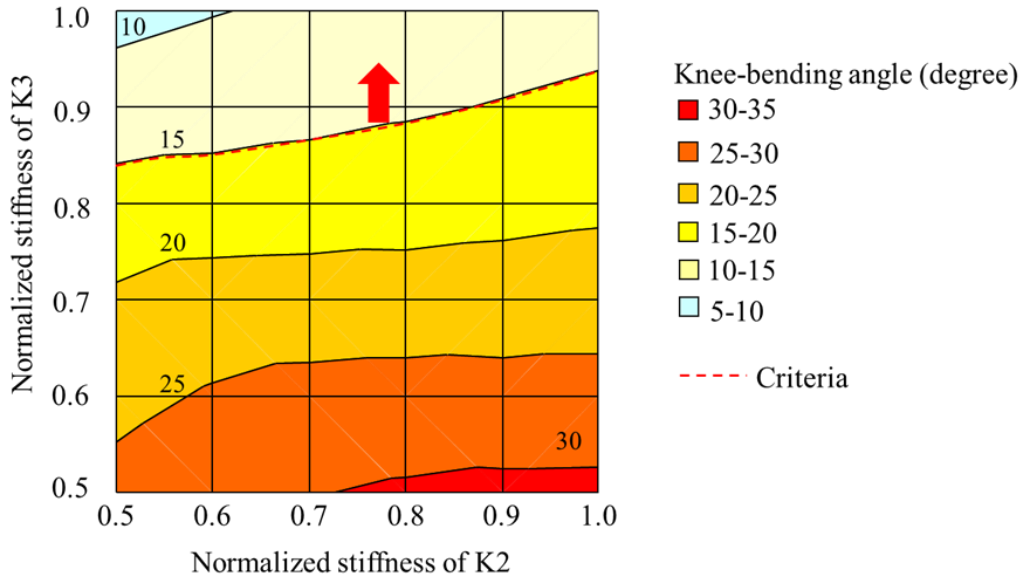

Figure 8.11. Distribution of the knee-bending angle using the model.

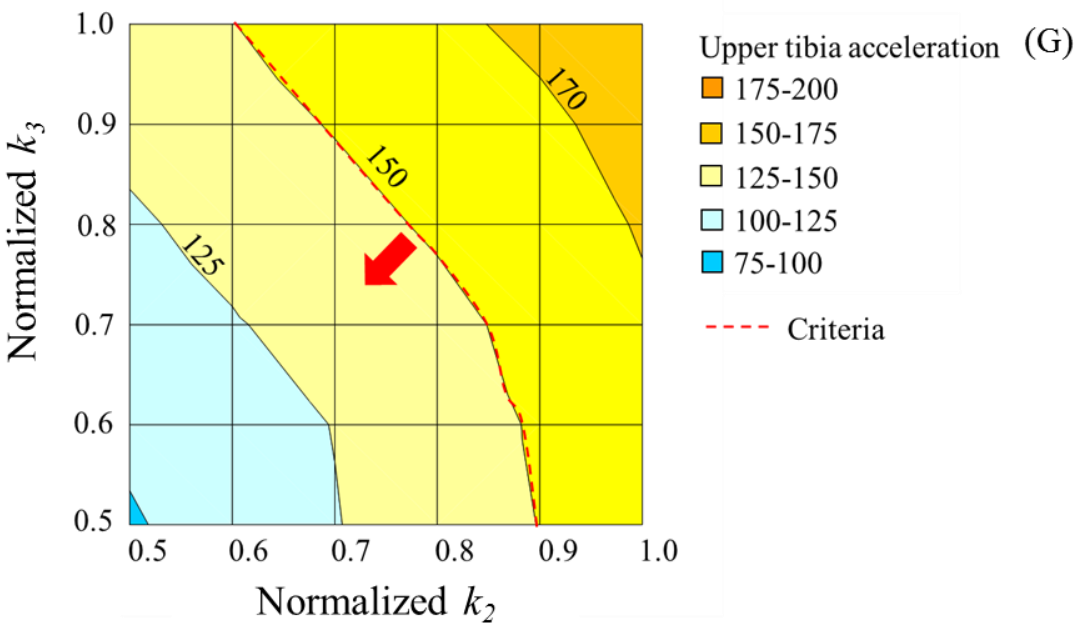

Figure 8.12. Distribution of the acceleration of the upper tibia using the model.

8.5 Discussion

The injury caused by the acceleration of the upper tibia by the lower legform impactor resembles the injury of the tibia around the knee joint. On the basis of the results of the parametric studies conducted using the model of the lower legform

impactor, it is inferred that the k_2 and the k_3 formed significant components of the acceleration of the upper tibia (see Figure 8.12). The distribution of the acceleration of the upper tibia shown in Figure 8.12 indicated that it was necessary to keep under certain levels of the k_2 and the k_3 in order to satisfy the injury criteria of the lower legform impactor for a vehicle. However, the k_3 shown in Figure 8.5 was considered at the center of the tibia, and it is difficult to imagine that F_3 causes the injury of the tibia around the knee joint of a pedestrian. The reason why the k_3 was sensitive to the acceleration of the upper tibia is that the tibia of the lower legform impactor was stiff, owing to which the rotational movement of the tibia was caused by F_3 . This rotational movement of the tibia decreased the acceleration of the upper tibia. If the flexibility of the tibia of the lower legform impactor is similar to that of the tibia of a human body, k_3 will be less sensitive to the acceleration of the upper tibia.

8.6 Conclusions

The rigid body and spring model (model) of the lower legform impactor was established and validated with the results of the FE model. The results obtained using the model showed good correlation with the results obtained using the FE model, and the model can be used to analyze the knee-bending angle and the acceleration of the upper tibia.

The knee-bending angle was shown as a function of the contact forces using the model. The contact force generated by the upper bumper absorber has a significant impact on the knee-bending angle.

Parametric studies involving a change in the upper bumper stiffness and the lower bumper stiffness were conducted using the model. The upper bumper stiffness has a significant impact on the knee-bending angle. The lower bumper stiffness has a significant impact on upper tibia acceleration, as observed in the case of the upper bumper stiffness. The sensitivity of the lower bumper stiffness to the acceleration of the upper tibia was discussed, and the lack of flexibility of the tibia of the lower legform impactor was considered to be the reason for this sensitivity.

9 General discussion and conclusion

9.1 Methodology

The injury mechanism of a pedestrian and the interactions between the pedestrian and a vehicle have been studied using a PMHS specimen, anthropometric dummies, and mathematical models. A human PMHS exhibits human-like kinematics and suffers from injuries. Tests performed using the PMHS specimen are not suitable for the evaluation of safety countermeasures owing to ethical issues and the limited resources. Mechanical dummies were developed. However, the impact response of full-body mechanical dummies was extremely sensitive to their initial posture. The repeatability the full-body mechanical dummies was disadvantageous for a parametric study.

Mathematical simulations are not subject to ethical issues and the limitation of resources. Such simulations are effective for studying the injury mechanism of a pedestrian and the interactions between a pedestrian and a vehicle. Multibody models and FE models are available for use in vehicle-pedestrian impacts. Methods to evaluate the bio-fidelity of mathematical simulations are divided into two steps. In the first step, the kinematics of a mathematical model is compared with that obtained from the PMHS test. In the second step, the injuries considered in the mathematical model are compared with those considered in the PMHS test. Multibody models and FE models are suitable for use in the first step, whereas only the FE models are suitable for use in the second step. In the past, the structure of the front end of a vehicle was much stiffer than a pedestrian's body; however, in future, the structure of the front end of a vehicle will be as stiff as a pedestrian's body owing to the safety countermeasure. The deformation of the front end of a vehicle will be the third step of the methods for evaluating the bio-fidelity of the mathematical simulations.

9.1.1 Evaluation of accuracy of deformation of the front end of a vehicle

The lower legform and the headform impact tests following the EEVC WG17 test protocol (European Enhanced Vehicle-Safety Committee, 1996) were conducted to validate the stiffness of the FE model of a sedan. Such test protocols are commonly used

for rating and regulation tests; thus, they can be easily used for validating the deformation of the front end of a vehicle, as described in chapters 2, 3, and 5.

9.1.2 Evaluation of kinematics of the mathematical model using the PMHS test

Previous studies using the human FE models were mostly conducted using a human FE model of AM50%ile size. The PMHSs used in the test always differed in terms of their height and mass from an AM50%ile pedestrian (see Table 2.2). THUMS was adjusted to the height and the mass of the tested PMHS by scaling, and comparison of the kinematics was improved in comparison to the result of Maeno and Hasegawa (2001). The impact response of the entire body of a pedestrian was not only sensitive to its initial posture but also sensitive to the height and the mass of the pedestrian.

9.1.3 Evaluation of injury considered in the mathematical model using the PMHS test

Fractures of the tibia and the fibula and the rupture of the ligaments of the knee joint were simulated by eliminating the FEs that exceeded the criteria of strain established by Yamada (1970) in chapter 2. The simulation results obtained using THUMS showed good correlations with the characteristics of the force versus deformation with the component tests of the knee joint, tibia, and fibula of the PMHS specimen. The risk of occurrence of fractures and ligament ruptures can be evaluated by eliminating the FEs on the basis of the criteria of strain.

9.1.4 Parametric studies

Extensive parametric studies were carried out to investigate the relationship between the injuries sustained by a pedestrian to the shape of the front end and the stiffness of vehicles in chapters 4 and 6. Newly developed FE models of urethane blocks that resembled that central section of the vehicles were used to address the complex interactions between a pedestrian and a vehicle. Results of the investigation of the interactions between the pedestrian and the vehicle, as presented in chapters 2, 3, and 5, indicated that the contact forces were transmitted through several contacting areas of the pedestrian. The kinematics and injuries of THUMS determined using the FE model of urethane blocks were similar to those determined using an FE model of the vehicle. The FE model of urethane blocks is suitable for use in parametric studies.

9.2 Important results from the present study

9.2.1 Bifurcation of lower leg injuries

Two types of lower leg injuries occur in the case of pedestrian-vehicle accidents. The first type of injury is the fracture of the tibia, and the second type of injury is the rupture of the knee-joint ligaments. Only one of these two types of injuries is often observed in pedestrian-vehicle accidents; in other words, both these types of injuries do not occur simultaneously in pedestrian-vehicle accidents. The reason why only one of these injuries is observed in pedestrian-vehicle accidents was clarified. The results of the FE analysis showed the bending of the tibia and the bending of the knee joint during a pedestrian-vehicle impact. First, the tibia and the knee joint bend simultaneously, increasing the risk of fracture of the tibia, which is then followed by the risk of rupture of the knee-joint ligaments. This finding suggests that it is necessary for the tibia of the test device to be flexible in order to evaluate both the risk of fracture of the tibia and the rupture of the knee-joint ligaments.

9.2.2 Cause of increase in the knee-bending angle of the lower legform impactor

The knee-bending angle of the lower legform impactor was described as a function of the height and the stiffness of the upper bumper absorber and the lower bumper absorber. The contact force generated by the upper bumper absorber had a significant impact on the knee-bending angle. Parametric studies involving a change in the stiffness of both the upper bumper and the lower bumper were conducted. The stiffness of the upper bumper had a significant impact on the knee-bending angle. The stiffness of the lower bumper had a significant impact on the acceleration of the upper tibia, as observed in the case of the upper bumper stiffness. The sensitivity of the stiffness of the lower bumper to the acceleration of the upper tibia was discussed, and the cause for this sensitivity was attributed to the lack of flexibility of the tibia of the lower legform impactor. This finding provided clear insights into the manner in which the knee joints bend when impacted by a vehicle.

9.2.3 Influence of the shape and stiffness of the front end of a vehicle

The stiffness of both the upper and the lower bumper absorbers was optimized for an AM50%ile pedestrian, an AF05%ile pedestrian, and a 6YO child pedestrian

impacted by a vehicle. The optimized stiffness of both the upper and the lower bumper absorbers indicated that neither the tibia fractured nor did the ligaments of the knee joint rupture when impacted by a vehicle. The stiffness of the upper bumper absorber was optimized for the AM50%ile pedestrians impacted by an SUV. The optimized stiffness of the upper bumper indicated that neither the tibia fractured nor did the ligaments of the knee joint rupture when impacted by a vehicle. However, the upper bumper absorber was too soft to be used for an SUV. A potential countermeasure to further optimize the stiffness of the upper and lower bumper absorbers involves the addition of a contact force to the tibia supported by the lower bumper absorber.

9.3 Future studies

In this research, bony fractures and ligament ruptures were studied. From Table 1.2, it is inferred that 30% of the injuries sustained by pedestrians include the AIS2-6 head injuries (see Table 1.2). Research on the mechanism of occurrence of brain injuries sustained by pedestrians is of high priority for establishing safety countermeasures. An FE model of THUMS version 3 already includes a detailed FE model of the brain and can be used in this research. Within the scope of the research of the brain injuries sustained by pedestrians, a greater number of simulations using FE models including parameters such as the vehicle impacting speed, vehicle impacting angle, postures of the pedestrian, shape of the front end of the vehicle, and stiffness of the front end of the vehicle will be necessary. To identify the critical parameters of the impacting configurations and the vehicle for the brain injuries, future parametric studies should be conducted on the basis of the Monte-Carlo simulation or stochastic simulations (Yasuki et al., 2003).

9.4 Conclusion

The key objective of the present thesis is to elucidate the mechanism of fracture of the tibia and the rupture of the knee-joint ligaments of a pedestrian. The main conclusions of this study are summarized as follows:

(1) An FE model of a pedestrian is reliable for examining the relationship between injuries such as the fracture of the tibia and the rupture of the knee-joint ligaments and characteristics such as the shape and stiffness of the impacting vehicle.

(2) The relationship between injuries such as the fracture of the tibia and the rupture of the knee-joint ligaments and characteristics such as the shape and stiffness of the impacting vehicle depended on the size and age of humans, such as in the case of an AM50%ile pedestrian, an AF05%ile pedestrian, and a 6YO child pedestrian. The FE models of these three pedestrians indicated that the kinematics and the injury mechanisms of the three pedestrians differed from each other.

(3) The FE model of a pedestrian was used to optimize the shape and the stiffness of a vehicle. With the optimized shape and stiffness of the vehicle, neither the tibia fractured nor did the ligaments of the knee joint rupture in the case of an AM50%ile pedestrian, an AF05%ile pedestrian, and a 6YO pedestrian. The FE model of the pedestrian can be one of the design tools for the safety of pedestrians in future.

(4) The rupture of the ligaments of the knee joint was related to the knee-bending angle, and the lower bumper absorber enabled the decrease in the knee-bending angle. The addition of contact forces of the tibia supported by the lower bumper absorber is a potential countermeasure for decreasing the knee-bending angle in the case where a pedestrian is impacted by an SUV.

(5) First, the tibia and the knee joint bent simultaneously, increasing the risk of fracture of the tibia; in case the tibia did not fracture, the ligaments of the knee joint were at a risk of undergoing rupture.

An FE model of a pedestrian is only now being used for the research of pedestrian safety measures. This method involving the use of the abovementioned pedestrian FE model is new and reliable for the research of the kinematics and the injuries of a pedestrian. The findings of this study may contribute to the enhancement of pedestrian safety research. The injury mechanism of soft tissues such as the brain and the internal organs was not included in this thesis; however, it should be researched using the pedestrian FE model in the near future.

References

Abe, H. (1996). *Data Book on Mechanical Properties of Living Cells, Tissues, and Organs.* New York, USA: Springer Verlag.

Akiyama, A., Okamoto, M., and Rangarajan, N. (2001). Development and Application of the New Pedestrian Dummy. *Proceedings of 17th ESV Conference, Report No. 463.* Amsterdam, The Netherlands: NHTSA.

Backaitis, S., Daniel, S., Cesari, D., and Cavallero, C. (1983). Comparison of Pedestrian Kinematics and Injuries in Staged Impact Tests with PMHSs and Mathematical 2D Simulations. *Report No. SAE 830186.* Warrendale, PA, USA: Society of Automotive Engineers.

Brun-Casssan, F., Vallee, H., Tarriere, C., Fayon, A., Got, C., Patel, A., and Hureau, J. (1983). Reconstruction of Actual Car-Pedestrian Collisions with Dummy and PMHSs. *Report No. SAE 830053.* Warrendale, PA, USA: Society of Automotive Engineers.

Cesari, D., Ramet, M., and Clair, P. (1980). Evaluation of Pelvic Fracture Tolerance in Side Impact. *Report No. SAE 801306.* Warrendale, PA, USA: Society of Automotive Engineers.

Cavallero, C., Cesari, D., Ramet, M., Billault, P., Farisse, J., Seiat-Gautier, B., and Bonnoit, J. (1983). Improvement of Pedestrian Safety: Influence of Shape of Passenger Car-Front Structures Upon Pedestrian Kinematics and Injuries: Evaluation Based on 50 PMHS Tests. *Report No. SAE 830624.* Warrendale, PA, USA: Society of Automotive Engineers.

Choi, H., Lee, I., and Haug, E. (1999). Advanced Finite Element Modeling of the Human Body for Occupant Safety; H-Model for the Next Millennium. *5th HanPam.* Seoul, Korea.

Daniel, S. (1982). The Role of the Vehicle Front End in Pedestrian Impact Protection. *Report No. SAE 820246.* Warrendale, PA, USA: Society of Automotive Engineers.

European Enhanced Vehicle-Safety Committee. (1996). *Improved Test Method to Evaluate Pedestrian Protection Afforded by Passenger Car.* EEVC Working Group Report.

Hayashi, S., Yasuki, T., and Kitagawa, Y. (2008). Occupant Kinematics and Estimated Effectiveness of Side Airbags in Pole Side Impacts Using a Human FE Model with Internal Organs. *Stapp Car Crash Journal. Vol. 52, pp. 363-377.* Warrendale, PA, USA: Society of Automotive Engineers.

Hayashi, S., Yasuki, T., Yamamae, Y., and Takahira, Y. (2006). A Study of Side Airbag Effectiveness in Reducing Chest Injury in Car-to-Car Side Impacts Using a Human FE Model. *Proceedings of 2006 International Research Council on the Biomechanics of Impacts, pp. 397-400.* Madrid, Spain: The IRCOBI Council.

Higuchi, K., and Akiyama, A. (1991). The Effect on the Vehicle Structure's Characteristics on Pedestrian Behavior. *Proceedings of the 13th ESV Conference, pp. 323-329.* USA: NHTSA.

Hoof, J., De Lange, R., and Wismans, J. (2003). Improving Pedestrian Safety Using Numerical Human Models. *Report No. SAE 2003-22-0018.* Warrendale, PA, USA: Society of Automotive Engineers.

IHRA. (1998). Pedestrian Safety Expert Meeting, IHRA/PS/26. *Pedestrian Safety Expert Meeting.*

Institute for Traffic Accident Research and Data Analysis. (2008). *Traffic Accident's Statistics Annual Report.* Tokyo, Japan: Institute for Traffic Accident Research and Data Analysis.

Irwin, A., and Mertz, A. (1997). Biomechanical Basis for the CRABI and Hybrid 3 Child Dummies. *Report No. SAE 973317.* Warrendale, PA, USA: Society of Automotive Engineers.

Ishikawa, H., Kajzer, J., and G, S. (1993). Computer Simulation of Impact Response of the Human Body in Car-Pedestrian Accidents. *Report No. SAE 933129.* Warrendale, PA, USA: Society of Automotive Engineers.

ISO/TC22/SC10/WG2. (1997). *Passenger Cars and Light Commercial Vehicle Pedestrian Protection–Impact Test Method for Pedestrian Leg and Knee. Document No. N552.*

Iwamoto, M., Kisanuki, Y., Watanabe, I., Furusu, K., Miki, K., and Hasegawa, J. (2002). Development of an FE Model of the Total Human Model for Safety (THUMS) and Application to Injury Reconstruction. *Proceeding of International*

Conference on the Biomechanics of Impacts, pp. 31-42. Munich, Germany: The IRCOBI Council.

Kajzer, J., Matsui, Y., Ishikawa, Y., Schroeder, G., and Bosch, U. (1999). Shearing and Bending Effects at the Knee Joint at Low Speed Lateral Loading. *Report No. SAE 1999-01-0712.* Warrendale, PA, USA: Society of Automotive Engineers.

Kajzer, J., Schroeder, G., Ishikawa, H., Matsui, Y., and Bosch, U. (1997). Shearing and Bending Effects at the Knee Joint at High Speed Lateral Loading. *Report No. SAE 973326.* Warrendale, PA, USA: Society of Automotive Engineers.

Kitagawa, Y., Hasegawa, J., and Yasuki, T. (2005). A Study of Knee Joint Kinematics and Mechanics using a Human FE Model. *Stapp Car Crash Journal. Vol. 49, pp. 117-131.* Warrendale, PA, USA: Society of Automotive Engineers.

Kitagawa, Y., Yasuki, T., and Hasegawa, J. (2008). Research Study on Whiplash Injury Lessening with Active Head Restraint using a Human FE Model. *Proceedings of 2008 International Research Council on the Biomechanics of Impacts, pp. 381-396.* Bern, Switzerland: The IRCOBI Council.

Konosu, A. (2002). Reconstruction Analysis for Car–Pedestrian Accidents using A Computer Simulation Model, *Review of Automotive Engineering JSAE, Vol. 23, No. 3, pp. 357–363.*: Tokyo, Japan: Society of Automotive Engineers of Japan.

Konosu, A., and Tanahashi, M. (2007). Development of a Biofidelic Flexible Pedestrian Legform Impactor type GT (Flex-GT). *Proceeding of 20th ESV Conference. Report No. 07-178.* Lyon, France: NHTSA.

Kuwahara, M., Yasuki, T., Kitagawa, Y., Hayashi, S., and Masuda, T. (2008). A Study of SRS Side Airbag Performance in Chest Protection in a Pole Side Impact using a Human FE Model. *Proceedings of 2008 FISITA. Report No. F2008-08-015.* Munich, Germany: FISITA.

Levine, R., Begeman, P., King, A. (1984). An Analysis of the Protection of Lateral Knee Bracing in Full Extension Using a cadaver Simulation of Lateral Knee Impact. *American Academic of Orthopedica Surgerical, August 17th.*

Linder, A., C, D., Clark, A., Fildes, B., Yang, J., and Otte, D. (2005). Mathematical Simulations of Real-world Pedestrian-Vehicle Collisions. *Proceeding of the19th ESV Conference. Report No. 05-285.* Washington, D.C., USA: NHTSA.

Maeno, T., and Hasegawa, J. (2001). Development of an FE model of the Total Human Model for Safety (THUMS) and Application to Car-Pedestrian Impacts. *Proceedings of the 16th ESV Conference, Report No. 494.* Amsterdam, The Netherlands: NHTSA

Masson, C., Arnoux, P-J., Brunet, C., and Cesari, D. (2005). Pedestrian injury Mechanisms and Criteria, A Coupled Experimental and Finite Element Approach. *Proceedings of the 19th ESV Conference, Report No. 05-0335.* Washington D.C., USA: NHTSA.

Matsui, Y., and Takabayashi, M. (2004). Effects of Upper Body Mass on Dynamic Behavior of Legform Impactor for Pedestrian Subsystem Tests. *Transaction of Society of Automotive Engineers of Japan, Vol. 35, No.2, pp. 211-216.*

Matsui, Y., and Konosu, A. (2002). Comparison of Pedestrian Subsystem Safety Tests Using Impactors and Full-Scale Dummy Tests. *Report No. SAE 2002-01-1021.* Warrendale, PA, USA: Society of Automotive Engineers.

McCalden, R., McGeough A., Baker, M., and Court-Brown, M. (1994). Age-related changes in the tensile properties of cortical bone. The relative importance of changes in porosity, mineralization, and microstructure. *Journal of Bone and Joint Surgery. Vol. 75, No. 8, pp. 1193-1205.* MA, USA.

McHenry, R. (1963). Analysis of the Dynamic of Automobile Passenger Restraint Systems. *Proceedings of the 7th Stapp Car Crash Conference, pp. 207-249.* Warrendale, PA, USA: Society of Automotive Engineers.

McPherson, G., and Kriewall, T. (1978). The Elastic Modulus of Fetal Cranial Bone: A First Step Towards an Understanding of the Biomechanics of Fetal Head Modeling. *Journal of Biomechanics , Vol. 13, No. 1, pp. 9-16.*

Mizuno, Y. (2005). Summary of IHRA Pedestrian Safety WG Activities-Proposed Test. *Proceedings of the 19th ESV Conference. Report No. 05-0138.* Washington, D.C., USA: NHTSA.

National Library of Medicine. (2008). *Visible Human Project.* National Library of Medicine.

National Police Agency. (2009). *Traffic Accidents Situation in 2008 (in Japanese).*

Nishimua, R., and Hasegawa, J. (2002). Development of the Human FEM Model for Child Pedestrian. *Proceeding of Annual Congress of Society of Automotive Engineers of Japan, Vol. 78, No. 02, Report No. 20025504.*

Okamoto, Y, Akiyama, A, Okamoto, M, and Kikuchi, Y. (2003). A Study of the Upper Leg Component Tests Compared with Pedestrian Dummy. *Proceedings of the 17th ESV Conference. Report No. 328.* Nagoya, Japan: NHTSA.

Ruan, J., El-Jawahri, R., Chai, L., and Prasad, P. (2003). Prediction and Analysis of Human Thoracic Impact Response and Injuries in PMHS Impacts using a Full Human Body Finite Element Model. *Stapp Car Crash Journal. Vol. 47, pp. 299-321.* Warrendale, PA, USA: Society of Automotive Engineers.

Schroeder, G., Fukuyama, K., Yamazaki, K., Kamiji, K., and Yasuki, T. (2008). Injury Mechanism of Pedestrians Impact Test with a Sport-Utility Vehicle and Minivan. *Proceedings of the 2008 International IRCOBI Conference, pp. 259-274.* Bern, Switzerland: The IRCOBI Council.

Severy, D., and Brink, H. (1966). Auto-Pedestrian Collision Experiments using Full-Scale Accident Simulation. *Report No. SAE 60080.* Warrendale, PA, USA: Society of Automotive Engineers.

Snedeker, G., Walz, F., Muser, M., Lanz, C., and Schroeder, G. (2005). Assessing Femur and Pelvis Injury Risk in Car-Pedestrian Collisions: Comparison of Full Body PMTO Impacts and a Human Body Finite Element Model. *Proceeding of the 19th ESV Conference. Report No.05-103.* Washington, D.C., USA: NHTSA.

Subit, D., Kerrigan, J., Crandall, J., Fukuyama, K., Yamazaki, K., Kamiji, K., and Yasuki, T. (2008). Pedestrian-Vehicle Interaction: Kinematics and Injury Analysis of Four Full-Scale Tests. *Proceedings of the 2008 International Research Council on the Biomechanics of Impacts, pp. 275-29:4.* Bern, Switzerland: The IRCOBI Council.

Takahashi, Y., Kikuchi, Y., Mori, F., and Konosu, A. (2003). Advanced FE Lower Limb Model for Pedestrians. *Proceedings of the 17th ESV Conference. Report No. 218.* Amsterdam, The Netherlands: NHTSA.

Takahashi, Y., Kikuchi, Y., Okamoto, M., Akiyama, A., Ivarsson, J., Bose, D., Subit, D., Shin, J., and Crandall, J. (2005). Biofidelity Evaluation for the Knee and Leg of

the POLAR Pedestrian Dummy. *Proceedings of the 19th ESV Conference. Report No. 05-0280.* Washington, D.C., USA: NHTSA.

Tamura, A., Nakahira, Y., Iwamoto, M., Watanabe, I., Miki, K., Hayashi, S., and Yasuki, T. (2006). The Influence of the Traction Force Due to Inertia of the Brain Mass on Traumatic Brain Injury during SUV-to-Pedestrian Impact. *Proceedings of the 2006 International Research Council on the Biomechanics of Impacts, pp. 361-364.* Madrid, Spain: The IRCOBI Council.

TASS. (2009). *MADYMO, Human Models Manual.* TASS.

TASS. (2011). The New MADYMO Pedestrian Facet Model. *E-news release Vol. 3.*

UN/ECE/WP29/GSRP. (2006). *Proposal for a global technical regulation on uniform provisions concerning the approval of vehicles with regard to their construction in order to improve the protection and to mitigate the severity of injuries to pedestrians and other vulnerable road users.* UN.

UN/ECE/WP29/GSRP/INF-GR-PS/Flex-TEG. (2007). Felx-GT development. UN.

Untarolu, C., Shin, J., Crandall, J., Takahashi, Y., Akiyama, A., and Kikuchi, Y. (2007). Pedestrian Kinematics Investigation with Finite Element Dummy Models Based on Anthropometry Scaling Method. *Proceedings of the 17th ESV Conference. Report No. 328.* Amsterdam, The Netherlands: NHTSA.

van Wijk, J., Wismans, J., Maltha, J., and Wittenbrood, J. (1983). MADYMO Pedestrian Simulations. *Report No. SAE 830060.* Warrendale, PA, USA: Society of Automotive Engineers.

Vezin, P., and Verriest, J. (2005). Development of a Set of Numerical Human Models for Safety. *Proceedings of the 19th ESV Conference. Report No. 05-0163.* Washington, D.C., USA: NHTSA.

Wittek, A., Konosu, A., Matsui, Y., Ishikawa, H., Sasaki, A., Shams, T., and McDonald, J. (2001). A New Legform Impactor for Evaluation of Car Aggressiveness in Car-Pedestrian Accidents. *Proceedings of the 17th ESV Conference, Report No.174.* Amsterdam, The Netherlands: NHTSA.

World Health Organization science group on the assessment of osteoporosis at primary health care level. (2004). World Health Organization. Retrieved from WHO: http://www.who.int/chp/topics/Osteoporosis.pdf

World Health Organization. (2004). *World Report on Road Traffic Injury Prevention.* World Health Organization.

Yamada, H. (1970). *Strength of Biological Materials. Baltimore.* MD, USA: The Williams and Wilkins Company.

Yang, J., and Kajzer, J. (1992). Computer Simulation of Impact Response of the Human Knee Joint in Car-Pedestrian Accidents. *Report No. SAE 922525.* Warrendale, PA, USA: Society of Automotive Engineers.

Yasuki, T., Okamoto, A., Okamoto, M. (2005). Achieving Design Target through Stochastic Analysis. *Proceedings of 17th ESV Conference. Reprt No. 547.* Nagoya, Japan: NHTSA.

Publications

This thesis is largely based on the earlier findings published in several papers as well as reviewed papers:

Reviewed papers

1. Yasuki, T. (2008). An Analysis of Lower Leg Impactor Behavior by Physics Model, *Journal of Biomechanical Science and Engineering, Vol. 3, No. 2, pp. 151-160.*

Chapter 8 is largely based on the above paper.

2. Yasuki, T., and Yamamae Y. (2010). Validation of Kinematics and Lower Extremity Injuries Estimated by Total Human Model for Safety in SUV-to-Pedestrian Impact Test, *Journal of Biomechanical Science and Engineering, Vol. 5, No. 4, pp. 340-356.*

(Chapter 2 is largely based on the above paper.)

3. Yasuki, T. (2007). Mechanism Analysis of Pedestrian Knee-bending Angle by Sedan-type Vehicle Using Human FE Model, *International Journal of Crashworthiness, Vol. 12, No. 4, pp. 329 -339.*

(Chapters 3 and 4 are largely based on the above paper.)

4. Yasuki, T. (2007). Mechanism Analysis of Pedestrian Knee-bending Angle by SUV-type Vehicles Using Human FE Model, *International Journal of Crashworthiness, Vol. 12, No. 6, pp. 645 -651*

(Chapters 5 and 6 are largely based on the above paper.)

5. Yasuki, T. and Yamamae, Y. (2005) A Study on Behavior of Legform Impactor, *Transactions - Society of Automotive Engineers of Japan, Vol. 36, No. 6, Paper No. 20054890.*

(Chapter 7 is largely based on the above paper.)

Papers

6. Yasuki, T. (2005) A Survey on the Biofidelity of the Knee-bending Angle of the TRL Lower Leg Impactor, *Proceedings of the 19th Enhanced Vehicle-Safety Conference, Paper No. 05-0101*.

(Chapter 7 is largely based on the above paper.)